Synthesis of novel first-row transition metal-*N*-heterocyclic carbene complexes

and

Synthesis of *N*-heterocyclic carbene-functionalized linkers for metal organic frameworks

By

Jacob Geoffrey Hoare

A Thesis Submitted to

Saint Mary's University, Halifax, Nova Scotia

in Partial Fulfillment of the Requirements for

the Degree of Bachelor of Science with Honours in Chemistry.

April, 2020, Halifax, Nova Scotia

Approved:	Dr. Robert Singer Professor
Approved:	Dr. Jason Masuda Chairperson

Date: April 26, 2022

Synthesis of novel first-row transition metal-*N*-heterocyclic carbene complexes

and

Synthesis of *N*-heterocyclic carbene-functionalized linkers for metal organic frameworks

By Jacob Geoffrey Hoare

Abstract

Although *N*-heterocyclic carbene ligands are highly versatile and powerful ligands in transition metal catalysis, complexes of *N*-heterocyclic carbenes with 3d metals are uncommon and frequently unstable. In order to explore the reactivity of some 3d metal-*N*-heterocyclic carbene complexes, two tridentate *NCN* pincer ligands were prepared: 1,3-bis(2-pyridylmethyl)imidazolium chloride and 1,3-bis(2-pyridylmethyl)benzimidazolium chloride. These ligands were coordinated to copper(II) and nickel(II) salts in air to yield a variety of 3d metal-*N*-heterocyclic carbene complexes. The counterion to the metal cation appears to have a significant influence on the coordination mode of the ligands and geometry around the metal centres. Synthesis of the novel metal complexes, as well as possible applications, are described herein.

Carbon dioxide is the primary contributor to climate change. As such, materials that can capture and fix carbon dioxide are important tools to limit climate change. One highly effective class of material for gas adsorption is metal-organic frameworks. In an effort to prepare a metal-organic framework with superior carbon dioxide capture and fixation capabilities, a series of linkers with *N*-heterocyclic carbene moieties were designed, of which two were successfully prepared. Thus far, efforts to prepare a metal-organic framework based on either of the two linkers have been unsuccessful.

Date: March 26, 2022

Acknowledgements

Firstly I would like to thank my supervisor, Dr. Robert Singer for his guidance and mentorship, and the opportunity to work in his lab. I would also like to thank my fellow group members Caylee MacDonald, Samantha Henneberry, Kalei Crowell, Olivia Singer, Megan Himmelman, Kaitlyn Blatt-Janmaat and in particular Jacob Campbell for helping to train me.

I would also like to thank the chemistry department technicians past and present, Alyssa Doué, Najwan Albarghouthi, and Bitu Hurisso for technical support and supplying materials, as well as Tanner George and Dr. Jason Masuda for their excellent crystallography work, Xiao Feng at the Dalhousie University mass spectrometry laboratory for running mass spectrometry on all of my samples and providing advice on the data interpretation, and Dr. Xiang Yang for collecting SEM and EDX data, and helping me to prepare SEM samples.

Finally, I would like to thank my friends, family, and Elisha Bennett for her love and support throughout my degree.

Table of contents **Page**

Abstract i
Acknowledgements ii
Table of contents iii
List of Figures vi
List of Schemes xi
List of tables xiii
List of symbols and abbreviations xiv
1. Synthesis of novel first-row transition metal-*N*-heterocyclic carbene complexes 1
1.1 Introduction 1
1.1.1 Transition metals in catalysis 1
1.1.2 *N*-heterocyclic carbenes 2
1.1.3 Target ligands and research questions 6
1.2 Results and discussion 8
1.2.1 Synthesis and characterisation of the ligands 8
1.2.2 Metal complexes of the pincer ligands (1) and (2) 13
1.3 Conclusions 35
1.4 Future work 36
1.5 Experimental 37
1.5.1 Materials and general considerations 37
1.5.2 Synthesis of ligands 38
1.5.3 Successful reactions of the ligands with transition metal salts 40
1.5.4 Unsuccessful reactions of the ligands with transition metal salts 46

2. Synthesis of *N*-heterocyclic carbene-functionalized linkers for metal organic frameworks 48
2.1 Introduction 48
2.1.1 Carbon dioxide capture 48
2.1.2 Metal-organic frameworks 49
2.1.3 Goals and target materials 56
2.2 Results and discussion 57
2.2.1 Synthesis of the linkers 57
2.2.2 Reactions of the linkers with metals 68
2.3 Conclusions 71
2.4 Future work 71
2.5 Experimental 73
2.5.1 Materials and general considerations 73
2.5.2 Successful syntheses of the linkers 73
2.5.3 Unsuccessful syntheses of the linkers 78
2.5.4 Reactions of the linkers with transition metal salts 82
3. References 85
4. Appendix 102
4.1 Appendix A: NMR spectra 102
4.2 Appendix B: crystallographic data 122
Structural information for 2 122
Structural information for 3 124

Structural information for 4 126

Structural information for 5 129

Structural information for 6 133

Structural information for 7 135

Structural information for 8 137

Structural information for 9 140

Structural information for 10 143

Structural information for 11 146

Structural information for 12 150

4.3 Mass spectral data 152

List of Figures **Page**

Figure 1: The general structure of an NHC, with arrows indicating both of the stabilizing effects from the adjacent nitrogen atoms (left) and the resonance hybrid of an NHC (right). R is typically a large, sterically hindered moiety, but substituents as small as methyl groups have also been used in NHC-metal complexes.[7] 2

Figure 2: The structure of Arduengo's carbene.[6] Note the bulky adamantyl groups that shield the carbene. 3

Figure 3: The generation of an imidazolylidene NHC by deprotonation of an imidazolium cation. 3

Figure 4: Bonding and backbonding interactions in a transition metal-NHC complex (left) and a transition metal-phosphine complex (right).[12–14] 4

Figure 5: The two main strategies of ligand design for NHC complexes of first-row transition metals; NHC ligands with harder base tethers (left) and a chelating multi-NHC (right).[16,24,27] 6

Figure 6: The structures of the two target pincer ligands. 7

Figure 7: The structure of the copper(II)-NHC complex prepared by O'Hearn *et al.* (left)[35] and the nickel(II)-NHC complex prepared by Luo *et al.* (right).[30] 7

Figure 8: The ^{1}H NMR spectrum of **1** collected in DMSO-*d*6, with all peak assignments shown. Note that the peak near 3.5 is residual water. 9

Figure 9: The asymmetric unit of **2**. R = 0.0715. Further structural details are provided in Appendix B. 11

Figure 10: Two cation of **2**, showing the π-stacking between ligands. Anions, solvent molecules, and hydrogen atoms have been omitted for clarity. 12

Figure 11: The ^{1}H NMR spectrum of **2** collected in DMSO-*d*6, with all peak assignments shown. Note that the peak near 3.5 ppm is residual water. 13

Figure 12: The asymmetric unit of **3**. R = 0.0451. Further structural details are provided in Appendix B. 14

Figure 13: The ^{1}H NMR spectrum of **3** in CD_3OD, showing the broad, poorly-defined peaks expected of a paramagnetic complex. Note that the peak near 4.9 ppm is water. 15

Figure 14: The cation of **4**. Hydrogens have been omitted for clarity. Selected bond lengths and angles are shown. R = 0.0338. Further structural details are provided in Appendix B. 17

Figure 15: The ligands used by Roy *et al.* (left) and Nielsen *et al.* (right).[41,43] 18

Figure 16: The asymmetric unit of **5**. Hydrogens, anions, and solvent molecules have been omitted for clarity. R = 0.0298 for the cation. Note that only a dichlorocuprate(I) anion could be identified; another counterion was observed by X-ray crystallography but its structure could not be determined. Further structural details are provided in Appendix B..... 19

Figure 17: The asymmetric unit of **6**. R = 0.0214. Further structural details are provided in Appendix B. 21

Figure 18: The ^{1}H NMR spectrum of **6** in CD_3CN, with the broad, sloping peaks indicative of a paramagnetic species. The possible C2 protons of imidazolium cations are indicated by the red box. Note that the two large peaks are methanol in the sample..... 22

Figure 19: The complex prepared by Wang *et al*.[47] 22

Figure 20: The asymmetric unit of **7**. R = 0.0451. Further structural details are provided in Appendix B. 23

Figure 21: The ^{1}H NMR spectrum of **7** in CD_3OD. Note that the peak near 4.9 ppm is water.. 24

Figure 22: the asymmetric unit of **8**. Note the diethyl ether solvate in the bottom left. R = 0.0460. 25

Figure 23: The cation of **9**. Hydrogens, both chloride anions, and solvent molecules have been omitted for clarity. R = 0.2732. 27

Figure 24: The ^{1}H NMR spectrum of 9 in CD_3OD. 27

Figure 25: The ^{13}C NMR spectrum of **9** in CD_3OD. 28

Figure 26: The crystal structure of **10**, with notable bond lengths labelled. R = 0.0539. 29

Figure 27: The ^{1}H NMR spectrum of **10** in DMSO-d6, showing the very broad peaks expected of a paramagnetic complex. 30

Figure 28: The possible structure of a 1D coordination polymer based on **10**. Note that for this coordination polymer to form, it would require an additional source of chloride, such as sodium chloride. 31

Figure 29: The asymmetric unit of **11**. R = 0.0587. 32

Figure 30: The possible structure of a 1D coordination polymer based on **11**. Note that for this coordination polymer to form, it would require an additional source of chloride, such as sodium chloride. 33

Figure 31: The asymmetric unit of **12**. R = 0.0631. 33

Figure 32: The ^{1}H NMR spectra of **11** (top) and **12** (bottom) collected in CD_3OD. Note that the large peaks at the upfield end of the window are due to methanol. 34

Figure 33: The ^{13}C NMR spectrum of **11** and **12**. 35

Figure 34: Research articles published per year for the search "'Carbon dioxide' capture" in Web of Science. 48

Figure 35: A simple schematic of a metal-organic framework. Black bars represent organic linkers, red circles represent metal nodes, and the blue sphere represents a void space. 50

Figure 36: The two approaches to postsynthetic modification of MOFs. Reproduced with permission from ACS Publications (https://pubs.acs.org/doi/10.1021/acscentsci.0c00690).[73].... 51

Figure 37: The main routes used to prepare ionic MOFs. Reproduced with permission from Elsevier Science & Technology Journals.[81] Route A to anionic MOFs: the linker of a neutral MOF is functionalized with an anionic moiety. Route B to anionic MOFs: an anionic ligand is coordinated to the node of a neutral MOF. Route A to cationic MOFs: a neutral linker is used with a cationic node. Route B to cationic MOFs: a cationic linker is used with a cationic node. Route C to cationic MOFs: the linker of a neutral MOF is functionalized with a cationic moiety. Route D to cationic MOFs: anions coordinating to the nodes of a neutral MOF are removed and replaced with non-coordinating guest anions. 53

Figure 38: A basic diagram of an anion-pillared MOF. The red circles are metal nodes, the black bars are organic linkers, and the blue bars are anionic pillars. 54

Figure 39: The coordination mode of a hexafluorosilicate pillar in a pillared ionic metal organic framework. L is the organic linker, M is the metal node. Note that formal charges have been excluded. 55

Figure 40: The interaction between a SIFSIX pillar and a guest carbon dioxide molecule. 56

Figure 41: The structures of the four target linkers in this work. 56

Figure 42: The environment around a node (M) of a hypothetical SIFSIX-pillared MOF with **13** as the linker. This is not a depiction of a repeating unit. Note that some formal charges and counterions have been excluded. 57

Figure 43: The ^{1}H NMR spectrum of an aliquot of the reaction between sodium hydride, sodium imidazolate, and 4-(chloromethyl)pyridine hydrochloride. Note the small peak near 9.8 ppm

indicating formation of **13**, along with 3 peaks between 4.6 and 5.6 ppm indicating three different sets of benzylic protons..... 60

Figure 44: The structure of the intermediate observed in the reaction mixture..... 61

Figure 45: The ^{1}H NMR spectra of 4-(chloromethyl)pyridine (top) and 4-(chloromethyl)pyridine *N*-oxide (bottom), indicating that the oxidation in question has gone to completion..... 62

Figure 46: The ^{1}H NMR spectrum of the reaction mixture of imidazole and 4-(chloromethyl)pyridine *N*-oxide. Note the lack of peaks above 9 ppm..... 63

Figure 47: Possible sites of nucleophilic attack on an alkyl-protected 4-(chloromethyl)pyridine. R = H, C_6H_5. 64

Figure 48: The ^{1}H NMR spectrum of the reaction mixture from the methylation of 4-(chloromethyl)pyridine with iodomethane. Note the many small peaks in the aromatic region indicating the formation of a mix of (likely polymeric) products. 64

Figure 49: the ^{1}H NMR spectrum and proposed structure of the precipitate formed from the reaction of glyoxal and two equivalents of 4-(aminomethyl)pyridine in water. 65

Figure 50: ^{1}H NMR spectrum of the crude reaction mixture containing **15** and a major by-product. Select peaks corresponding to the benzimidazolium and pyridinium salts are indicated. Note that the pyridinium salt shown is a proposed structure of the by-product. 68

Figure 51: A SEM image of the brown precipitate collected from the reaction of **13** and $NiSiF_6 \cdot 6H_2O$ (left) and an EDX spectrum of the same material (right). 70

List of Schemes **Page**

Scheme 1: The reaction conditions used to prepare **1**. 8

Scheme 2: The optimal conditions for the preparation of **2**. The reaction was heated to reflux for 5 days. 10

Scheme 3: The species isolated from the reaction of 1,3-bis(2-pyridylmethyl)imidazolium chloride with copper(II) acetate monohydrate, in the order that they are isolated. Anions and solvent molecules have been omitted. 14

Scheme 4: The synthesis of nickel(II) complex **6** from ligand **1** and nickel(II) chloride hexahydrate. 20

Scheme 5: The synthesis of complex **7** from **2** and copper(II) acetate monohydrate. 23

Scheme 6: The synthesis of complexes **8** and **9** from **2** and nickel(II) acetate tetrahydrate. 25

Scheme 7: The synthesis of the cation of **9** used by Luo *et al*.[30] 26

Scheme 8: The synthesis of **10** from ligand **2** and copper(II) chloride dihydrate. 29

Scheme 9: The synthesis of **11** and **12** from ligand **2** and nickel(II) chloride hexahydrate. 31

Scheme 10: The reaction and competitive side reaction in the most obvious route to the linkers. 58

Scheme 11: The expected pathway of the reaction to produce the target linkers. Note that **13** is being used as an example structure. 66

Scheme 12: The general reaction conditions used to produce the 1-(pyridylmethyl)imidazoles **17** – **20**, precursors to the target ligands **13 – 16**. 66

Scheme 13: The general reaction conditions used to prepare the target ligands **13** – **16**. Only **13** and **14** were isolated, although the formation of **15** and **16** was observed by NMR. 67

Scheme 14: The proposed synthesis of **15** and **16** by ring building. 71

Scheme 15: The structure and proposed synthesis of a rigid linker with neutral donating sites.. 72

List of tables **Page**

Table 1: The conditions explored for the synthesis of **13**. 58

Table 2: The reaction conditions between **13** or **14** and metal cations in an effort to prepare a MOF. 68

List of symbols and abbreviations

NHCs: *N*-heterocyclic carbenes

NMR: nuclear magnetic resonance

IR: infrared

DMSO: dimethylsulfoxide

THF: tetrahydrofuran

Å: angstrom (10^{-10} cm)

1D: one-dimensional

CO_2: carbon dioxide

FT-IR: Fourier transfrom infrared spectroscopy

ATR: attenuated total reflection

ESI-MS: electrospray ionization mass spectrometry

HRMS: high-resolution mass spectrometry

MOF: metal-organic framework

3D: three-dimensional

SIFSIX: hexafluorosilicate

2D: two-dimensional

DMF: *N*,*N*-dimethylformamide

MMPP: magnesium monoperoxyphthalate

$CDCl_3$: chloroform-d

DCM: dichloromethane

SEM: scanning electron microscopy

EDX: energy-dispersive X-ray

1. Synthesis of novel first-row transition metal-*N*-heterocyclic carbene complexes

1.1 Introduction

1.1.1 Transition metals in catalysis

Transition metal catalysis is an essential component of the synthesis of a variety of economically and societally important materials.[1] In particular, second- and third-row transition metals have been used to catalyse a wide variety of extremely powerful reactions, perhaps most notably palladium-catalysed carbon-carbon cross-coupling reactions.[2] Although second- and third-row transition metals catalyse a wide variety of very useful reactions, they are typically expensive, toxic, and low abundance.[3] As a result, extensive work has been directed toward finding alternatives. For the most part, organocatalysis does not share the limitations of transition metal catalysis and is therefore one alternative. However, organocatalysts are often less efficient and require higher catalyst loading than transition metal catalysts; thus they are often not economically viable.[1] The other option is catalysis with first-row transition metals, which provide the benefits of transition metal catalysis but are more abundant and not as toxic as heavier transition metals.[3] As such, significant work has also been directed to finding suitable complexes of first-row transition metals to catalyse reactions that have historically been catalysed by heavier metals.[3] One major challenge in adapting first-row transition metals to catalysing these reactions is that most first-row transition metals have fewer readily available oxidation states available, and thus tend to react by one-electron pathways; heavier transition metals with more accessible oxidation states tend to react by two-electron processes.[3,4] Nonetheless, a variety of first-row transition metal catalysts have been designed for reactions typically catalysed by 2nd and 3rd-row transition metals.

1.1.2 *N*-heterocyclic carbenes

1.1.2.1 Structure and synthesis of *N*-heterocyclic carbenes

N-heterocyclic carbenes (NHCs) are an unusually stable class of carbenes in which the carbenic carbon is stabilized by the presence of adjacent nitrogen atoms (Figure 1).[5] The carbenic carbon is thought to exist in a singlet state with a vacant P orbital and a lone pair of electrons. The adjacent nitrogen atoms stabilise the carbene by mesomerically donating electron density into the vacant orbital and inductively withdrawing electron density from the lone pair of electrons. These stabilizing effects mean that NHCs are a rare example of a class of carbenes that can sometimes be isolated, but sterically hindered substituents are often necessary for an NHC to be isolable, as they help to shield the NHC.[6] For example, Arduengo *et al.* isolated the first example of a stable carbene from the 1,3-bis(1-adamantyl)imidazolium cation in 1991 (Figure 2).[6]

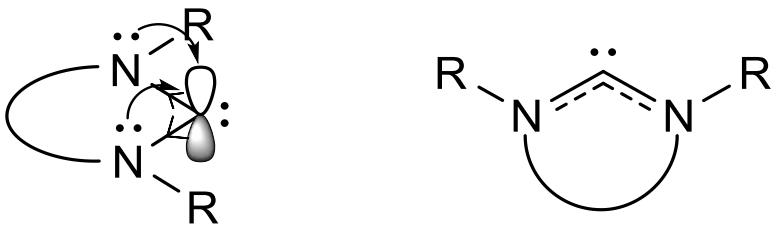

Figure 1: The general structure of an NHC, with arrows indicating both of the stabilizing effects from the adjacent nitrogen atoms (left) and the resonance hybrid of an NHC (right). R is typically a large, sterically hindered moiety, but substituents as small as methyl groups have also been used in NHC-metal complexes.[7]

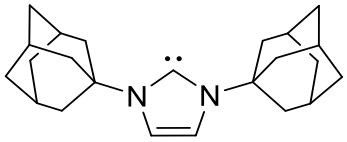

Figure 2: The structure of Arduengo's carbene.[6] Note the bulky adamantyl groups that shield the carbene.

NHCs are typically prepared from deprotonation of the corresponding azolium cation, as shown in Figure 3.[8] The most common azolium cations used in the preparation of NHCs are imidazolium and imidazolinium cations, but a wide range of cations have been explored.[8] The R groups of NHCs can also be varied, allowing the sterics and electronics of the molecule to be tuned; this, in turn, controls the reactivity.[8,9] For example, an NHC with smaller R groups will typically be more reactive, as the carbene is more accessible.

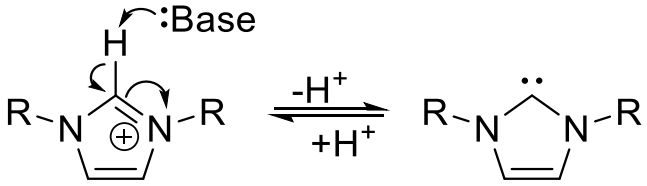

Figure 3: The generation of an imidazolylidene NHC by deprotonation of an imidazolium cation.

1.1.2.2 Synthesis and catalytic activity of transition metal *N*-heterocyclic carbene complexes

The first example of an NHC-transition metal complex was a mercury(II) complex prepared in 1968, yet NHCs were still considered too unstable to see widespread use.[10] NHCs only began garnering attention as potential ligands after Arduengo *et al*. isolated a free carbene in 1991,[6] and even more so after Herrmann *et al*. demonstrated that a bis(NHC)palladium(II) complex was a very effective catalyst for the Heck reaction.[7] Since then, NHCs have gradually supplanted

phosphines as the ligands of choice in catalysis with noble metal complexes. This is unsurprising as both NHCs and phosphines are strongly σ-donating and weakly π-accepting ligands and both are soft bases.[8,11] NHCs are able to undergo backbonding to the P orbital of the carbenic carbon, while phosphines undergo backbonding to P-C antibonding orbitals (Figure 4).[8,11–14] However, NHCs are even more strongly electron-donating than phosphines. This was demonstrated by Nolan *et al.* by coordination of a series of NHCs and phosphines to tetracarbonylnickel(0) and observation of the carbonyl stretch.[15]

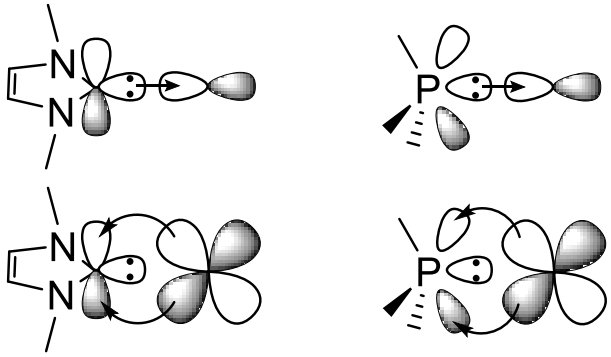

Figure 4: Bonding and backbonding interactions in a transition metal-NHC complex (left) and a transition metal-phosphine complex (right).[12–14]

Because NHCs are so strongly electron-donating, they are useful in catalysis as they help to stabilize high-energy intermediates that sometimes form in catalytic cycles and can reduce decomposition of the catalyst.[5,11] NHCs can also allow the isolation of highly electron-deficient species – an air-stable copper(III) complex, for example.[16]

1.1.2.3 *N*-heterocyclic carbene-first-row transition metal complexes

Catalysts are of immense industrial and economic importance.[3] The majority of catalysts are based on noble metals which are low in abundance and expensive.[3] Hence, significant work has

been directed to finding first-row transition metal complexes that can catalyse reactions that have previously only been performed using noble metal catalysts, as first-row transition metals are generally cheaper and more abundant.[3,17,18]

NHCs are soft bases so they typically do not coordinate well to hard or intermediate first-row transition metals due to the unfavourable hard-soft acid-base pairing. There are a few exceptions in which a monodentate NHC ligand has been coordinated to a first-row transition metal – notably nickel(0)[15] and copper(I)[19–21] – but these are softer than most other first-row transition metals. Because of the widespread use of NHCs in catalysis with noble metals, significant work as been directed to preparing NHC complexes with first-row transition metals in order to enhance their catalytic abilities. Two main strategies have been developed to prepare stable NHC-first-row transition metal complexes. The first strategy is to incorporate a hard base into the NHC-containing ligand, as shown in Figure 5; the hard base acts as a tether, keeping the NHC close to the metal centre.[22–25] Anionic tethers – such as aryloxides – are typically used with early transition metals,[22,23,26,27] while neutral tethers such as pyridines are often used with late transition metals.[24,25,28–32] The second strategy involves taking advantage of the chelate effect by incorporating multiple NHCs into a single ligand (Figure 5).[16,33] Often both strategies are used together. Using a tether is by its nature taking advantage of the chelate effect, and many ligands incorporate multiple NHCs and hard bases.[17,24,32]

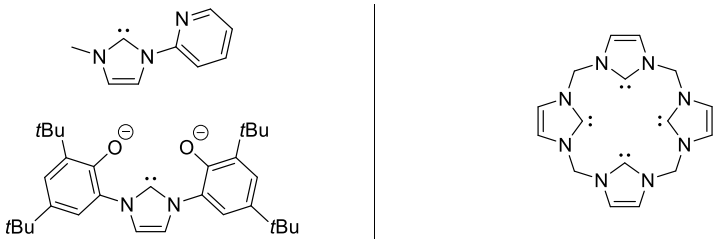

Figure 5: The two main strategies of ligand design for NHC complexes of first-row transition metals; NHC ligands with harder base tethers (left) and a chelating multi-NHC (right).[16,24,27]

At this point the majority of work with NHC-first-row transition metal complexes is simply exploring the synthesis of these complexes. The cases in which catalytic activity of the prepared complexes has been explored have, for the most part, been promising.[17,27,28,32] This is likely due to the strong electron donation from NHCs, which helps to stabilize high oxidation state intermediates and allow first-row transition metals to more readily undergo 2-electron transfer processes.[34] For example, a copper(II) complex with a tetradentate ligand containing two NHCs and two pyridines proved to be an effective catalyst for the Chan-Evans-Lam reaction.[32] This reaction is typically catalysed by copper(II) species, but can sometimes require high catalyst loadings; the prepared catalyst was effective at lower loadings.[32] Zhou *et al*. found that a bimetallic nickel(II)-NHC complex was an effective catalyst for Suzuki-Miyaura and Kumada-Corriu cross-coupling reactions, both of which are normally catalysed by palladium complexes.[17] This highlights the potential use of NHCs in first-row transition metal catalysis.

1.1.3 Target ligands and research questions

The desired ligands for this work are both pincer ligands, with two pendant pyridine arms attached to a central imidazolium cation that can give rise to an NHC (Figure 6).

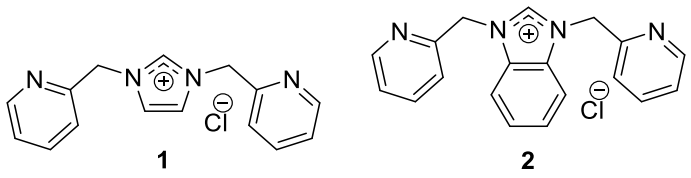

Figure 6: The structures of the two target pincer ligands.

Because each of these ligands has two pyridines to act as tethers, they are expected to be able to complex to some first-row transition metals, mainly copper and nickel.[24,30,31,35] In particular, some previous work with ligand **1** demonstrated that it reacts with copper(II) hexafluorosilicate to generate an air and moisture-stable copper(II)-NHC complex (Figure 7),[35] and previous work with **2** found that it could coordinate to nickel(II) in a 2:1 ratio of ligand to metal.[30]

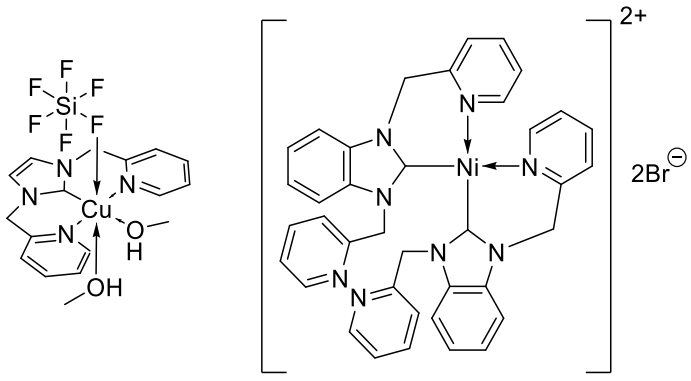

Figure 7: The structure of the copper(II)-NHC complex prepared by O'Hearn *et al.* (left)[35] and the nickel(II)-NHC complex prepared by Luo *et al.* (right).[30]

However, the ligands may not always saturate the metal centre, allowing other ligands to bind and potentially allowing the complexes to be catalytically active. Thus, the coordination of these ligands to first-row transition metals is worthy of further exploration. Specifically, it was expected

that the anion associated with the metal cation could affect the structure of the metal complexes. To this end, a series of eight reactions were planned, fulfilling every combination of imidazolium or benzimidazolium-based pincer ligand, nickel(II) or copper(II) cation, and chloride or acetate anion.

1.2 Results and discussion

1.2.1 Synthesis and characterisation of the ligands

Both pincer ligands were prepared based on literature procedures that add both pyridine arms in a single step, with slight modifications to the workup of 1,3-bis(2-pyridylmethyl)imidazolium chloride (**1**) and the synthesis and workup of 1,3-bis(2-pyridylmethyl)benzimidazolium chloride (**2**).[9,35–37]

1 was synthesized by heating an ethanolic solution at reflux of imidazole, two equivalents of 2-(chloromethyl)pyridine hydrochloride, and excess sodium carbonate for 72 hours (Scheme 1). The product was worked up by first removing sodium carbonate, bicarbonate, and chloride by gravity filtration, followed by precipitation of the product with diethyl ether to afford **1** in 70% yield.

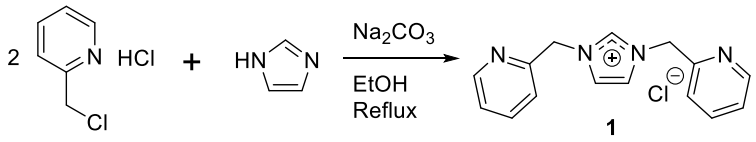

Scheme 1: The reaction conditions used to prepare **1**.

After the reaction, nuclear magnetic resonance (NMR) and infrared (IR) spectra of **1** were recorded and compared to literature reports.[35,37–39] The ^{1}H NMR spectrum of **1** is shown in Figure 8.

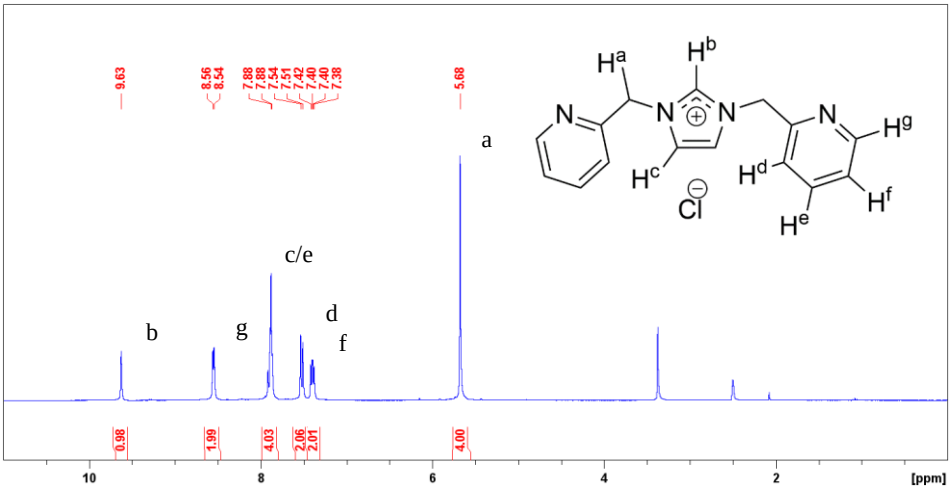

Figure 8: The ^{1}H NMR spectrum of **1** collected in DMSO-*d*6, with all peak assignments shown. Note that the peak near 3.5 is residual water.

There are several notable features in the ^{1}H NMR spectrum of **1**. The first is the singlet at 9.63 ppm. This peak is due to the C2 proton (proton b) of the imidazolium ring, and is highly diagnostic of imidazolium cations; very few other functional groups give sharp peaks in this region of the ^{1}H NMR spectrum. The chemical shift of this peak also correlates to the acidity, or lack of electron density, of that proton. The next feature of note is the multiplicity of the peaks corresponding to the hydrogen atoms of the 2-substituted pyridine rings; these split into two doublets and two doublets of doublets. Although one peak overlaps with the C4/C5 protons of the imidazolium ring (proton c) the splitting pattern is still recognizable. Finally, the benzylic protons (peak a) appear as a singlet in an otherwise empty region of the spectrum, and integrate to 4 relative to the C2 proton; this peak – and the region around it – can indicate the presence of impurities in the sample, as the major by-product of this reaction also has benzylic protons that appear in the same region of the spectrum or overlap the benzylic proton peak in the product. Thus, the ratio of the C2 proton

peak to the benzylic proton peak – as well as the presence or absence of other peaks near the benzylic proton peak – is a good measure of the purity of the sample.

2 was prepared slightly differently. It was found that using an exact 2:1 ratio of benzimidazole to 2-(chloromethyl)pyridine hydrochloride led to the formation of an impurity, likely poly(2-methylpyridinium chloride), which could not be readily separated from the desired product. However, it was found that reducing the amount of 2-(chloromethyl)pyridine hydrochloride suppressed formation of this impurity, at the expense of yield. The conditions shown in **Scheme 2** were found to be optimal.

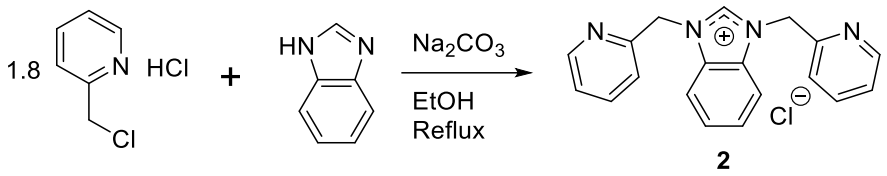

Scheme 2: The optimal conditions for the preparation of **2**. The reaction was heated to reflux for 5 days.

After the reaction was complete, sodium carbonate, bicarbonate, and chloride were removed by gravity filtration and the solvent was removed by rotary evaporation. The resulting brown oil was taken up in dichloromethane and filtered again to remove any residual sodium carbonate, bicarbonate, and chloride. **2** was recrystallized by vapour diffusion of diethyl ether into the dichloromethane solution in typical yields of 30-40%. It could also be recrystallized by vapour diffusion of diethyl ether into a methanolic solution in lower yield; the asymmetric unit of **2** is shown in Figure 9. Interestingly, when the brown oil obtained from rotary evaporation was triturated with THF the product precipitated as a light brown solid. Unfortunately, this workup could not be further developed due to time constraints.

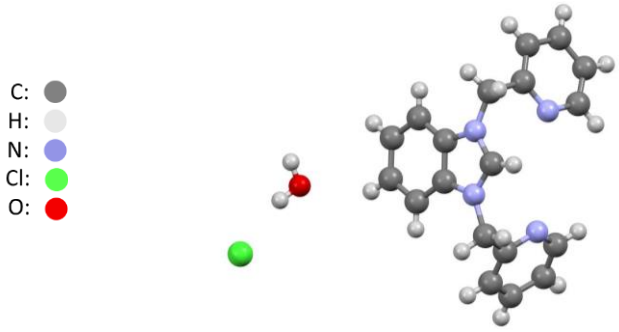

Figure 9: The asymmetric unit of **2**. R = 0.0715. Further structural details are provided in Appendix B.

Interestingly, the compound crystallised as a hydrate. This is likely because it was recrystallised from wet solvents in humid conditions. It could be dehydrated by heating, vacuum, or azeotropic distillation in toluene. There is also literature precedent for metathesizing the cation of **2** to a hexafluorophosphate, which is anticipated to make the compound more hydrophobic.[40] This ligand crystallizes in molecular pairs, as shown in Figure 10. The benzimidazolium cores undergo π-stacking with a distance between the planes of the two benzimidazolium cores of approximately 3.5Å. The two benzimidazolium cores also lie antiparallel to each other; the imidazolium end of one lies above the phenyl end of the other. This packing arrangement is a common feature in many of the transition metal complexes of **2** that were isolated in this work.

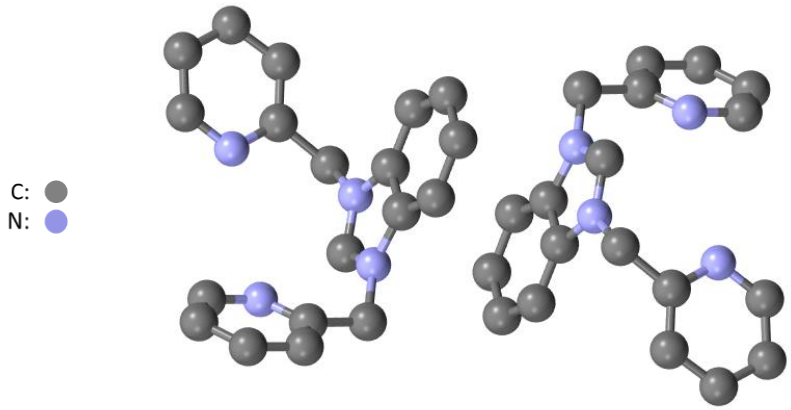

Figure 10: Two cation of **2**, showing the π-stacking between ligands. Anions, solvent molecules, and hydrogen atoms have been omitted for clarity.

The NMR and IR spectra of **2** were collected and are in good agreement with literature data.[9,36] The ^{1}H NMR spectrum is shown in Figure 11. This NMR spectrum shares many of the same features as the ^{1}H NMR spectrum of **1**, most notably the benzylic proton peak (proton a) and the C2 proton peak (peak b). The C2 proton peak is 0.8 ppm further downfield in **2** than in **1**, indicating that it is less electron-dense and may be more acidic. The 2-substituted pyridine splitting pattern is also more apparent in this compound than in **1**. Protons c and d were assigned using ^{1}H-^{13}C HMBC and ^{1}H-^{1}H COSY NMR spectra.

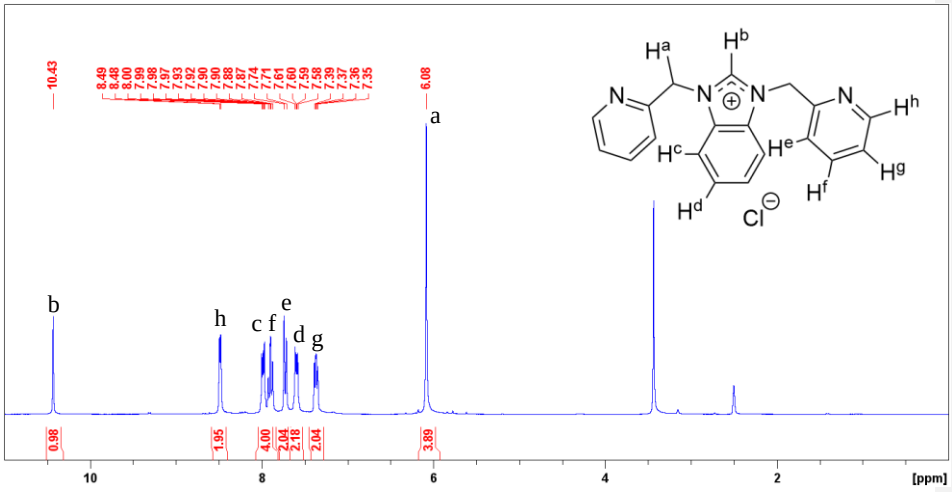

Figure 11: The ^{1}H NMR spectrum of **2** collected in DMSO-*d*6, with all peak assignments shown. Note that the peak near 3.5 ppm is residual water.

1.2.2 Metal complexes of the pincer ligands (1) and (2)

1.2.2.1 Reaction of 1,3-bis(2-pyridylmethyl)imidazolium chloride and copper(II) acetate monohydrate

The reaction of 1,3-bis(2-pyridylmethyl)imidazolium chloride with one equivalent of copper(II) acetate monohydrate performed in methanol with no effort to exclude air or moisture affords several different isolable species (**Scheme 3**). These species can be recrystallized from a single reaction at different times using a variety of conditions; this suggests that the reaction may progress through several isolable intermediates before arriving at the trimeric copper(I) cluster **5**.

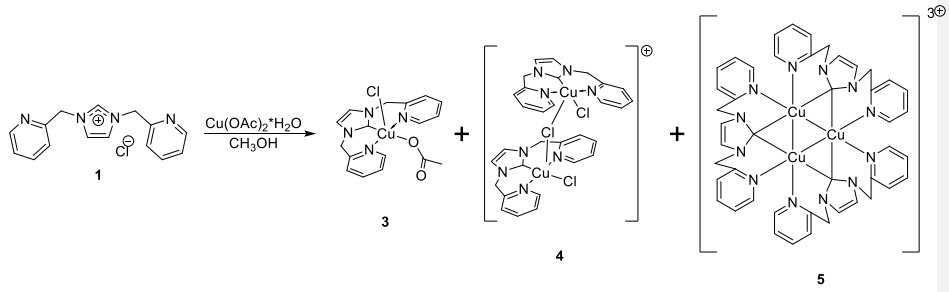

Scheme 3: The species isolated from the reaction of 1,3-bis(2-pyridylmethyl)imidazolium chloride with copper(II) acetate monohydrate, in the order that they are isolated. Anions and solvent molecules have been omitted.

3 was isolated as a dark blue crystalline solid by vapour diffusion of diethyl ether into an aliquot of the reaction mixture after 24 hours. The asymmetric unit is shown in Figure 12.

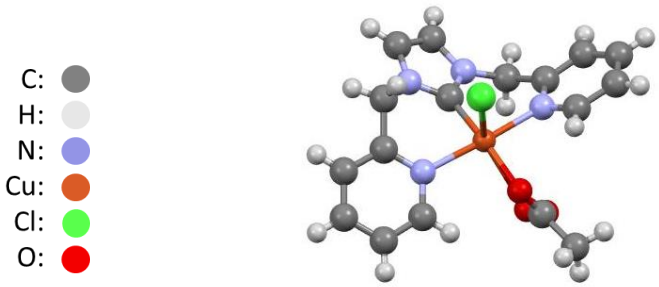

Figure 12: The asymmetric unit of **3**. R = 0.0451. Further structural details are provided in Appendix B.

The Cu-Cl bond length in **3** is 2.605Å. This is longer than is typical for a copper-chlorine bond, indicating a Jahn-Teller distortion; this effect is characterized by a lengthening or shortening of the axial bonds in a transition metal complex, and has been observed in other complexes of copper(II) with a tridentate pincer ligand and axial chloride ligand.[41] The Cu-O distances to the

two oxygen atoms of the acetate anion are different; the oxygen atoms aligned to the equatorial position is 1.975Å, while the other Cu-O distance is 2.728Å. This may indicate that the acetate anion is coordinating as a monodentate ligand, and the copper(II) centre is in a square pyramidal geometry.

Copper(II) has an odd number of electrons and is expected to be paramagnetic. The ^{1}H NMR spectrum of **3** shows the broad, poorly-resolved peaks that one would expect of a paramagnetic complex (Figure 13). Notably, there is no visible peak in the range where C2 protons of imidazolium cations typically appear; this suggests that the complex exists as a NHC in solution as well as the solid state.

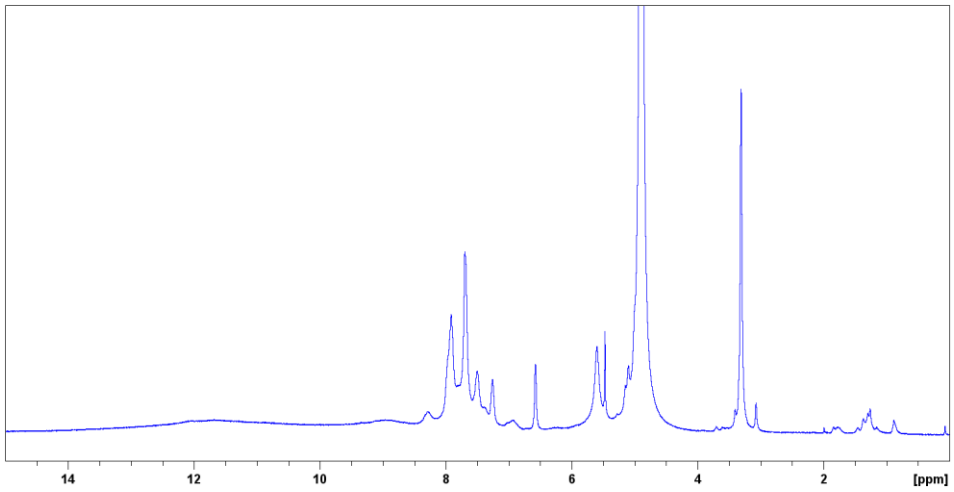

Figure 13: The ^{1}H NMR spectrum of **3** in CD_3OD, showing the broad, poorly-defined peaks expected of a paramagnetic complex. Note that the peak near 4.9 ppm is water.

Given that **3** has two labile ligands – the chloride and acetate anions – it could be applicable as a precatalyst. Copper(II)-NHC complexes have been used as catalysts in Chan-Evans-Lam couplings[32] and Ullmann-type etherifications.[42] Notably, both reactions are thought to involve a

formal copper(III) intermediate, which is likely stabilized by the strongly electron-donating NHC ligand.

The coordination mode of the ligand is the same as in the species prepared by O'Hearn and Singer (Figure 7).[35] This is unsurprising, as the procedure used to prepare it is similar. However, the copper(II) NHC complex isolated by O'Hearn and Singer was not observed to rearrange to species analogous to **4** and **5**.

Complex **4** was recrystallized by vapour diffusion of diethyl ether into an aliquot of the reaction mixture after one week (Figure 14). Although a crystal structure was determined, the amount of material isolated was insufficient for full characterization to be completed. Complex **4** is similar to some previously prepared complexes of copper(II) with tridentate pincer ligands and bridging chlorides.[41,43] The anion in **4** is a dichlorocuprate(I). At this stage some copper has been reduced from the +2 oxidation state to +1. The source of electrons for this reduction has not been determined; it is possible that methanol is the reducing agent. Although this complex could be catalytically active in similar processes to **3**, it seems to be less stable.

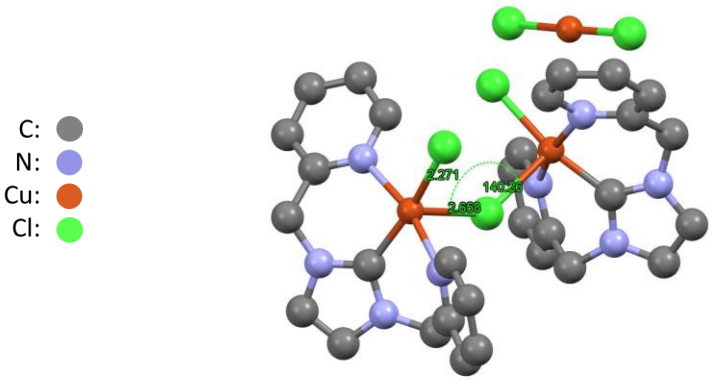

Figure 14: The cation of **4**. Hydrogens have been omitted for clarity. Selected bond lengths and angles are shown. R = 0.0338. Further structural details are provided in Appendix B.

Like **3**, the two copper(II) centres in **4** have a square pyramidal geometry. The axial Cu-Cl bond length is much longer than the equatorial Cu-Cl bond length (2.658Å and 2.271Å respectively). This is indicative of a Jahn-Teller distortion. The Cu-Cl-Cu bond angle of 140.28° is similar to that of the complexes prepared by Nielsen *et al.* using a bis(2-pyridylmethyl)amine ligand, as opposed to the work of Roy *et al.* which found bond angles of 180°.[41,43] Notably, the ligand used by Roy *et al.* was entirely planar, but the ligand used by Nielsen *et al.* was not; it had sp^3-hybridized carbons that introduced a slight torsion to the structure, similar to **1** (Figure 15).[41,43] The other structures observed by Roy *et al.* and Nielsen *et al.* were not observed in this work, nor did they describe complexes analogous to **5**.

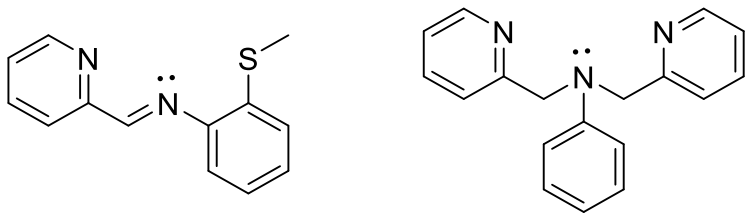

Figure 15: The ligands used by Roy *et al.* (left) and Nielsen *et al.* (right).[41,43]

5 was recrystallized by vapour diffusion of diethyl ether into methanol after approximately one month (Figure 16). Like **4**, the amount of material isolated was not sufficient for characterization beyond X-ray crystallography. The anions observed by X-ray crystallography appear to be dichlorocuprate(I) and trichlorocuprate(I); the dichlorocuprate(I) anion was also observed by ESI-MS, but the other counterion has not been adequately identified. Although such clusters are known, they are typically prepared by treating the NHC precursor imidazolium cation with copper(I) oxide.[40] This synthesis seems to be the first example of the preparation of this cation *via* a copper(II)-NHC complex. The reducing agent for this reduction has not been determined.

Previous work with this cationic cluster found that it is a good NHC transfer reagent for the synthesis of other NHC complexes, and is intensely luminescent. [40,44,45] However, its catalytic abilities appear not to have been evaluated.

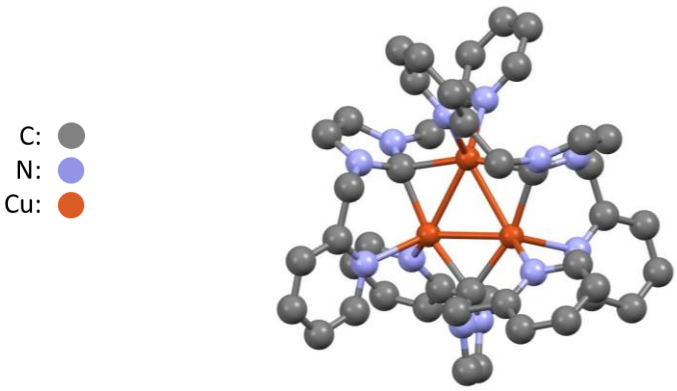

Figure 16: The asymmetric unit of **5**. Hydrogens, anions, and solvent molecules have been omitted for clarity. R = 0.0298 for the cation. Note that only a dichlorocuprate(I) anion could be identified; another counterion was observed by X-ray crystallography but its structure could not be determined. Further structural details are provided in Appendix B.

Interestingly, the NHC ligands in this complex appear to be bridging between the copper(I) atoms. This is unusual and merits further study of the orbital geometry by computational methods. It is possible that the NHC is in a triplet state, however, this is unlikely as triplet carbenes are not stabilized by adjacent nitrogen atoms, so NHCs are thought to exist in the singlet state. It is also possible that this is a 3-coordinate 2-electron bond, as is sometimes observed with bridging hydrides and alkyl anions, as was suggested by Díez-González *et al*.[46] Notably, no computationam

1.2.2.2 Reaction of 1,3-bis(2-pyridylmethyl)imidazolium chloride and nickel(II) acetate tetrahydrate

The reaction of equimolar 1,3-bis(2-pyridylmethyl)imidazolium chloride and nickel(II) acetate tetrahydrate was performed in methanol with no effort to exclude air or moisture. An amorphous, intractable brown solid was produced. No characterizable product was isolated.

1.2.2.3 Reaction of 1,3-bis(2-pyridylmethyl)imidazolium chloride and copper(II) chloride dihydrate

The reaction of equimolar 1,3-bis(2-pyridylmethyl)imidazolium chloride and copper(II) chloride dihydrate was performed in methanol with no effort to exclude air or moisture. An amorphous, intractable brown solid was produced. No characterizable product was isolated.

1.2.2.4 Reaction of 1,3-bis(2-pyridylmethyl)imidazolium chloride and nickel (II) chloride hexahydrate

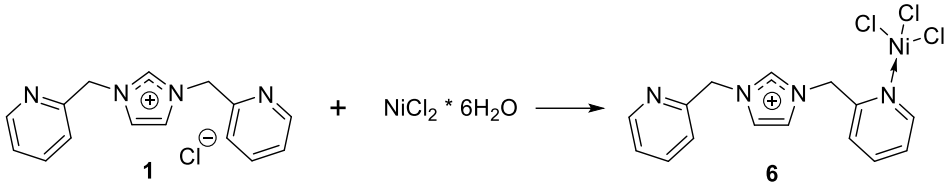

Scheme 4: The synthesis of nickel(II) complex **6** from ligand **1** and nickel(II) chloride hexahydrate.

The reaction of 1,3-bis(2-pyridylmethyl)imidazolium chloride and nickel(II) chloride hexahydrate was performed in methanol with no effort to exclude air or moisture. Nickel(II) complex **6** was isolated as light blue blocky crystals from the vapour diffusion of diethyl ether into acetonitrile or methanol (Figure 17).

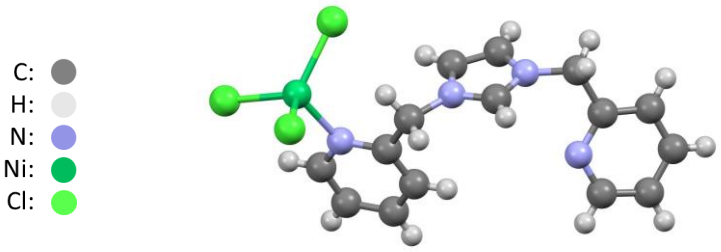

Figure 17: The asymmetric unit of **6**. R = 0.0214. Further structural details are provided in Appendix B.

This structure exhibits a different coordination mode for ligand **1**. It is possible that this is a result of the presence of chloride anions, as analogous coordination modes have been observed from the reaction of 1,3-bis(2-pyridylmethyl)benzimidazolium chloride with nickel(II) chloride hexahydrate or copper(II) chloride dihydrate, but not nickel(II) acetate tetrahydrate or copper(II) acetate monohydrate. Treatment with a base may allow this structure to convert to a nickel(II)-NHC complex, but this was not explored in this work due to time constraints.

The ^{1}H NMR spectrum of this complex suggests that it is paramagnetic (Figure 18). This makes sense, as a tetrahedral 16-electron complex should have 2 unpaired electrons based on the expected d-orbital splitting. Interestingly, there are two peaks in the region of C2 protons of imidazolium cations; this may indicate the existence of two different structures in solution.

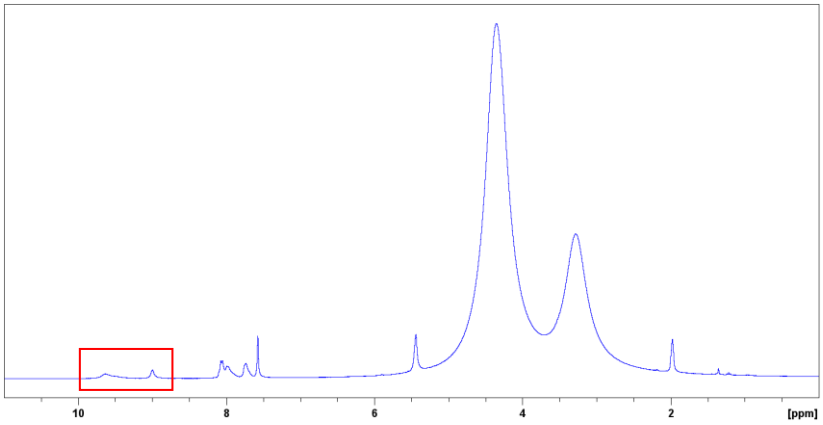

Figure 18: The ^{1}H NMR spectrum of **6** in CD_3CN, with the broad, sloping peaks indicative of a paramagnetic species. The possible C2 protons of imidazolium cations are indicated by the red box. Note that the two large peaks are methanol in the sample.

A similar nickel(II) complex was prepared by Wang *et al.* from an imidazolium ligand with one picolyl arm and one imidazolium arm, who found that it catalysed ethylene polymerization following activation with methylaluminoxane (Figure 19).[47] The effect of having a second, non-coordinating pyridine on the catalytic activity of this ligand is worth examination, especially given the findings of Luo *et al.* who found that a non-coordinating pendant pyridine improved the activity of a nickel(II)-based electrocatalyst for hydrogen reduction, likely by recruiting protons to the metal centre.[30]

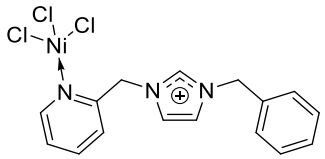

Figure 19: The complex prepared by Wang *et al.*[47]

1.2.2.5 Reaction of 1,3-bis(2-pyridylmethyl)benzimidazolium chloride and copper(II) acetate monohydrate

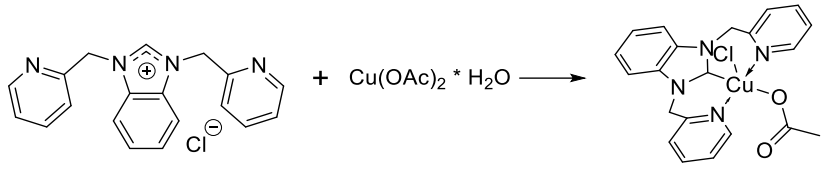

2 **7**

Scheme 5: The synthesis of complex **7** from **2** and copper(II) acetate monohydrate.

The reaction of 1,3-bis(2-pyridylmethyl)benzimidazolium chloride with copper(II) acetate monohydrate was performed in methanol with no effort to exclude air or moisture. Dark blue crystals of **7** were isolated by vapour diffusion of diethyl ether into methanol (Figure 20).

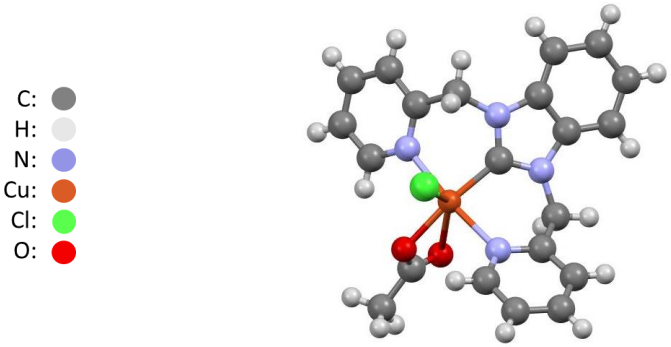

Figure 20: The asymmetric unit of **7**. R = 0.0451. Further structural details are provided in Appendix B.

This is a second example of a copper(II)-NHC complex, and is extremely similar to **3**. As such, it is expected that this species can undergo the same series of rearrangements as **3**, however this has yet to be determined. Notably, a trinuclear cluster analogous to **5** is known for ligand **2**.[40]

The ^{1}H NMR spectrum of **7** suggests that the material is not pure (Figure 21). This could be due to further reaction; **7** is analogous to **3**, and it has been shown that **3** undergoes further reaction to several other products. Copper(II) also has an odd number of electrons, so it is expected that **7** is paramagnetic; this also helps to explain the somewhat broad, oddly-shaped peaks in the ^{1}H NMR spectrum.

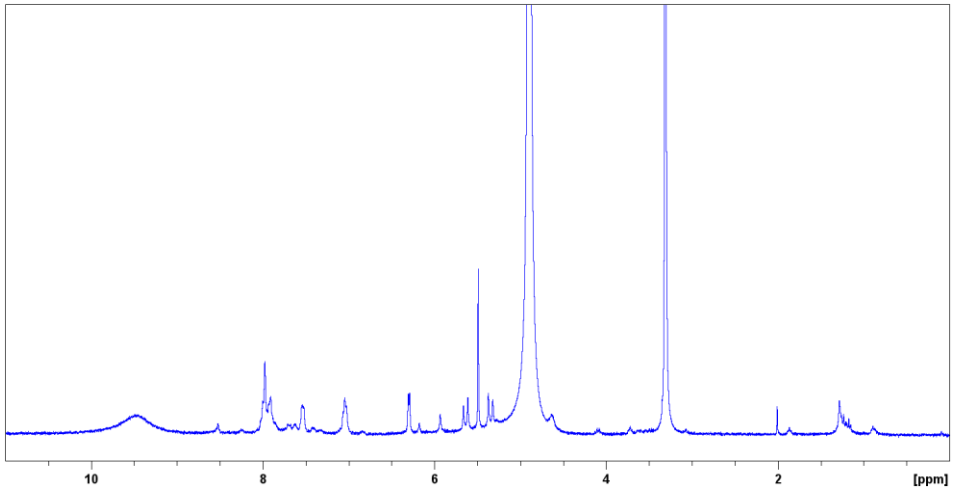

Figure 21: The ^{1}H NMR spectrum of **7** in CD_3OD. Note that the peak near 4.9 ppm is water.

1.2.2.6 Reaction of 1,3-bis(2-pyridylmethyl)benzimidazolium chloride and nickel(II) acetate tetrahydrate

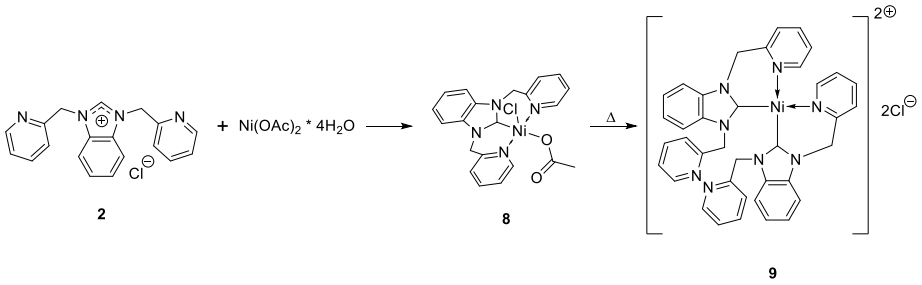

Scheme 6: The synthesis of complexes **8** and **9** from **2** and nickel(II) acetate tetrahydrate.

The reaction of 1,3-bis(2-pyridylmethyl)benzimidazolium chloride with nickel(II) acetate tetrahydrate was performed in methanol with no effort to exclude air or moisture. Blue crystals of **8** were isolated by vapour diffusion of diethyl ether into methanol (Figure 22). It crystallized as a diethyl ether solvate.

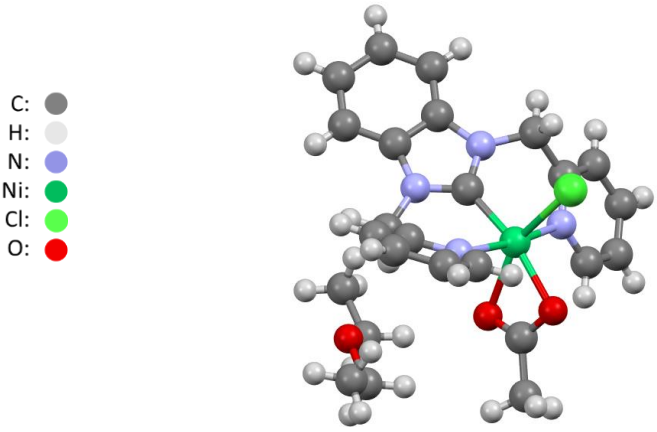

Figure 22: the asymmetric unit of **8**. Note the diethyl ether solvate in the bottom left. R = 0.0460.

This is the first example of a nickel(II)-NHC complex in this work. Such complexes are known, but are uncommon.[17,24,25,30,40] Previous examples have mostly been prepared through transmetallation from Ag(I) complexes or oxidation of Raney nickel in air, with the NHC as a proton source. One previous example used a weak base route similar to this work, but only **9** was isolated (**Scheme 7**).[30]

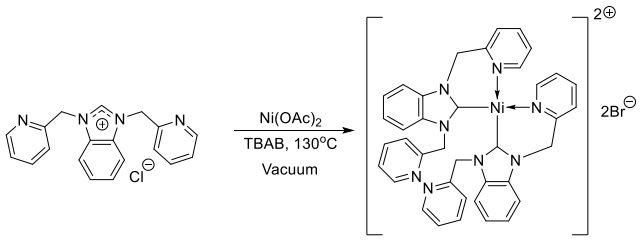

Scheme 7: The synthesis of the cation of **9** used by Luo *et al*.[30]

Heating of **8** provided **9**, which was recrystallized as yellow needles by vapour diffusion of diethyl ether into methanol (Figure 23). This structure has not been fully refined, as is evident from the high R value. It is therefore possible that the shown structure is not entirely accurate; however, the cation was also observed by mass spectrometry.

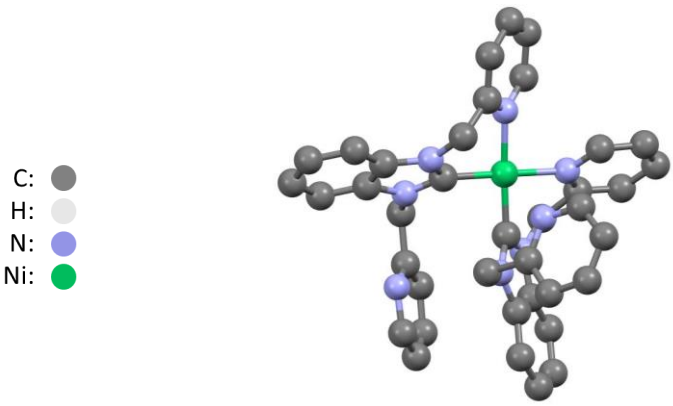

Figure 23: The cation of **9**. Hydrogens, both chloride anions, and solvent molecules have been omitted for clarity. R = 0.2732.

The cation in Figure 23 is known, although it has not been prepared *via* this route before.[30] In previous work this cation was prepared by heating to 130°C in an ionic liquid, but in this case a much lower temperature of 50°C was used with methanol as the solvent. **8** seems to be a precursor to the formation of **9** under high-temperature conditions.

The ^{1}H NMR spectrum of **9** is shown in Figure 24. This complex is expected to be diamagnetic, so the peak broadening is likely due to ligand exchange; each cation is coordinating through one of its two pendant pyridines, and these likely exchange in solution. This would result in the two coordinating NHCs converting between a *cis* and *trans* relationship to each other. Variable-temperature NMR experiments could be used to study this behaviour. Notably, the C2 proton peak is absent, indicating formation of NHCs. Due to the overlapping and width of the peaks, they could not be accurately integrated.

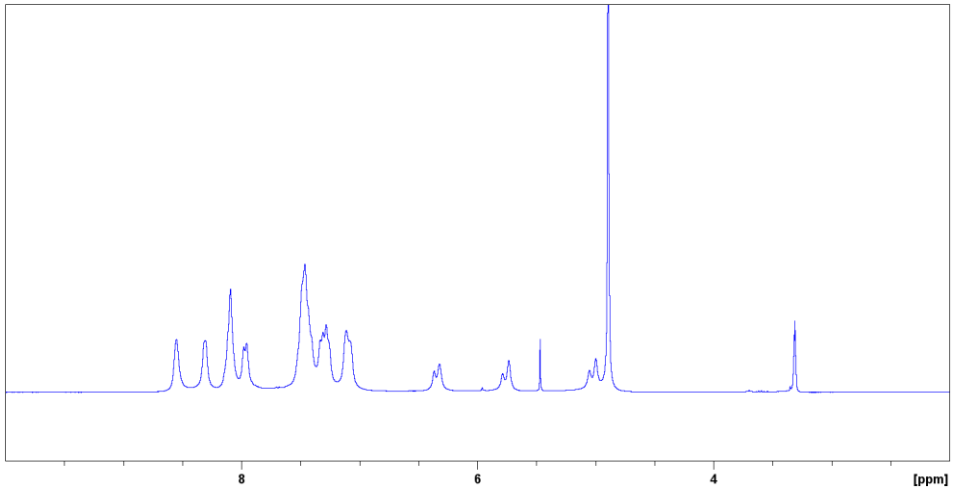

Figure 24: The ^{1}H NMR spectrum of 9 in CD_3OD.

Interestingly, the $^{13}C\{^{1}H\}$ NMR has 19 distinct peaks (Figure 25). Coupling is highly unlikely as the spectrum is proton-decoupled, so the only atom to which the carbon nuclei could couple is nickel and the only spin-active nickel isotope, ^{61}Ni, is approximately 1.1% abundant;[48] although C-Ni coupling could give rise to satellites, it would not likely give rise to peaks of the observed intensity. **2** has 19 carbons, so 19 peaks are possible assuming the structure is coordinated such that it is completely unsymmetric, as is the case in **9**. This is in contrast to the ^{1}H NMR spectrum shown in Figure 24, where the hydrogen atoms of the coordinating and non-coordinating pyridines appear to have averaged out given the number of peaks present in the ^{1}H-NMR spectrum.

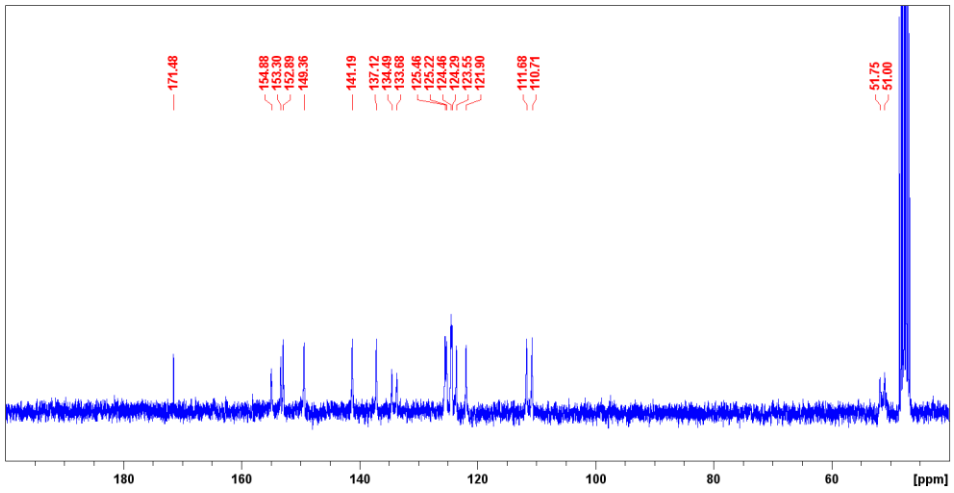

Figure 25: The ^{13}C NMR spectrum of **9** in CD_3OD.

1.2.2.7 Reaction of 1,3-bis(2-pyridylmethyl)benzimidazolium chloride and copper(II) chloride dihydrate

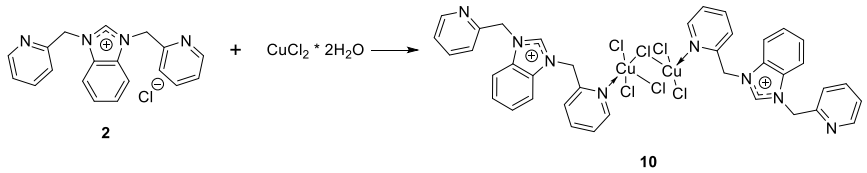

Scheme 8: The synthesis of **10** from ligand **2** and copper(II) chloride dihydrate.

The reaction of 1,3-bis(2-pyridylmethyl)benzimidazolium chloride with copper(II) chloride dihydrate was performed in methanol with no effort to exclude air or moisture. Light green crystals of **10** precipitated immediately on addition of the 1,3-bis(2-pyridylmethyl)benzimidazolium chloride solution to the copper(II) chloride dihydrate solution (Figure 26).

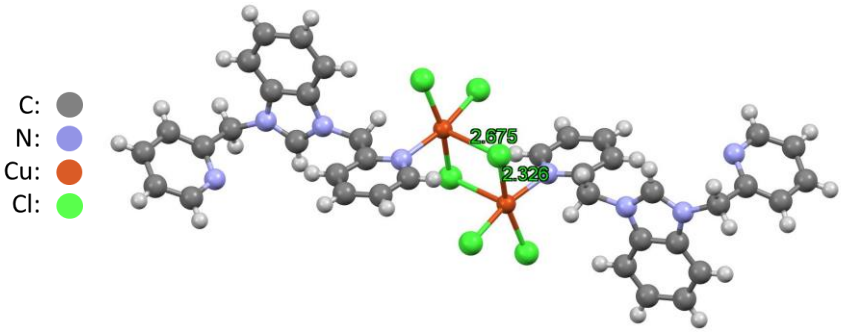

Figure 26: The crystal structure of **10**, with notable bond lengths labelled. R = 0.0539.

In this case, the pincer ligand coordinates through a single pyridine, reminiscent of **6**. Unlike in **6**, however, the complexes dimerize, giving rise to a square pyramidal geometry around each of the two copper atoms. The axial Cu-Cl bond is significantly longer than the equatorial Cu-Cl

bonds – as shown in Figure 26 – indicating a Jahn-Teller distortion. Geometry around the copper atoms is square pyramidal ($\tau_5 = 0.0168$).

10 is predicted to be paramagnetic given that copper(II) has an odd number of electrons, and the ^{1}H NMR spectrum exhibits the broad, undefined peaks expected of a paramagnetic complex (Figure 27). There is still a distinct peak above 10 ppm, likely corresponding to the C2 proton of the benzimidazolium cation. Beyond this, no peaks can be readily assigned.

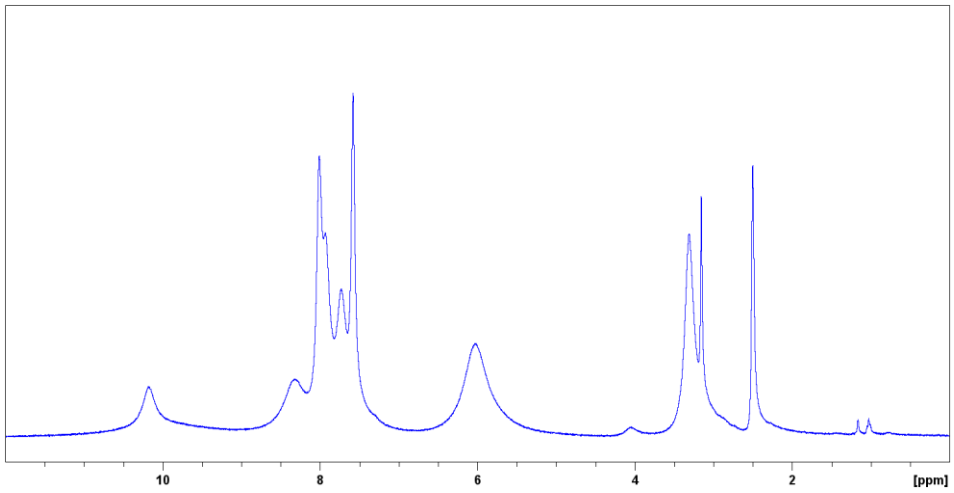

Figure 27: The ^{1}H NMR spectrum of **10** in DMSO-d6, showing the very broad peaks expected of a paramagnetic complex.

It is possible that **10** could be used to produce an imidazolium-functionalized coordination polymer, with 1,3-bis(2-pyridylmethyl)benzimidazolium cations acting as linkers and $Cu_2Cl_6^{2-}$ anions acting as nodes. This would likely form an anionic 1D coordination polymer (Figure 28).

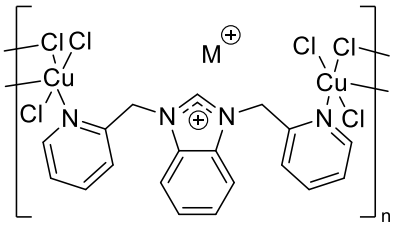

Figure 28: The possible structure of a 1D coordination polymer based on **10**. Note that for this coordination polymer to form, it would require an additional source of chloride, such as sodium chloride.

1.2.2.8 Reaction of 1,3-bis(2-pyridylmethyl)benzimidazolium chloride and nickel(II) chloride hexahydrate

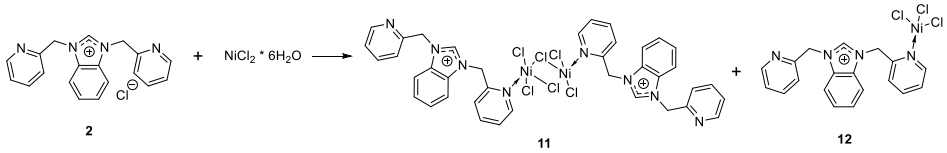

Scheme 9: The synthesis of **11** and **12** from ligand **2** and nickel(II) chloride hexahydrate.

The reaction of 1,3-bis(2-pyridylmethyl)benzimidazolium chloride with nickel(II) chloride hexahydrate was performed in methanol with no effort to exclude air or moisture. Several different species were recrystallized from this reaction. **11** was recrystallized as blue blocks by vapour diffusion of diethyl ether into methanol, along with a red crystalline material, the structure of which has yet to be determined (Figure 29).

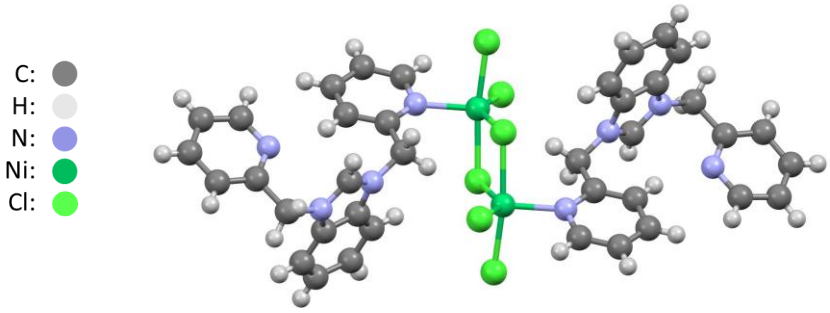

Figure 29: The asymmetric unit of **11**. R = 0.0587.

The geometry around the nickel atoms appears to be between square pyramidal and trigonal bipyramidal, possibly leaning toward the latter ($\tau_5 = 0.541$). All Ni-Cl bond lengths are similar, with the longest (2.463Å) being the pseudoaxial bond of the bridging chlorides and the shortest (2.313Å) being the pseudoequatorial monodentate chlorides; this is a much smaller difference than was observed in **10**.

It is possible that **11** – like **10** – could be used to produce an imidazolium-functionalized coordination polymer, with 1,3-bis(2-pyridylmethyl)benzimidazolium cations acting as linkers and $Ni_2Cl_6^{2-}$ anions acting as nodes. This would likely form an anionic 1D coordination polymer (Figure 30).

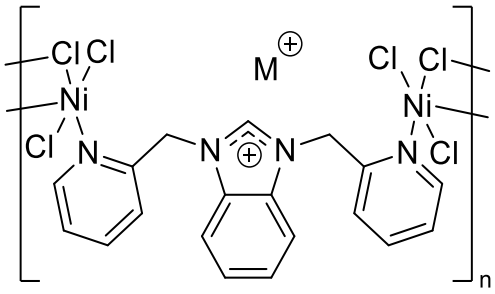

Figure 30: The possible structure of a 1D coordination polymer based on **11**. Note that for this coordination polymer to form, it would require an additional source of chloride, such as sodium chloride.

11 was dissolved in methanol and recrystallized by vapour diffusion with acetone instead of diethyl ether to yield **12** (Figure 31). This compound is analogous to **6**; as such, both should be tested for similar applications.

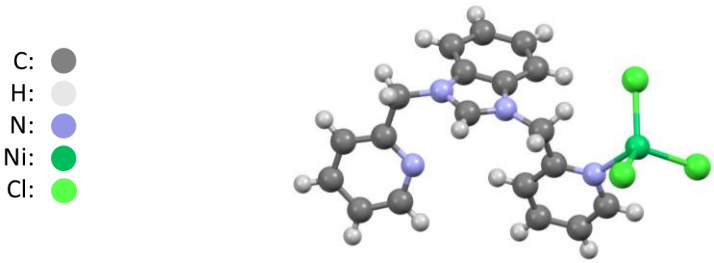

Figure 31: The asymmetric unit of **12**. R = 0.0631.

Notably, both **11** and **12** appear to exist as the same species in methanolic solution, as demonstrated by their ^{1}H NMR spectra (Figure 32). The peaks are somewhat broadened in these spectra compared to the peaks of the free ligand; this could be due to an equilibrium between several different coordination modes around both the nickel(II) centre and the ligand. Notably, the C2 proton peak that is characteristic of imidazolium cations appears at 8.13 ppm, and is much

smaller than one would expect; this suggests that the major structure present in solution may be a nickel(II)-NHC complex that only gets protonated and changes its coordination mode during recrystallization. This is also suggested by the fact that the sum of the integrals in the ^{1}H NMR spectrum of **11** and **12** is approximately 14; the cation of **2** has 15 protons, while the NHC derived from it has 14.

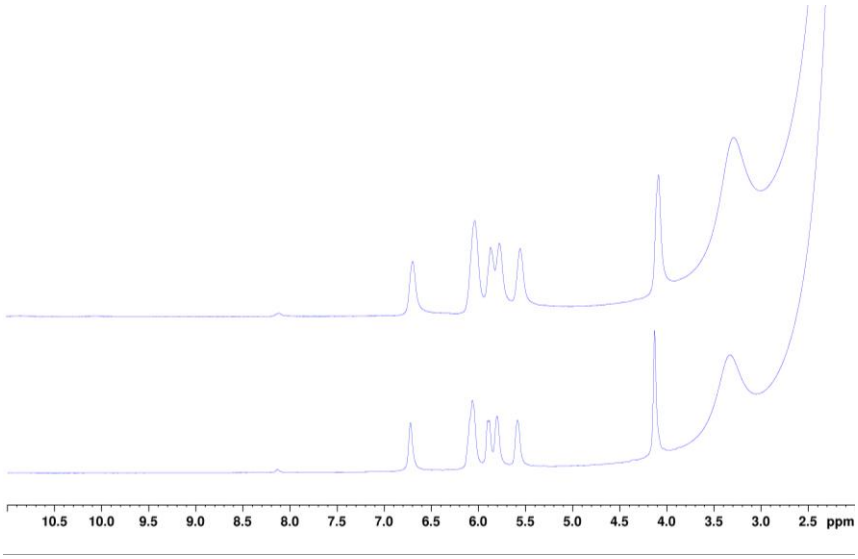

Figure 32: The ^{1}H NMR spectra of **11** (top) and **12** (bottom) collected in CD_3OD. Note that the large peaks at the upfield end of the window are due to methanol.

The ^{13}C NMR spectra of **11** and **12** are also identical, and have one notable feature; they only show nine peaks, while the ligand **2**, from which **11** and **12** were prepared, has ten carbon environments (Figure 33). There are several points above 200 ppm which could be signals, but cannot be confidently distinguished from the baseline.

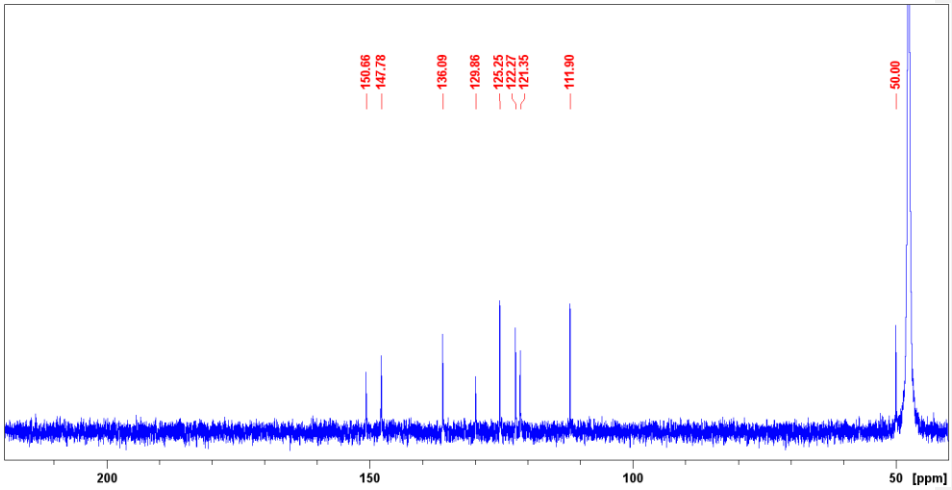

Figure 33: The ^{13}C NMR spectrum of **11** and **12**.

1.3 Conclusions

Two NHC-based pincer ligands with pendant pyridines, **1** and **2**, were synthesized in moderate to good yield from the desired imidazole core and 2-(chloromethyl)pyridine hydrochloride. These two ligands were complexed to chloride and acetate salts of copper(II) and nickel(II). The two ligands exhibited two different coordination modes: they either coordinate as a tridentate pincer ligand when metal acetate salts are used, or coordinate through a single pyridine when metal chlorides are used, leaving a non-coordinating imidazolium cation. Notably, complexes **10** and **11** have structural features that suggest that they could be used as precursors for NHC-functionalized coordination polymers. All complexes were prepared in the presence of moisture. These complexes were characterized by X-ray crystallography, IR spectroscopy, NMR spectroscopy, and mass spectrometry where possible.

1.4 Future work

The most straightforward next steps in this work are further characterization of all complexes **3** – **12**; several complexes could not be isolated in sufficient yield for NMR spectroscopy, and some of those that were may not have been pure. In addition to NMR spectroscopy, magnetic susceptibility measurements could be used to study the electron configuration of the complexes.

It is likely that **1** does react with nickel(II) acetate tetrahydrate and copper(II) chloride dihydrate, despite the fact that no product was isolated. Isolation of a product from these reactions should be attempted.

The C2 proton of **2** is likely more acidic than that of **1**, as suggested by ^{1}H NMR spectroscopy; thus, the isolation of a free NHC derived from **2** should be attempted. The isolation of such a species would allow much greater flexibility and scope in reactions with transition metals.

The pathways involved in the formation of **3**, **4**, and **5** should be elucidated; in particular the electron source for the reduction of copper(II) to copper(I) should be determined. Performing two reactions in *t*-butanol and 1-butanol could be a means to determine whether alcohol solvents act as the reducing agent, because *t*-butanol can not be oxidized to a carbonyl but 1-butanol can be. Thus, if only the reaction with 1-butanol is observed to form **5** the reduction can be attributed to the solvent. In addition, isolation of **3** and **4** to observe whether they can then convert to **5** would also help to determine whether any as yet unidentified species in the reaction mixture are involved in the reaction. Similarly, the conversion of **7** to species analogous to **4** and **5** should be explored; such a process is likely possible – a cluster analogous to **5** but with ligand **2** is known[40] – but was not observed in this work.

The formation of **10** and **11** suggests that it may be possible to produce a 1D coordination polymer from **2**, two equivalents of copper(II) chloride dihydrate or nickel(II) chloride hexahydrate, and at least two equivalents of a chloride source such as sodium chloride. This possibility should be explored, as such a material could be an effective CO_2 capture material. **10** and **11** could also be tested for their ability to capture CO_2 in their own right.

The catalytic activity of several of the prepared complexes should be explored. **3** and **7** may be effective catalysts of Chan-Evans-Lam and Ullmann-type couplings, as other copper(II)-NHC complexes have been observed to catalyse those reactions.[32,42] The nickel(II)-NHC complexes **8** and **9** should also be explored as catalysts; although it was found that **9** was a poor electrocatalyst for proton reduction, its ability to catalyse other reactions is unexplored.[30] Zhou *et al.* demonstrated that a nickel(II)-NHC complex could catalyse Suzuki-Miyaura and Kumada-Corriu couplings; these complexes should be tested for catalytic activity in those reactions.[17] It may also be possible to reduce both **8** and **9** to nickel(0)-NHC complexes, which may also exhibit catalytic activity in appropriate reactions.

1.5 Experimental

1.5.1 Materials and general considerations

All reagents and solvents were purchased from Millipore Sigma, Alfa Aesar, Fisher Scientific, or Oakwood chemicals and used without further purification unless otherwise specified. Deuterated NMR solvents were purchased from Cambridge Isotopes. NMR spectra were collected using a Bruker 300 MHz Ultrashield spectrometer. IR spectra were collected using a Bruker ALPHA ATR with a single reflection ZnSe crystal. ESI-MS data were collected by Xiao Feng at Dalhousie University using a Bruker Compact QTOF mass spectrometer. X-ray diffraction data was collected by Tanner George or Dr. Jason Masuda using a Bruker D8 VENTURE

diffractometer equipped with a PHOTON III CMOS detector using monochromated Mo Kα radiation (λ = 0.71073 Å) from an Incoatec micro-focus sealed tube at 100-150 K. Structure solutions were determined by Dr. Jason Masuda and Tanner George. The structures were solved using SHELXT and all non-hydrogen atoms were refined anisotropically with SHELXL using a combination of shelXle and OLEX2 graphical user interfaces. Final crystal structure images were prepared using Mercury.[49]

1.5.2 Synthesis of ligands

1.5.2.1 Synthesis of 1,3-bis(2-pyridylmethyl)imidazolium chloride (1)

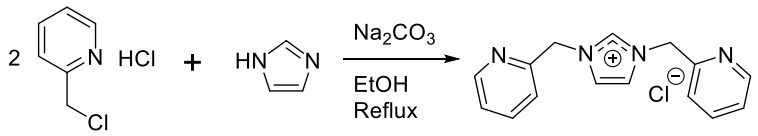

In a 50mL round-bottom flask equipped with a magnetic stir bar, imidazole (0.681g, 10.00mmol) was dissolved in 20mL of ethanol. Powdered sodium carbonate (5g) and 2-(chloromethyl)pyridine (3.280g, 20.00mmol) were added, and the mixture stirred at room temperature for 10 minutes then heated to reflux for 72 hours. After cooling to room temperature, the mixture was gravity filtered through fluted filter paper and the filter washed with 20mL of ethanol. Diethyl ether was added to the filtrate until the mixture became turbid, then a further 20mL of diethyl ether was added. The mixture was cooled overnight in the freezer, during which time the precipitate settled. The precipitate was collected by vacuum filtration and washed with diethyl ether to afford 1,3-bis(2-pyridylmethyl)imidazolium chloride as a brown solid (70%).

FT-IR (ATR, cm^{-1}): 3144.35 (m), 1703.14 (m), 1636.73 (s), 1594.64 (s), 1562.03 (s), 1438.58 (s).

^{1}H NMR (DMSO-d6, 300MHz): δ 9.65 (s, 1H), 8.55 (d, J=4.48 Hz, 2H), 7.92 – 7.86 (m, 4H), 7.53 (d, J=7.82 Hz, 2H), 7.39 (dd, ^{3}J=5.60 Hz, ^{3}J=7.33 Hz, 2H), 5.68 (s, 4H).

^{13}C NMR (DMSO-d6, 75MHz): δ 153.7, 149.6, 137.8, 137.6, 123.7, 123.3, 122.6, 53.0.

ESI-MS (+): Calcd for $C_{15}H_{15}N_4^+$ m/z: 251.1. Found 251.1.

HRMS (+): Calcd for $C_{15}H_{15}N_4^+$ m/z: 251.1291. Found 251.1282.

1.5.2.2 Synthesis of 1,3-bis(2-pyridylmethyl)benzimidazolium chloride (2)

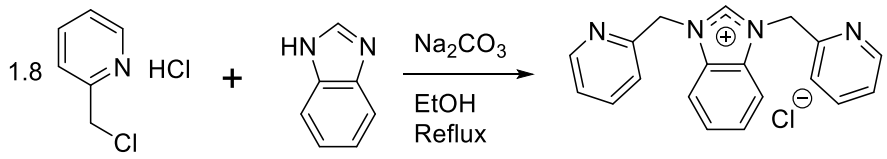

Benzimidazole (10.00mmol, 1.181g) was dissolved in 10mL of ethanol in a 50mL round-bottom flask charged with a stir bar. Sodium carbonate (3g) and 2-(chloromethyl)pyridine hydrochloride (18mmol, 2.953g) were added, and the inside of the flask was washed with 10mL of ethanol to rinse down material that had stuck to the sides. This mixture was stirred at room temperature for 5 minutes, then heated to reflux for 4 days. After 4 days, the reaction mixture was cooled to room temperature and gravity filtered. The solvent was removed by rotary evaporation, providing a brown oil. This was redissolved in 10mL of dichloromethane and filtered through a Kimwipe plug. The product was recrystallised by vapour diffusion of diethyl ether into the dichloromethane solution to afford blocky yellow-brown crystals (0.909g, 30%).

FT-IR (ATR, cm^{-1}): 3380.74 (s), 1633.99 (m), 1594.58 (m), 1563.35 (m), 1438.15 (m).

^{1}H NMR (DMSO-d6, 300MHz): δ 10.43 (s, 1H), 8.49 (d, J=4.02 Hz, 2H), 7.99 (dd, ^{3}J=6.30 Hz, ^{4}J=3.14 Hz, 2H), 7.90 (td, J^{3}=7.70 Hz, J^{4}=1.66 Hz, 2H), 7.73 (d, J=7.70 Hz, 2H), 7.60 (dd, ^{3}J=6.27 Hz, ^{4}J=3.11 Hz, 2H), 7.37 (m, 2H), 6.08 (s, 4H).

^{13}C NMR (DMSO-d6, 75MHz): δ 153.1, 149.6, 144.1, 137.6, 131.3, 126.7, 123.7, 122.8, 114.1, 50.9.

ESI-MS (+): Calcd for $C_{19}H_{17}N_4^+$ m/z: 301.1. Found 301.1.

HRMS (+): Calcd for $C_{15}H_{15}N_4^+$ m/z: 301.1448. Found 301.1448.

1.5.3 Successful reactions of the ligands with transition metal salts

1.5.3.1 Synthesis of 3

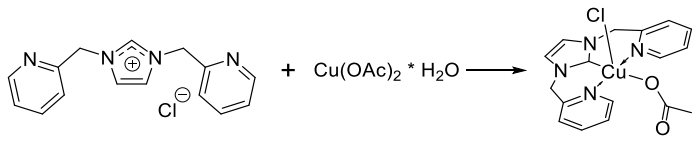

In a 20mL scintillation vial equipped with a stir bar, 1,3-bis(2-pyridylmethyl)imidazolium chloride (3.00mmol, 0.860g) was dissolved in 5mL of methanol. Separately, copper(II) acetate monohydrate (3.00mmol, 0.599g) was dissolved in 5mL of methanol. The two solutions were mixed and stirred at room temperature. After a few hours, the colour of the solution had changed from brown to green-blue. After 24 hours, the solution was dark blue. An aliquot was removed and vapour diffusion with diethyl ether afforded blue, blocky crystals of **3**.

FT-IR (ATR, cm^{-1}): 3124.01 (m), 2936.70 (m), 2822.27 (m), 1566.97 (s), 1389.67 (s), 1029.21 (s), 755.36 (s).

ESI-MS (+): Calcd for $C_{17}H_{17}CuN_4O_2^+$ [M-Cl] m/z: 372.1. Found 372.1.

1.5.3.2 Synthesis of (4)

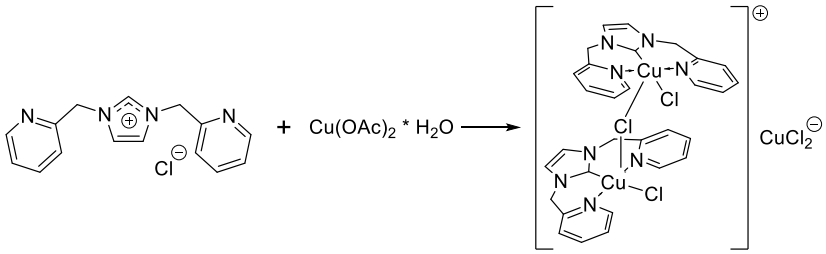

An aliquot of the reaction mixture from which **3** was isolated was removed after one week, and vapour diffusion of diethyl ether into the aliquot afforded single crystals of **4**. The quantity of material isolated was insufficient for further characterization.

1.5.3.3 Synthesis of (5)

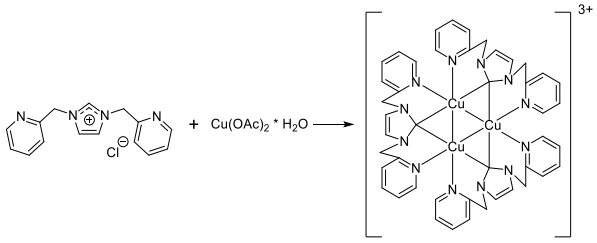

An aliquot of the reaction mixture from which **3** was isolated was removed after one month, and vapour diffusion of diethyl ether into the aliquot afforded single crystals of **5**.

ESI-MS (-): Calcd for $CuCl_2^-$ m/z: 134.9. Found 134.9.

1.5.3.4 Synthesis of (6)

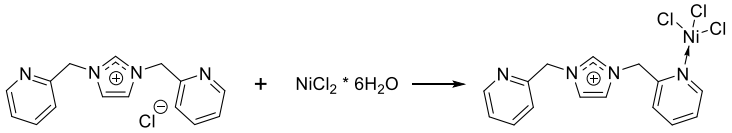

In a 50mL round-bottom flask equipped with a stir bar, 1,3-bis(2-pyridylmethyl)imidazolium chloride (5.00mmol, 1.434g) was dissolved in 10mL of acetonitrile. Separately, nickel(II) chloride hexahydrate (5.00mmol, 1.188g) was dissolved in 10mL of methanol. The two solutions were mixed and stirred for 24 hours at room temperature, during which time the mixture took on a green-yellow colour. The solvents were removed by rotary evaporation, affording a blue-green residue. This was dissolved in minimal acetonitrile and precipitated by addition of diethyl ether to afford **6** as a blue powder which was collected by vacuum filtration (0.851g, 40.9%). Single crystals of **6** suitable for single-crystal X-ray diffraction were obtained by vapour diffusion of diethyl ether into acetonitrile and methanol solutions of **6**.

FT-IR (ATR, cm^{-1}): 3140.77 (w), 2944.35 (w), 2830.91 (w), 1594.85 (w), 1570.66 (w), 1428.98 (m), 1019.52 (s), 744.62 (m).

1.5.3.5 Synthesis of (7)

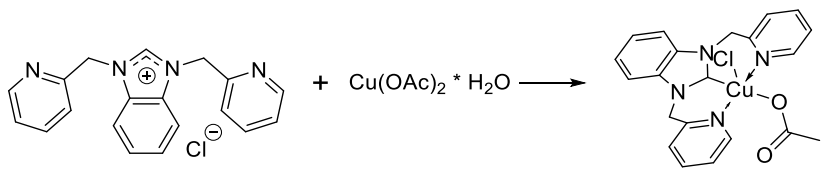

In a 20mL scintillation vial equipped with a stir bar, 1,3-bis(2-pyridylmethyl)benzimidazolium chloride (1.00mmol, 0.337g) was dissolved in 5mL of methanol. Separately, copper(II) acetate monohydrate (1.00mmol, 0.200g) was dissolved in 5mL of methanol. The two solutions were

mixed and stirred at room temperature. The solution immediately changed colour from brown to very dark blue, and a dark blue precipitate began to form. After stirring for 24 hours at room temperature, the precipitate was centrifuged and washed with 3x5mL of methanol. It was found that the precipitate was sparingly soluble in methanol, and vapour diffusion of diethyl ether into a methanol solution afforded **15** as dark blue, blocky crystals suitable for single-crystal X-ray diffraction.

FT-IR (ATR, cm^{-1}): 3021.61 (w), 1602.98 (s), 1387.24 (s), 774.23 (s), 752.66 (s).

1.5.3.6 Synthesis of (8)

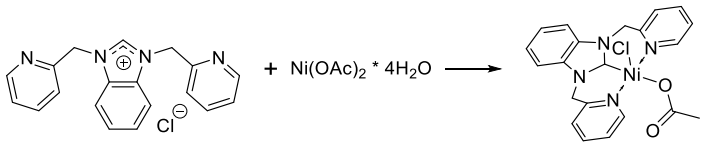

In a 20mL scintillation vial equipped with a stir bar, 1,3-bis(2-pyridylmethyl)benzimidazolium chloride (1.00mmol, 0.337g) was dissolved in 5mL of methanol. Separately, nickel(II) acetate tetrahydrate (1.00mmol, 0.249g) was dissolved in 5mL of methanol. The two solutions were mixed and stirred at room temperature for 24 hours, during which time the mixture took on a blue colour. Single crystals of **8** were obtained by vapour diffusion of diethyl ether into the methanol solution. Due to the thermal instability of **8**, it could not be fully characterized.

1.5.3.7 Synthesis of (9)

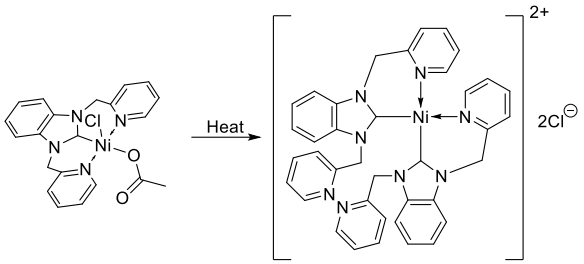

A solution of **8** in methanol was heated gently for 10 minutes, at which point yellow crystals of **9** precipitated.

^{1}H NMR (CD_3OD, 300MHz): δ 8.55-7.95 (m), 7.46-7.11 (m), 6.35 (d), 5.76 (d), 5.03 (d).

^{13}C NMR (CD_3OD, 75MHz): δ 171.5, 154.9, 153.3, 152.9, 149.4, 141.2, 137.1, 134.5, 133.7, 125.5, 125.2, 124.5, 124.3, 123.6, 121.9, 111.7, 110.7, 51.8, 51.0.

ESI-MS (+): Calcd for $C_{38}H_{32}N_8Ni^{2+}$ m/z: 329.1. Found 329.1. Calcd for $C_{38}H_{32}ClN_8Ni^{+}$ m/z: 693.2. Found 693.2.

HRMS (+): Calcd for $C_{38}H_{32}N_8Ni^{2+}$ m/z: 329.1046. Found 329.1047.

1.5.3.8 Synthesis of (10)

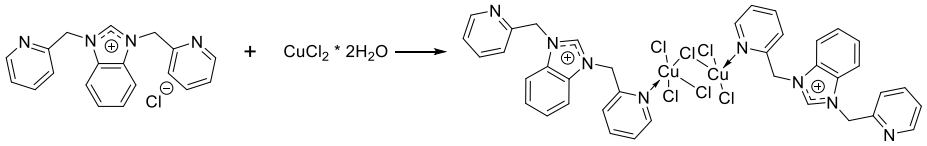

In a 20mL scintillation vial equipped with a stir bar, 1,3-bis(2-pyridylmethyl)benzimidazolium chloride (1.00mmol, 0.337g) was dissolved in 5mL of methanol. Separately, copper(II) chloride dihydrate (1.00mmol, 0.170g) was dissolved in 5mL of methanol. The copper(II) chloride solution

was added to the solution of **2** and light green plate-like crystals of **10** suitable for single-crystal X-ray diffraction began precipitating immediately. These were collected by centrifugation and washed with 3x5mL of methanol.

FT-IR (ATR, cm^{-1}): 3011.13 (w), 1553.02 (m), 1428.21 (m), 1186.07 (m), 766.65 (s), 753.76 (s).

1.5.3.10 Synthesis of (11)

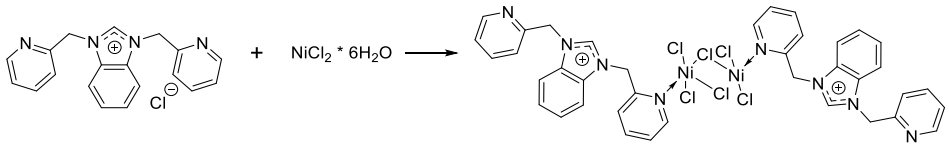

In a 20mL scintillation vial equipped with a stir bar, 1,3-bis(2-pyridylmethyl)benzimidazolium chloride (1.00mmol, 0.337g) was dissolved in 5mL of methanol. Separately, nickel(II) chloride hexahydrate (1.00mmol, 0.238g) was dissolved in 5mL of methanol. The two solutions were mixed and stirred at room temperature for 3 days, during which time the mixture took on a yellow colour. Light blue single crystals of **11**, along with red crystals of an unknown material, were isolated by vapour diffusion of diethyl ether into the methanolic solution.

FT-IR (ATR, cm^{-1}): 3126.51 (m), 3057.09 (m), 1594.50 (m), 1571.98 (m), 1435.02 (s), 1185.54 (m), 1026.10 (m), 755.23 (s).

^{1}H NMR (CD_3OD, 300MHz): δ 6.72 (s, 2H), 6.06 (s, 4H), 5.85 (m, 4H), 5,58 (s, 2H), 4.13 (s, 4H).

^{13}C NMR (CD_3OD, 75MHz): δ 150.7, 147.8, 136.1, 129.9, 125.3, 122.3, 121.4, 111.9, 50.0.

1.5.3.9 Synthesis of (12)

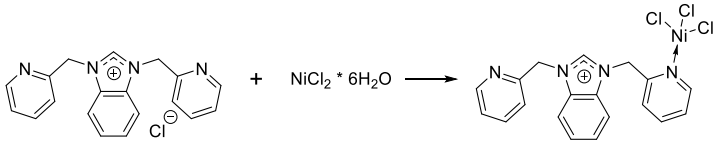

Dark blue single crystals of **12** were obtained by vapour diffusion of acetone into an aliquot of the methanolic solution from which **11** was also isolated.

FT-IR and NMR spectra are identical to those of **11**.

1.5.4 Unsuccessful reactions of the ligands with transition metal salts

1.5.4.1 Reaction of 1,3-bis(2-pyridylmethyl)imidazolium chloride with nickel(II) acetate tetrahydrate

In a 20mL scintillation vial equipped with a stir bar, 1,3-bis(2-pyridylmethyl)imidazolium chloride (1.00mmol, 0.287g) was dissolved in 5mL of methanol. Separately, nickel(II) acetate tetrahydrate (1.00mmol, 0.249g) was dissolved in 5mL of methanol. The two solutions were mixed and stirred at room temperature for three days, during which time the mixture took on a dark brown colour. Vapour diffusion of diethyl ether, acetone, and THF into aliquots of the reaction was attempted. No products were successfully isolated.

1.5.4.2 Reaction of 1,3-bis(2-pyridylmethyl)imidazolium chloride with copper(II) chloride dihydrate

In a 20mL scintillation vial equipped with a stir bar, 1,3-bis(2-pyridylmethyl)imidazolium chloride (1.00mmol, 0.287g) was dissolved in 5mL of methanol. Separately, copper(II) chloride dihydrate (1.00mmol, 0.170g) was dissolved in 5mL of methanol. The two solutions were mixed and stirred at room temperature for three days, during which time the mixture took on a dark brown

colour. Vapour diffusion of diethyl ether, acetone, and THF into aliquots of the reaction was attempted. No products were successfully isolated.

2. Synthesis of *N*-heterocyclic carbene-functionalized linkers for metal organic frameworks

2.1 Introduction

2.1.1 Carbon dioxide capture

As the most significant contributor to climate change, it is essential that the output of carbon dioxide from human activities is decreased However, it is becoming clear that simply decreasing future output is not enough; it is also important that the current atmospheric carbon dioxide content is decreased.[50,51] As such, carbon dioxide capture technologies have gained significant interest in recent years (Figure 34).[50] Similarly, carbon dioxide fixation technology has also gained significant interest as a means to use carbon dioxide as a feedstock for useful materials.[52,53]

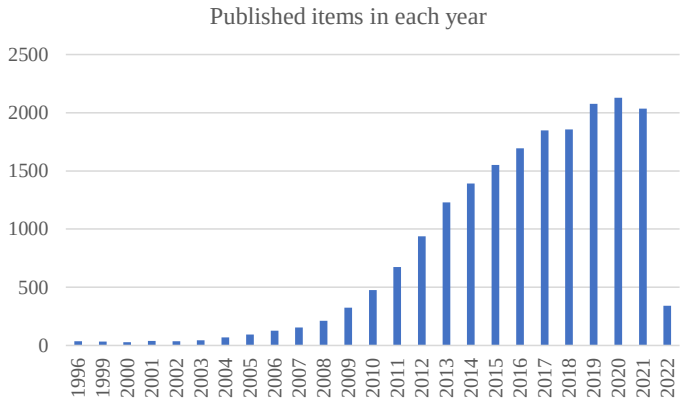

Figure 34: Research articles published per year for the search "'Carbon dioxide' capture" in Web of Science.

Several methods have been developed for carbon dioxide capture, but all fall into one of two broad categories: physisorption and chemisorption.[52] Physisorption processes are governed by

weak intermolecular reactions, and are therefore readily reversible.[54] Similarly, materials relying on physisorption typically have lower capacities than those that use chemisorption.[54] Chemisorption, on the other hand, involves formation of covalent bonds to the guest molecule, and therefore requires more energy to reverse and allows higher loadings.[54] Because chemisorption involves formation of new bonds, it also has the effect of activating some guest molecules.

Most sorbents for carbon dioxide take advantage of its Lewis acidic carbon atom; thus, many function as Lewis bases.[50,52,55,56] In the case of chemisorption, this also has the effect of activating carbon dioxide, allowing some materials to catalyse its fixation.[55,56] Most notably, amines have historically been used as chemisorbents for carbon dioxide.[55] More recently, NHCs have seen more use in carbon dioxide chemisorption and fixation.[56,57] Carbon dioxide fixation can take place through a range of different pathways, but the most common is reaction of activated carbon dioxide with an epoxide to form a cyclic carbonate.[56,58,59]

2.1.2 Metal-organic frameworks

2.1.2.1 Synthesis of metal-organic frameworks

Metal-organic frameworks (MOFs) are a class of coordination polymers with a crystalline, multidimensional structure.[60] They are prepared from metallic "nodes" and organic "linkers". The nodes can be individual metal atoms or ions or small clusters, and the linkers typically coordinate through carboxylates or *N*-heterocycles. Each linker coordinates to two or more nodes, and each node supports multiple linkers around it (Figure 35).[60] The end result is a multidimensional coordination polymer.

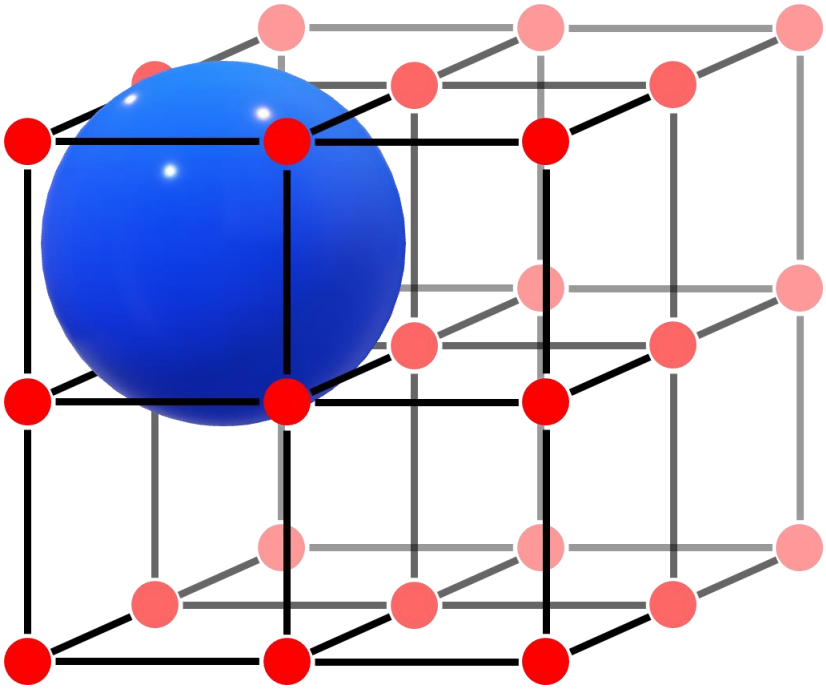

Figure 35: A simple schematic of a metal-organic framework. Black bars represent organic linkers, red circles represent metal nodes, and the blue sphere represents a void space.

As shown in Figure 35, MOFs are highly porous with large internal void spaces and a high internal surface area.[60,61] As a result of these properties, MOFs have a wide variety of potential applications including separations,[62–64] storage,[65,66] catalysis,[57,66,67] sensing,[68–70] and sometimes ion exchange.[70–72] The structures of MOFs can be constructed for a specific task in one of two main ways: presynthetic modification or postsynthetic modification.[60,73] Presynthetic modification involves alteration of the linkers or nodes prior to construction of the MOF, while postsynthetic modification involves construction of the MOF first, then modification of the framework (Figure 36).

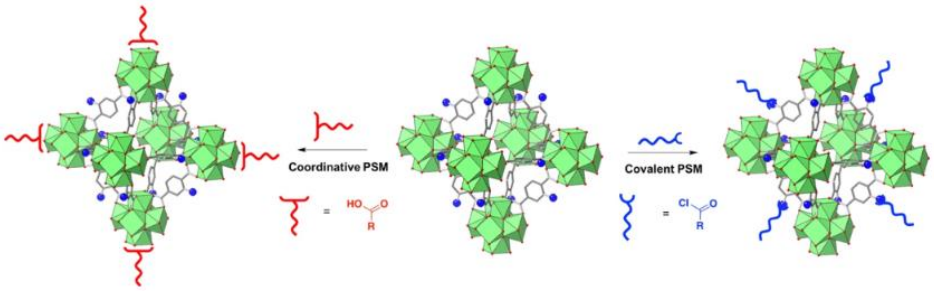

Figure 36: The two approaches to postsynthetic modification of MOFs. Reproduced with permission from ACS Publications (https://pubs.acs.org/doi/10.1021/acscentsci.0c00690).[73]

2.1.2.2 Applications of metal-organic frameworks

2.1.2.2.1 Separation and adsorption

Due to their high internal volumes and surface areas, MOFs are ideal materials for adsorptions and separations.[66] The high volume allows storage of a large quantity of substrate while the high surface area allows the MOF to interact selectively with a mixture of compounds. Most often, MOFs are applied to separation and storage of gaseous substrates. The high internal volume of MOFs means that they typically fill with guest molecules, so the primary issue is designing MOFs with a high affinity for a particular substrate so that they can separate a single species from a mixture. There are two main design principles used to improve selectivity: size exclusion – in which the pore size of the MOF is controlled such that only some guest molecules can fit[62,74] – and tuning the internal pore environment such that the target substrate interacts favourably with it.[63,64,75] This pore environment can be controlled either by functionalizing a linker to have desirable properties and building a MOF from it (presynthetic modification) or by building the desired functionalities off the structure when it is already incorporated into a MOF (postsynthetic modification).[60,73]

Recently, a novel behaviour has been observed in MOFs with flexible morphologies, in which the MOF will change conformation when exposed to a substrate to increase the internal volume.[76] This behaviour is known as "breathing" and can be due to several different factors.[76] The most common of these is a flexible linker that undergoes a conformational change as the amount of guest molecules changes.[76] However, breathing behaviour can also be due to interactions between guest molecules and the linkers or nodes altering the coordination geometry in the structure.[76]

2.1.2.2.2 Catalysis

Metal organic frameworks are also useful as heterogeneous catalysts. MOFs can be used as supports for catalysts such as nanoparticles, by immobilizing the catalyst within the pores of the MOF.[77] This can allow the catalyst to be separated from the reaction more easily. MOFs can also be catalytically active in their own right. There are two main strategies to make MOFs catalytically active; the MOF can be constructed such that there are defects in the framework – exposing coordinatively unsaturated metal nodes[78–80] – or the MOF can be constructed from a catalytically active linker.[57,80] Catalytic linkers can be prepared prior to assembly (the presynthetic route) or by treating the MOF to make it catalytic after synthesis.[57,80] For example, Das and Nagajara described a MOF constructed from linkers containing imidazolium moieties, which was doped with copper(I) to produce a copper(I)-NHC complex on the linkers of the MOFs.[57] This material proved to both have a high affinity for carbon dioxide due to the free imidazolium moieties and be catalytically active in the reaction of carbon dioxide with alkynes at the copper(I) centres.[57]

2.1.2.3 Ionic metal-organic frameworks

Ionic MOFs are a subclass of MOFs in which the charges of the ligands and cations do not balance.[81] As a result, the MOF has a net charge that must be balanced. Ionic MOFs can be prepared by a variety of routes (Figure 37).

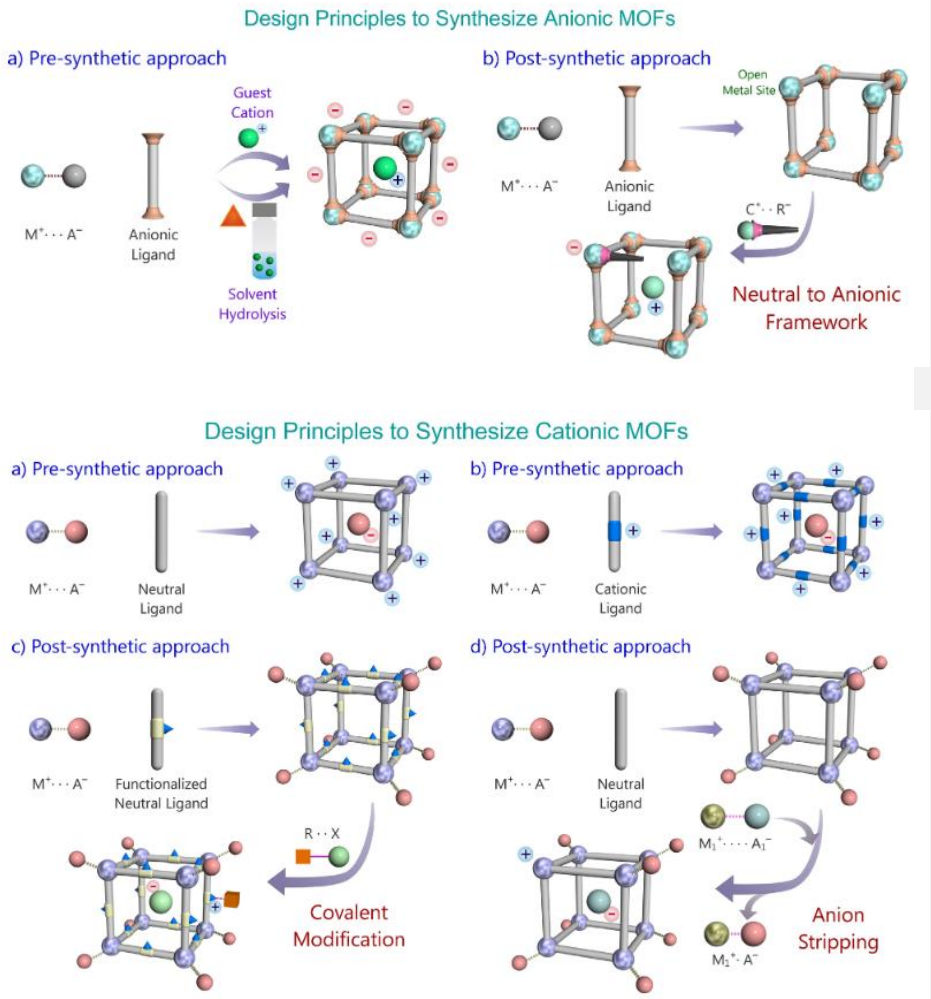

Figure 37: The main routes used to prepare ionic MOFs. Reproduced with permission from Elsevier Science & Technology Journals.[81] Route A to anionic MOFs: the linker of a neutral MOF is functionalized with an anionic moiety. Route B to anionic MOFs: an anionic ligand is coordinated to the node of a neutral MOF. Route A to cationic MOFs: a neutral linker is used with a cationic node. Route B to cationic MOFs: a cationic linker is used with a cationic node. Route C to cationic MOFs: the linker of a neutral MOF is functionalized with a

cationic moiety. Route D to cationic MOFs: anions coordinating to the nodes of a neutral MOF are removed and replaced with non-coordinating guest anions.

The counterions of an ionic MOF can either be free in the pores of the framework, or – in the case of cationic MOFs – incorporated into the structure of the lattice.[81] Often, this incorporation involves the formation of a 2D cationic sheet, with the anions acting as "pillars" between the sheets, as shown in Figure 38; thus, they have been dubbed pillared ionic MOFs.[75,82,83] Ionic MOFs have the same range of properties and applications as neutral MOFs, but can also be used for ion exchange and sensing.[81]

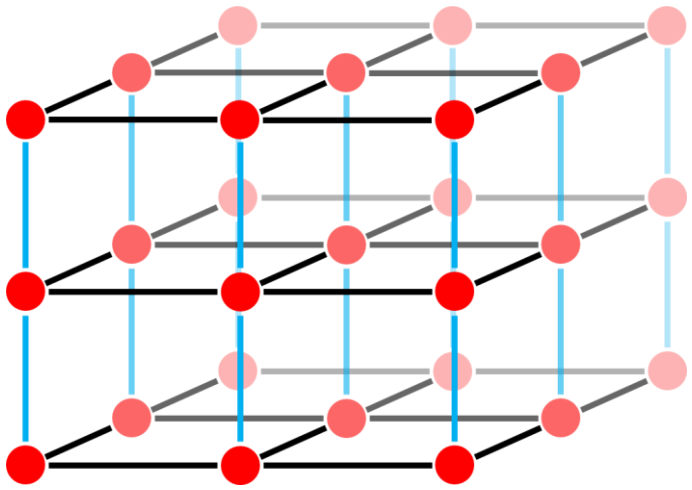

Figure 38: A basic diagram of an anion-pillared MOF. The red circles are metal nodes, the black bars are organic linkers, and the blue bars are anionic pillars.

2.1.2.3.1 Hexafluorosilicate pillared metal organic frameworks

One of the more common pillars used in ionic MOFs is hexafluorosilicate, SiF_6^{2-} (often referred to as SIFSIX).[64,75,82–84] This anionic pillar is typically used in MOFs with linkers that coordinate

through pyridine moieties, and coordinates weakly to two metal cations through the axial fluorine atoms (Figure 39).[64,75,82–84]

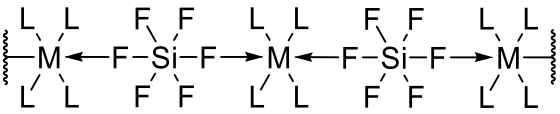

Figure 39: The coordination mode of a hexafluorosilicate pillar in a pillared ionic metal organic framework. L is the organic linker, M is the metal node. Note that formal charges have been excluded.

The four axial fluorine atoms are therefore free to interact with substrates, and give hexafluorosilicate-pillared MOFs a high affinity for Lewis acidic species such as acetylene or carbon dioxide.[64,75,82–84] Interestingly, the hexafluorosilicate anion is also hydrophobic, and as a result hexafluorosilicate-pillared MOFs can have a low affinity for water.[75] It has been demonstrated that the driving factor for the high carbon dioxide affinity in hexafluorosilicate-pillared MOFs is an electrostatic interaction between the equatorial fluorine atoms of the hexafluorosilicate anion and the carbon atom of the carbon dioxide (Figure 40).[75,85] Notably, computational work by Forrest *et al*. also found that in SIFSIX-pillared MOFs with sufficiently large pores, a secondary interaction between an oxygen atom of one carbon dioxide molecule and the carbon atom of another helps to increase the carbon dioxide capacity of the material.[85]

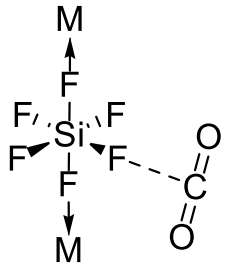

Figure 40: The interaction between a SIFSIX pillar and a guest carbon dioxide molecule.

2.1.3 Goals and target materials

The overarching goal of this work is to synthesize an ionic MOF incorporating hexafluorosilicate pillars and NHCs. To this end, a series of imidazolium salts with neutral coordinating sites were designed (Figure 41). These linkers all contain a central imidazolium or benzimidazolium cation with two pyridylmethyl "arms" that should allow them to coordinate to two metal centres and form coordination polymers. The methylene spacers between the pendant pyridines and the cationic cores mean that these linkers are somewhat flexible; this could allow a MOF prepared from this linker to exhibit breathing behaviour.

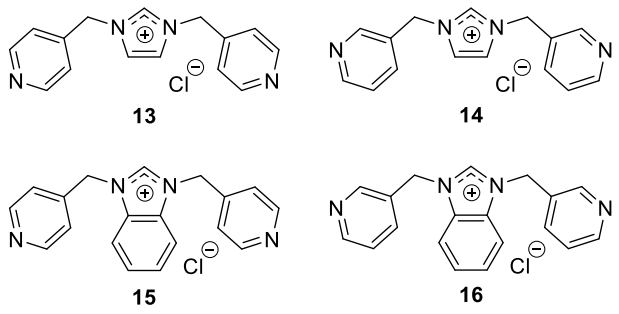

Figure 41: The structures of the four target linkers in this work.

Based on previous studies of SIFSIX-pillared MOFs with pyridine-based linkers such as 4,4'-bipyridine[86] and 1,2-bis(4-pyridyl)acetylene[87], it is expected that the metal nodes should have octahedral geometry with the linkers at the four equatorial positions and the SIFSIX pillars at the two axial positions (Figure 42).

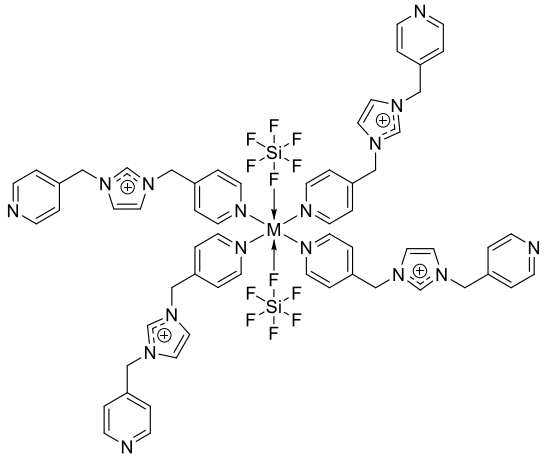

Figure 42: The environment around a node (M) of a hypothetical SIFSIX-pillared MOF with **13** as the linker. This is not a depiction of a repeating unit. Note that some formal charges and counterions have been excluded.

2.2 Results and discussion

2.2.1 Synthesis of the linkers

The synthesis of the target linkers in this work is challenging, as the most obvious route – shown in **Scheme 10** – presents a major drawback; the starting material, (chloromethyl)pyridine, polymerizes at a rate competitive with the desired reaction. The resulting polymeric material is not easily separable from the desired product when present in large amounts.

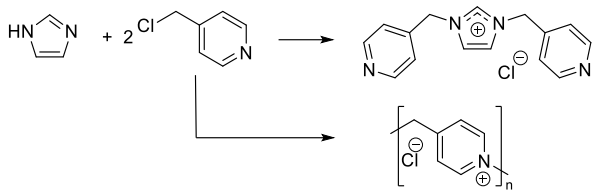

Scheme 10: The reaction and competitive side reaction in the most obvious route to the linkers.

As such, there are very few reports of this class of linkers in the literature; the successful synthesis of **13** has been reported on one occasion[88] and O'Hearn outlined several unsuccessful approaches – and was unable to replicate the results of Siraj and Spicer.[89] Thus, **13** was selected as a model for the four target linkers and several synthetic routes were explored, summarized in Table 1.

Table 1: The conditions explored for the synthesis of **13**.

Entry #	**Strategy**	**Reactants**
1	Imidazolate	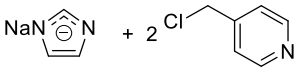
2	Protecting group	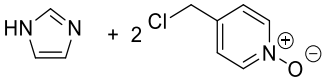
3	Protecting group	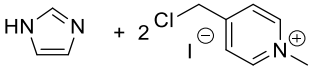
4	Protecting group	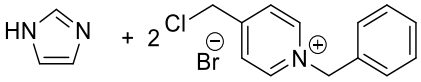
5	Ring building	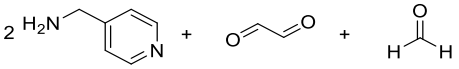
6	Sequential addition	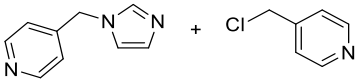

The first route explored was the route used by Siraj and Spicer, in which an imidazolate anion is generated first, then reacted with two equivalents of 4-(chloromethyl)pyridine hydrochloride.[88] O'Hearn found that generation of the imidazolate anion with sodium hydride also led to decomposition of the solvents DMF and acetonitrile, and the products of these decomposition processes could not be separated.[89] As such, THF was selected as a solvent that would not decompose in the presence of sodium hydride. An additional alteration was made from the procedure used by Siraj and Spicer; instead of freebasing the 4-(chloromethyl)pyridine separately then adding it to the solution of sodium imidazolate, two equivalents of solid 4-(chloromethyl)pyridine hydrochloride was added directly to the mixture containing one equivalent of sodium imidazolate and two equivalents of sodium hydride in dry THF cooled on ice. This is because it was observed that 4-(chloromethyl)pyridine beings to polymerize as soon as it is freebased, before it can be added to the reaction. After stirring for 5 days at room temperature, an aliquot of the reaction mixture was analyzed by ^{1}H NMR and the distinctive C2 proton peak above 9 ppm was not observed. The reaction was refluxed for a further four days, but ^{1}H NMR still did not show the distinctive C2 proton peak. It was clear that THF was a poor solvent for this reaction, so after cooling the reaction to room temperature the volume was decreased under vacuum and acetonitrile was added. After an additional 3 days, ^{1}H NMR showed the presence of a small C2 proton peak, but it was clear that the reaction was still extremely slow (Figure 43).

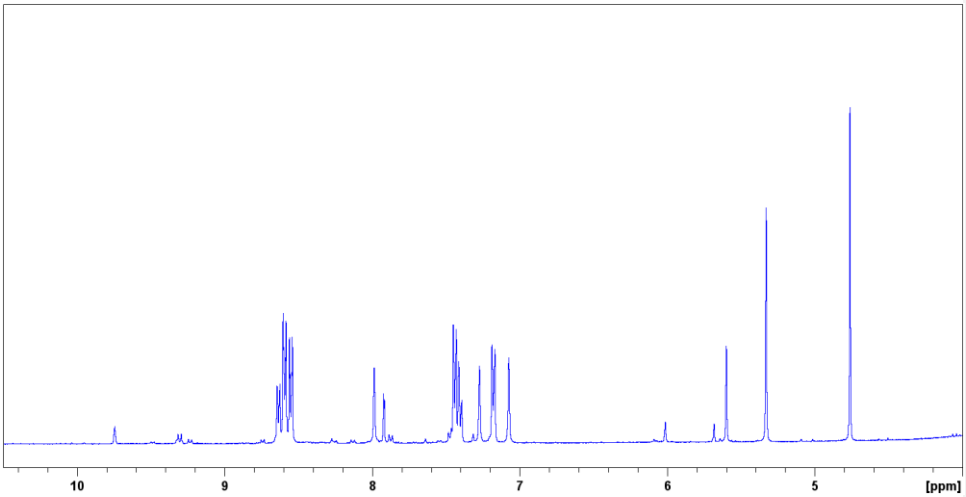

Figure 43: The ^{1}H NMR spectrum of an aliquot of the reaction between sodium hydride, sodium imidazolate, and 4-(chloromethyl)pyridine hydrochloride. Note the small peak near 9.8 ppm indicating formation of **13**, along with 3 peaks between 4.6 and 5.6 ppm indicating three different sets of benzylic protons.

The ^{1}H NMR spectrum in Figure 43 also has a small doublet at 9.3 ppm, indicating the formation of the polymeric by-product. Since the ^{1}H NMR spectrum suggests that there is a large amount of this by-product relative to the desired product, the reaction was abandoned. The other notable feature in this NMR spectrum is the three singlets around 4.8, 5.3, and 5.6 ppm, corresponding to 4-(chloromethyl)pyridine, an intermediate shown in Figure 44, and the desired product. The structure of this intermediate was determined later, and it would prove key to the eventual synthesis of **13** and **14**.

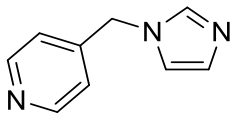

Figure 44: The structure of the intermediate observed in the reaction mixture.

After the route described by Siraj and Spicer could not be replicated, a variety of protecting groups for the reactive nitrogen atom in 4-(chloromethyl)pyridine were attempted. The first of these was a *N*-oxide.

4-(chloromethyl)pyridine *N*-oxide was synthesized from 4-(chloromethyl)pyridine hydrochloride with magnesium monoperoxyphthalate (MMPP) and sodium carbonate in water. However, this process has several limitations. First, the reaction time is highly inconsistent; the time taken for the reaction to reach completion varied from 24 hours to 5 days even when the reaction conditions were kept as consistent as possible. Similarly, the physical appearance – colour and turbidity – of the reaction also varied, as did the amount of MMPP required to achieve complete oxidation. Second, previous work by Tilley *et al.* found that 4-(chloromethyl)pyridine *N*-oxide can not be isolated out of solution, as it decomposes.[90] This was corroborated in this work. Nonetheless, a high-purity product was isolated by adding brine to the reaction mixture and extracting with THF. Conversion could be monitored by extracting from the reaction mixture into $CDCl_3$ in a test tube and performing ^1H NMR (Figure 45). The spectroscopic handle in this case is the upfield shift of one of the aromatic signals.

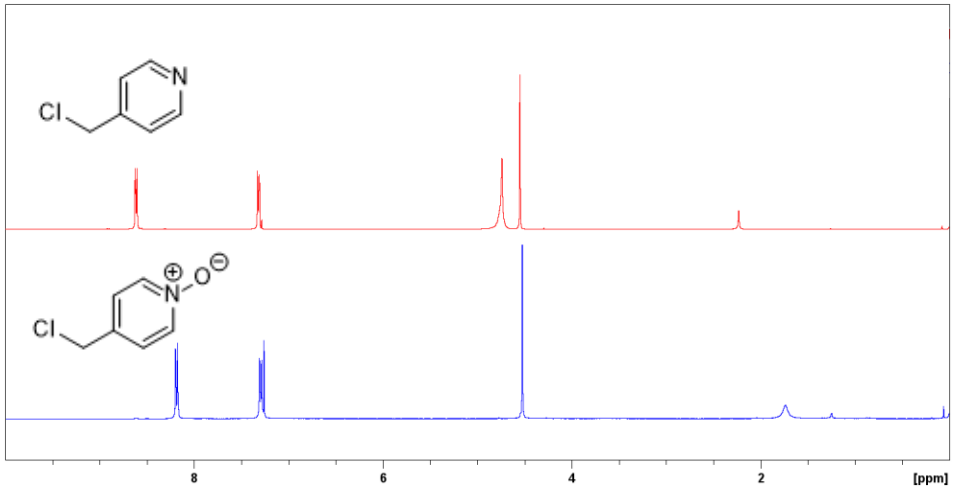

Figure 45: The ^{1}H NMR spectra of 4-(chloromethyl)pyridine (top) and 4-(chloromethyl)pyridine *N*-oxide (bottom), indicating that the oxidation in question has gone to completion.

However, this approach meant that determining yield was challenging. When 0.1 equivalents of imidazole was added to the extract, ^{1}H NMR spectroscopy of the reaction mixture even after a long reaction time indicated that the only product was a monosubstituted imidazole (Figure 46).

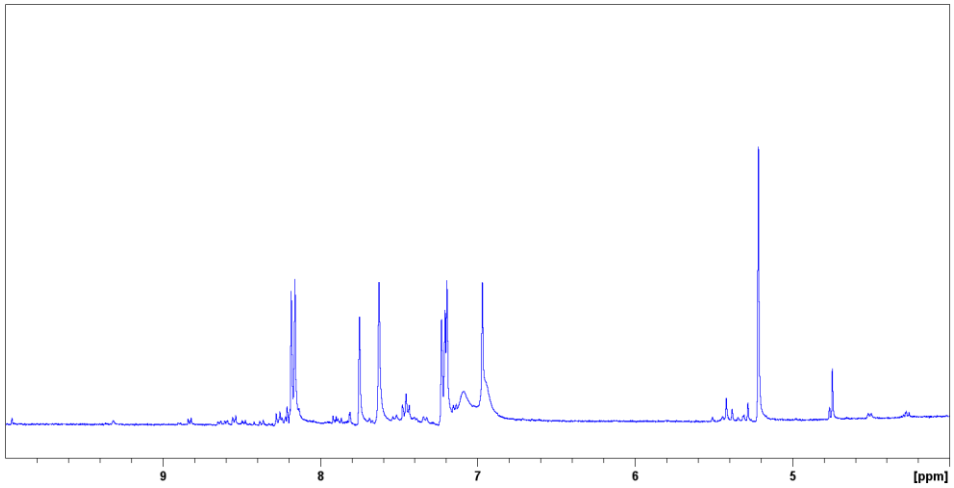

Figure 46: The ^{1}H NMR spectrum of the reaction mixture of imidazole and 4-(chloromethyl)pyridine *N*-oxide. Note the lack of peaks above 9 ppm.

Due to the combination of extremely low yields and the unreliable nature of the oxidation, this approach was abandoned.

The other two protecting groups that were explored were *N*-methyl and *N*-benzyl groups. These were far from optimal protecting groups, as they could be removed by nucleophiles – such as imidazole. Indeed, one known method to remove *N*-methyl groups from pyridinium cations is to treat with 1-methylimidazole,[91] so it seems unlikely that the methyl group in particular would be a suitable protecting group. However, it is possible that nucleophilic attack at the benzylic carbon would be preferred because chloride is a better leaving group than pyridinium (Figure 47).

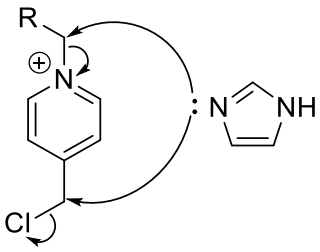

Figure 47: Possible sites of nucleophilic attack on an alkyl-protected 4-(chloromethyl)pyridine. R = H, C_6H_5.

Methylation of 4-(chloromethyl)pyridine was attempted with iodomethane in acetonitrile. However, this method was unsuccessful as the polymerization of 4-(chloromethyl)pyridine was competitive with methylation (Figure 48).

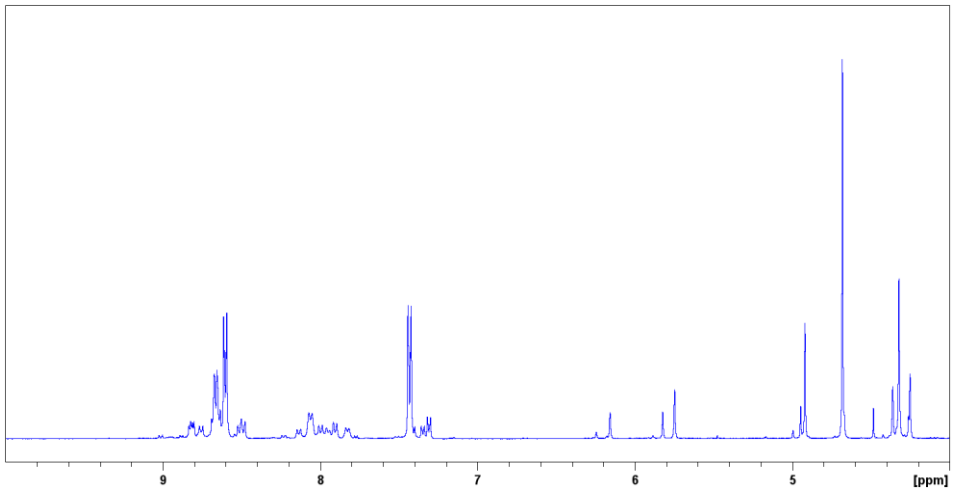

Figure 48: The ^{1}H NMR spectrum of the reaction mixture from the methylation of 4-(chloromethyl)pyridine with iodomethane. Note the many small peaks in the aromatic region indicating the formation of a mix of (likely polymeric) products.

Benzylation with benzyl bromide in methanol had the same problem as methylation with iodomethane; the rate of polymerization was competitive with it. Thus, both alkyl protecting groups were abandoned.

The last unsuccessful route explored avoided 4-(chloromethyl)pyridine completely, instead building the imidazolium core from glyoxal, formaldehyde, hydrochloric acid, and two equivalents of 4-(aminomethyl)pyridine. This route was chosen because by changing the starting material one avoids the polymerization reaction entirely. When glyoxal and the amine were mixed in water, a yellow precipitate formed rapidly; using a combination of 1D and 2D NMR spectra, a structure was tentatively assigned (Figure 49). Although the reaction conditions were varied extensively, this was the only product that could be isolated – and no pure material could be isolated from many reactions.

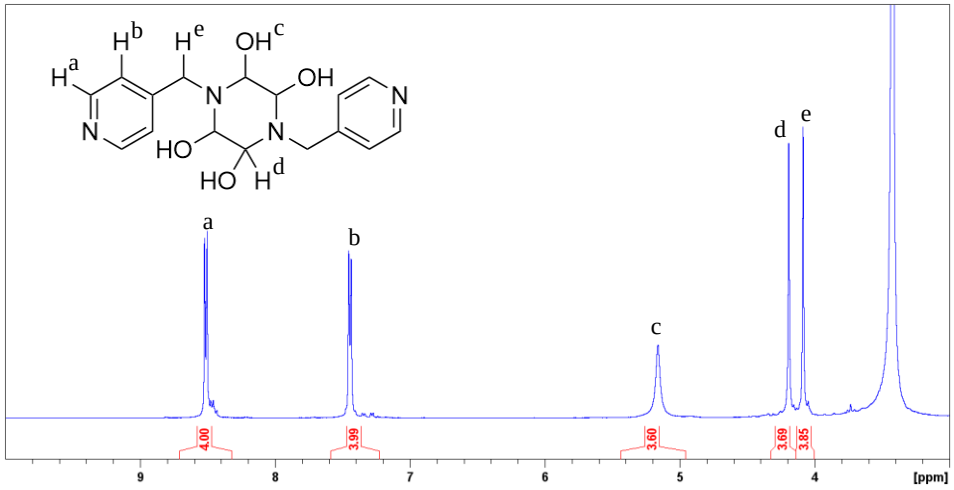

Figure 49: the ^{1}H NMR spectrum and proposed structure of the precipitate formed from the reaction of glyoxal and two equivalents of 4-(aminomethyl)pyridine in water.

Upon re-examination of the NMR data from the using sodium imidazolate and further consideration of the reaction pathway, another approach was developed. It was hypothesized that the reaction must pass through a monosubstituted imidazole intermediate – shown in **Scheme 11** – and that isolation of this intermediate would allow greater control over the reaction conditions in the second step.

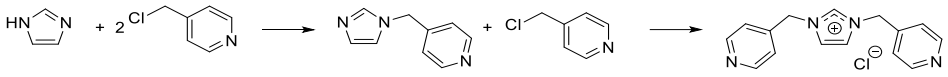

Scheme 11: The expected pathway of the reaction to produce the target linkers. Note that **13** is being used as an example structure.

To this end, the four monosubstituted intermediates were prepared based on a literature method that was modified for microwave-assisted synthesis.[92] One equivalent of 3- or 4-(chloromethyl)pyridine hydrochloride was mixed with the desired core and excess sodium hydroxide in acetonitrile, then microwaved at 80°C for 1 hour. This produced the monosubstituted azoles **17** – **20** in very good to excellent yields (**Scheme 12**).

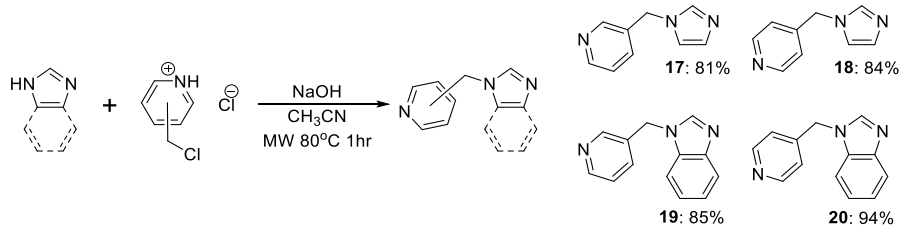

Scheme 12: The general reaction conditions used to produce the 1-(pyridylmethyl)imidazoles **17** – **20**, precursors to the target ligands **13 – 16**.

These monosubstituted azoles were refluxed with 0.25 equivalents of 3- or 4-(chloromethyl)pyridine hydrochloride and excess sodium carbonate in acetonitrile for 24 hours

(**Scheme 13**). The intermediate was used in excess as this meant that the desired product would be kinetically favoured over the polymer. The target linkers were recrystallized, and the excess intermediates could be recovered from the supernatant by rotary evaporation and extraction from water into DCM.

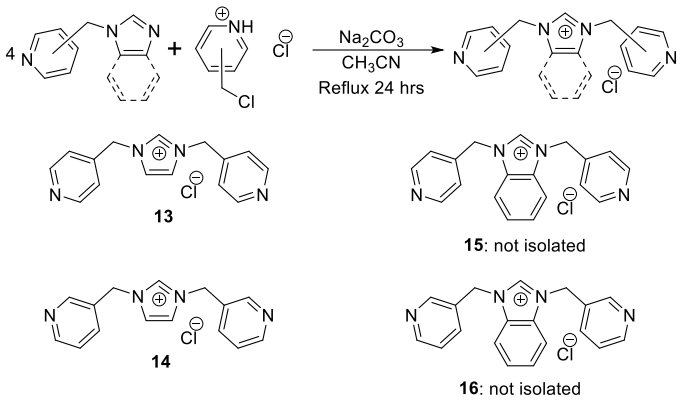

Scheme 13: The general reaction conditions used to prepare the target ligands **13** – **16**. Only **13** and **14** were isolated, although the formation of **15** and **16** was observed by NMR.

13 and **14** were isolated in moderate yields *via* this method, but **15** and **16** were not. The NMR spectrum of the reaction of **20** with 4-(chloromethyl)pyridine – shown in Figure 50– suggests that reaction at the nitrogen atom of the pendant pyridine is preferred to reaction at the nitrogen atom at the 3-position benzimidazole. The NMR spectrum of the reaction of **19** with 3-(chloromethyl)pyridine indicates the same. Both NMR spectra show the presence of a pyridinium salt in similar concentrations to the target benzimidazolium salt. Efforts to separate the target compound have been unsuccessful.

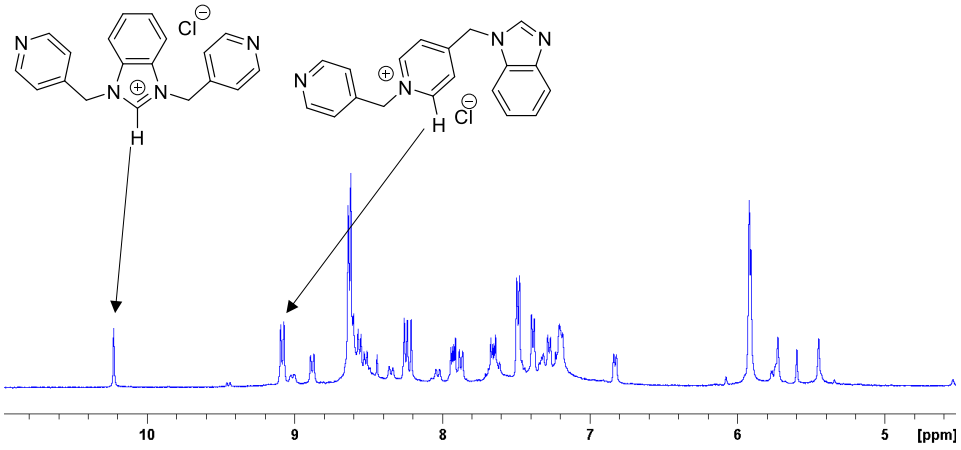

Figure 50: ^{1}H NMR spectrum of the crude reaction mixture containing **15** and a major by-product. Select peaks corresponding to the benzimidazolium and pyridinium salts are indicated. Note that the pyridinium salt shown is a proposed structure of the by-product.

2.2.2 Reactions of the linkers with metals

Several efforts were made to prepare and isolate metal complexes of **13** and **14**, however none yielded a product on which structural characterization could be performed. Only nickel(II) and copper(II) cations were used in these efforts, however, other conditions, such as temperature, solvent, counterion to the metal salt of the starting material, reaction time, and recrystallization conditions were varied (Table 2).

Table 2: The reaction conditions between **13** or **14** and metal cations in an effort to prepare a MOF.

Entry #	**Linker**	**Metal salt**	**Other reagents**	**Reaction conditions**
1	13	$NiSiF_6 \cdot 6H_2O$		Ethanol/water, RT
2	13	$CuSO_4 \cdot 7H_2O$	$(NH_4)_2SiF_6$	Ethanol/water, RT
3	13	$Cu(BF_4)_2 \cdot xH_2O$		Methanol, RT

4	13	$NiSiF_6 \cdot 6H_2O$		Ethylene glycol, MW 120°C
5	13	$NiCl_2 \cdot 6H_2O$		Methanol, RT
6	13	$NiCl_2 \cdot 6H_2O$		Refluxing ethanol then RT ethylene glycol
7	13	$Cu(BF_4)_2 \cdot xH_2O$	$(NH_4)_2SiF_6$	Water, RT, then heating
8	14	$NiSiF_6 \cdot 6H_2O$		Methanol, RT
9	13	$NiSiF_6 \cdot 6H_2O$	HCl, then triethylamine	Methanol, RT
10	14	$Cu(BF_4)_2 \cdot xH_2O$	$(NH_4)_2SiF_6$	Methanol/water, RT
11	13	$NiSiF_6 \cdot 6H_2O$		Water, 100°C

In Entry 1, a room temperature ethanolic solution of **13** was layered onto a cold aqueous solution of nickel(II) hexafluorosilicate hexahydrate. A brown precipitate began to form immediately at the interface. As a control reaction, a room temperature ethanolic solution of **13** was layered onto a cold aqueous solution of potassium hexafluorosilicate; no precipitate formed, indicating that the nickel cations are essential to the formation of the precipitate. This precipitate was examined by scanning electron microscopy (SEM) and energy-dispersive X-ray (EDX) spectroscopy (Figure 51). SEM images showed that the material is not microcrystalline; instead, it is an extremely porous, amorphous solid. EDX spectroscopy showed that all expected elements were present. However, no evidence about the connectivity in the sample could be determined.

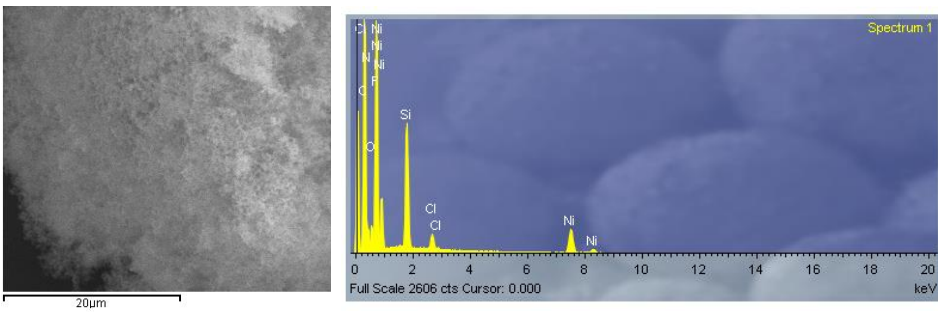

Figure 51: A SEM image of the brown precipitate collected from the reaction of **13** and $NiSiF_6 \cdot 6H_2O$ (left) and an EDX spectrum of the same material (right).

Entry 2 is analogous to entry 1, but copper cations were used instead of nickel cations. Also, ammonium hexafluorosilicate was used as the hexafluorosilicate source. Again, a brown precipitate began to form immediately at the solvent interface.

All other entries were efforts to prepare a crystalline product, and all resulted in the formation of an amorphous brown precipitate. Entries 5 and 6 were an effort to prepare a 2D coordination polymer from the linker and nickel(II) chloride hexahydrate, which could be pillared in a second step. Entries 4, 7, and 11 all involved heating the reaction mixture in an effort to encourage crystallization. Entry 9 proceeded *via* a different pathway; it was observed that the brown precipitate produced in prior reactions was soluble in acid, so it was dissolved in acid and a vapour diffusion with triethylamine was performed in order to force it to precipitate more slowly.

It was found that the brown precipitate was sparingly soluble in ethylene glycol, but it could not be recrystallized. Interestingly, when a solution in ethylene glycol was left for one month at room temperature, it changed colour from a brown solution to light red. This product could not be recrystallized either.

It is possible that the flexibility of the linkers is hindering their ability to form crystalline MOFs.

2.3 Conclusions

Two ligands with central imidazolium cations and two pendant pyridines with the proper substitution pattern to act as linkers in MOFs were synthesized in moderate yield by a novel stepwise addition route. Unfortunately, the other two target linkers could not be isolated by this route, although they were detected in solution. Reaction of both linkers with copper(II) and nickel(II) salts in a variety of conditions yield poorly soluble, amorphous brown solids. Examination of some of these materials by SEM and EDX revealed that they are extremely porous, with elemental composition corresponding to the desired product, but no information regarding connectivity could be obtained.

2.4 Future work

The two main directions for this work moving forward would be the development of synthetic routes to **15** and **16**, as well as synthesis of a crystalline MOF based on **13** or **14**. Some other possible avenues to investigate would be a new target linker with a more rigid structure, and exploring CO_2 sorption by the amorphous materials.

It is possible that a protecting group or ring-building method is necessary for the synthesis of **15** and **16**. A ring-building method from o-diaminobenzene and pyridinecarboxaldehyde – as shown in **Scheme 14** – may be effective.

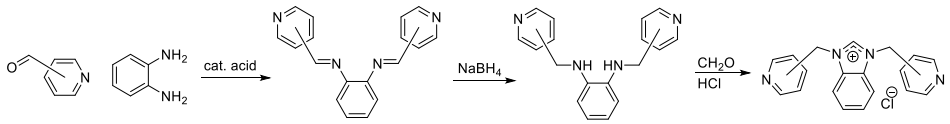

Scheme 14: The proposed synthesis of **15** and **16** by ring building.

Further efforts toward the synthesis of a crystalline MOF will likely involve simply varying conditions. For example, DMSO and DMF may be suitable solvents for this reaction. It is also possible that heating will be required to form a crystalline product.

It may also be worth exploring gas sorption by the amorphous materials collected from the reaction of **13** and **14** with nickel(II) and copper(II) salts; although these materials are amorphous, they may still be effective in CO_2 capture.

One final avenue of exploration would be the development of a more rigid NHC-functionalised linker. It is possible that the reason that all observed products from the reactions of **13** and **14** yielded amorphous products is that both linkers are flexible, so a rigid linker could help to lead to a crystalline product. There is some literature precedence for this; a MOF prepared from a rigid dicarboxylate NHC linker was found to be crystalline,[93] and when decorated with copper(I) atoms on some of the NHCs in the pores, was highly effective in CO_2 uptake and fixation.[57] It is likely that a similar linker with neutral donors may be applicable in this work, and could be synthesized by ring building from formaldehyde, glyoxal, a Brønsted acid, and an amine (**Scheme 15**).

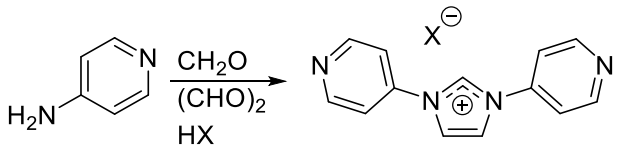

Scheme 15: The structure and proposed synthesis of a rigid linker with neutral donating sites.

2.5 Experimental

2.5.1 Materials and general considerations

All reagents and solvents were purchased from Millipore Sigma, Alfa Aesar, Fisher Scientific, or Oakwood chemicals and used without further purification unless otherwise specified. Deuterated NMR solvents were purchased from Cambridge Isotopes. NMR spectra were collected using a Bruker 300 MHz Ultrashield spectrometer. IR spectra were collected using a Bruker ALPHA ATR with a single reflection ZnSe crystal. ESI-MS data was collected by Xiao Feng at Dalhousie University using a Bruker Compact QTOF mass spectrometer. Scanning electron microscopy and energy dispersive X-ray spectroscopy were performed by Xiang Yang using a TESCAN Mira3 LMU scanning electron microscope and Oxford Instruments INCA X-max 80mm^2 EDS system.

2.5.2 Successful syntheses of the linkers

2.5.2.1 Synthesis of 1,3-bis(4-pyridylmethyl)imidazolium chloride (13)

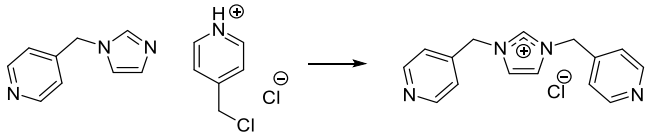

In a 50mL round-bottom flask equipped with a stir bar, 1-(3-pyridylmethyl)imidazole (10.00mmol, 1.592g) was dissolved in 20mL of acetonitrile. Powdered sodium carbonate (3g) was added, followed by 4-(chloromethyl)pyridine hydrochloride (2.50mmol, 0.410g). This mixture was stirred at room temperature for 5 minutes, then a condenser was attached and the mixture was heated to reflux for 24 hours. After cooling to room temperature, the reaction was gravity filtered and the filter paper was washed with acetonitrile. Solvent was removed from the filtrate by rotary evaporation, and the resulting black oil was dissolved in minimal methanol. Vapour diffusion with

diethyl ether afforded 1,3-bis(4-pyridylmethyl)imidazolium chloride. The supernatant was decanted and the precipitated 1,3-bis(4-pyridylmethyl)imidazolium chloride was washed with diethyl ether. The supernatant and washings were combined and solvent was removed by rotary evaporation, redissolved in 20mL of deionized water, and extracted with 3x10mL of dichloromethane. The organic fraction was dried of magnesium sulfate and gravity filtered. Solvent was removed by rotary evaporation to recover the excess 1-(4-pyridylmethyl)imidazole. 1,3-bis(4-pyridylmethyl)imidazolium chloride was afforded as a hygroscopic dark brown solid (0.287g, 40%).

IR (ATR, cm^{-1}): 3035.47 (m), 2979.98 (m), 1632.02 (s), 1601.24 (s), 1415.80 (s).

^{1}H NMR (DMSO-d_6, 300MHz): δ 9.50 (s, 1H), 8.63 (d, *J*=5.91 Hz, 4H), 7.92 (s, 2H), 7.36 (d, *J*=5.80 Hz, 4H), 5.55 (s, 4H)

^{13}C NMR (DMSO-d_6, 75MHz): δ 150.7, 144.0, 137.9, 123.9, 123.1, 51.4

ESI-MS (+): Calcd for $C_{15}H_{15}N_4^+$ m/z: 251.1. Found 251.1.

HRMS (+): Calcd for $C_{15}H_{15}N_4^+$ m/z: 251.1291. Found 251.1285.

2.5.2.2 Synthesis of 1,3-bis(3-pyridylmethyl)imidazolium chloride (14)

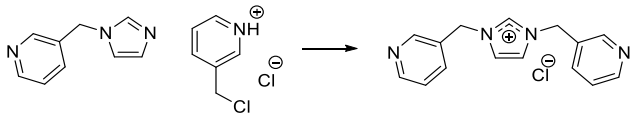

Compound **14** was prepared following the same procedure used for **13**. **14** was isolated as a dark brown hygroscopic solid (0.251g, 35%).

FT-IR (ATR, cm^{-1}): 3055.63 (m), 2993.62 (m), 1594.81 (s), 1578.98 (s), 1558,75 (s), 1427.63 (s).

^{1}H NMR (DMSO-d6, 300MHz): δ 9.74 (s, 1H), 8.72 (s, 2H), 8.57 (d, J=4.66 Hz, 2H), 7.93 (m, 4H), 7.43 (dd, J=4.70 Hz, 2H), 5.55 (s, 4H).

^{13}C NMR (DMSO-d6, 75MHz): δ 150.0, 149.8, 136.9, 136.5, 130.6, 124.0, 123.0, 49.7.

ESI-MS (+): Calcd for $C_{15}H_{15}N_4^+$ m/z: 251.13. Found 251.1.

HRMS (+): Calcd for $C_{15}H_{15}N_4^+$ m/z: 251.1291. Found 251.1285.

5.2.5 Synthesis of 1-(3-pyridylmethyl)imidazole (17)

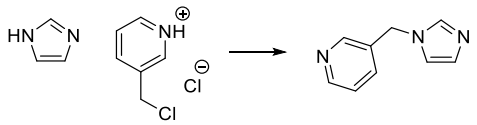

In a 50mL round-bottom flask equipped with a stir bar, imidazole (10.00mmol, 0.681g) was dissolved in 20mL of acetonitrile. Powdered sodium hydroxide (30mmol, 1.20g) was added, followed by 3-(chloromethyl)pyridine hydrochloride (10.00mmol, 1.640g). The reaction was stirred for 5 minutes a room temperature, then the reaction vessel was placed in a CEM Discover SP microwave reactor with the following parameters: 50 W, 80°C, 1 hour, high stirring. After the reaction vessel had cooled, the acetonitrile was removed by rotary evaporation. The resulting solid residue was taken up in 30mL of deionized water and extracted with 5x15mL of dichloromethane. The dichloromethane fraction was dried over anhydrous magnesium sulfate and gravity filtered. Solvent was removed by rotary evaporation and the resulting orange solid was dried under high vacuum (1.289g, 81%).

FT-IR (ATR, cm^{-1}): 3105.58 (w), 1671.63 (w), 1593.90 (w), 1578.52 (m), 1504.51 (s), 1480.21 (m), 1427.20 (s).

^{1}H NMR (DMSO-d_6, 300MHz): δ 8.57 (d, *J*=3.97 Hz, 1H), 8.50 (s, 1H), 7.54 (s, 1H), 7.41 (d, *J*=7.81 Hz, 1H), 7.27 (m, 1H), 7.09 (s, 1H), 6.88 (s, 1H), 5.13 (s, 2H).

^{13}C NMR (DMSO-d_6, 75MHz): δ 140.0, 148.8, 137.4, 135.0, 132.0, 130.5, 124.0, 119.2, 48.4.

ESI-MS (+): Calcd for $C_9H_{10}N_3$ (M+H) m/z: 160.2. found 160.1.

HRMS (+): Calcd for $C_9H_{10}N_3$ (M+H) m/z: 160.0869. found 160.0863.

5.2.6 Synthesis of 1-(4-pyridylmethyl)imidazole (18)

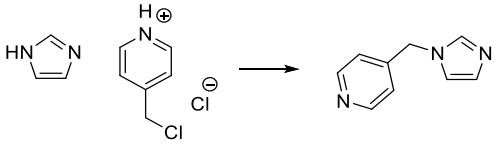

Compound **18** was prepared following the same procedure used for **17** from imidazole (10.00mmol, 0.681g) and 4-(chloromethyl)pyridine hydrochloride (10.00mmol, 1.640g). **8** was isolated as a yellow solid (1.336g, 84%). Single crystals of **8** suitable for single-crystal X-ray crystallography were obtained by slow evaporation of an acetone solution.

FT-IR (ATR, cm^{-1}): 3106.22 (w), 1673.87 (w), 1601.66 (s), 1563.67 (w), 1504.64 (s), 1415.74 (s).

^{1}H NMR ($CDCl_3$, 300MHz): δ 8.59 (d, *J*=5.99 Hz, 2H), 7.56 (s, 1H). 7.14 (s, 1H), 6.99 (d, *J*=5.91 Hz, 2H), 6.90 (s, 1H), 5.15 (s, 2H)

^{13}C NMR ($CDCl_3$, 75MHz): δ 150.7, 145.4, 137.8, 130.6, 121.6, 119.5, 49.6.

ESI-MS (+): Calcd for $C_9H_{10}N_3$ (M+H) m/z: 160.2. found 160.1.

HRMS (+): Calcd for $C_9H_{10}N_3$ (M+H) m/z: 160.0869. found 160.0863.

5.2.7 Synthesis of 1-(3-pyridylmethyl)benzimidazole (19)

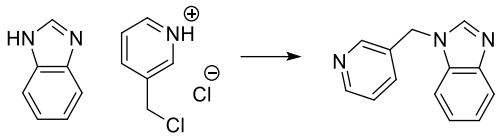

Compound **19** was prepared following the same procedure used for **17** from benzimidazole (10.00mmol, 1.181g) and 3-(chloromethyl)pyridine hydrochloride (10.00mmol, 1.640g). **9** was isolated as a pale yellow solid (1.779g, 85%).

FT-IR (ATR, cm^{-1}): 3087.36 (w), 1707.06 (m), 1494.11 (m), 1427.28 (m), 1360.27 (m).

^{1}H NMR ($CDCl_3$, 300MHz): δ 8.56 (m, 2H), 7.97 (s, 1H), 7.83 (m, 1H) 7.39 (d, *J*=7.91 Hz, 1H), 7.25 (m, 4H), 5.36 (s, 2H)

^{13}C NMR ($CDCl_3$, 300MHz): δ 149.8, 148.5, 143.9, 143.0, 134.7, 133.5, 131.3, 124.0, 123.5, 122.6, 120.5, 109.9, 46.3

ESI-MS (+): Calcd for $C_{13}H_{11}N_3$ (M+H) m/z: 210.1. found 210.1.

HRMS (+): Calcd for $C_{13}H_{11}N_3$ (M+H) m/z: 210.1026. found 210.1032.

5.2.8 Synthesis of 1-(4-pyridylmethyl)benzimidazole (20)

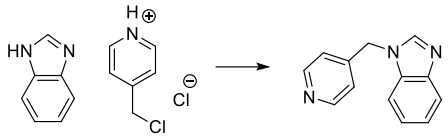

Compound **20** was prepared following the same procedure used for **17** from benzimidazole (10.00mmol, 1.181g) and 4-(chloromethyl)pyridine hydrochloride (10.00mmol, 1.640g). **10** was isolated as a pale yellow solid (1.967g, 94%).

FT-IR (ATR, cm^{-1}): 3055.61 (w), 2928.17 (w), 1602.44 (s), 1496.07 (s), 1459.02 (m), 1416.33 (m).

^{1}H NMR ($CDCl_3$, 300MHz): δ 8.57 (d, J=6.04 Hz, 2H), 7.99 (s, 1H), 7.87 (d, *J*=8.33 Hz, 1H), 7.29 (m, 2H), 7.20 (d, *J*=7.77 Hz, 1H), 7.02 (d, *J*=5.98 Hz, 2H), 5.39 (s, 2H)

^{13}C NMR ($CDCl_3$, 300MHz): δ 150.6, 144.7, 144.0, 143.3, 133.7, 123.6, 122.8, 121.5, 120.8, 109.8, 47.6

ESI-MS (+): Calcd for $C_{13}H_{11}N_3$ (M+H) m/z: 210.1. found 210.1.

HRMS (+): Calcd for $C_{13}H_{11}N_3$ (M+H) m/z: 210.1026. found 210.1032.

2.5.3 Unsuccessful syntheses of the linkers

2.5.3.1 Synthesis of 1,3-bis(3-pyridylmethyl)benzimidazolium chloride (16)

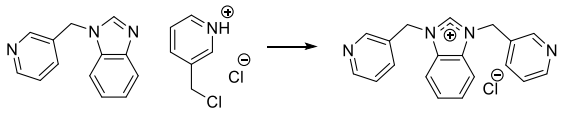

In a 50mL round-bottom flask equipped with a stir bar, 1-(3-pyridylmethyl)benzimidazole (10.00mmol, 2.093g) was dissolved in 20mL of acetonitrile. Powdered sodium carbonate (3g) was added, followed by 3-(chloromethyl)pyridine hydrochloride (2.50mmol, 0.410g). This mixture was stirred at room temperature for 5 minutes, then a condenser was attached and the mixture was heated to reflux for 24 hours. After cooling to room temperature, an aliquot of the reaction mixture was collected and dried under high vacuum. The resulting dark brown residue was dissolved in DMSO-d6. The ^{1}H NMR spectrum collected on the sample indicated that **16** was a minor component of the mixture.

2.5.3.2 Synthesis of 1,3-bis(4-pyridylmethyl)benzimidazolium chloride (15)

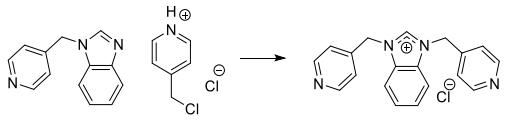

The synthesis of **15** was attempted analogously to **16**, and it was found that **15** was a similarly minor component of the reaction mixture.

2.5.3.3 *N*-oxidation of 4-(chloromethyl)pyridine

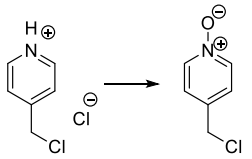

In a round-bottom flask equipped with a stir bar, 4-(chloromethyl)pyridine (10.00mmol, 1.640g) was dissolved in deionized water (15mL). Magnesium monoperoxyphthalate (10.00mmol, 6.183g) and sodium carbonate (7.5mmol, 0.795g) were added and the reaction was stirred at room temperature for 1 hour, at which point more magnesium monoperoxyphthalate (5.00mmol, 3.091g) was added. The reaction was stirred for a further 6 hours, at which point more magnesium monoperoxyphthalate (5.00mmol, 3.091g) was added. After 24 hours from starting the reaction, 5mL of water and 5mL of brine were added and the product was extracted with 3x10mL of THF. The extract was dried over magnesium carbonate and filtered, and imidazole (1.00mmol, 0.640g) was added. Conversion was monitored by ^{1}H NMR.

^{1}H NMR ($CDCl_3$, 300MHz): δ 8.19 (d, J=7.08Hz, 2H), 7.30 (d, J=6.96Hz, 2H), 4.52 (s, 2H).

Commented [J2]:

2.5.3.4 *N*-methylation of 4-(chloromethyl)pyridine with iodomethane

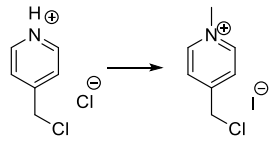

In a round-bottom flask equipped with a stir bar, 4-(chloromethyl)pyridine (5.00mmol, 0.820g) was suspended in acetonitrile (10mL). sodium bicarbonate (10.00mmol, 1.060g) was added, followed by iodomethane (5.50mmol, 0.342mL). The reaction mixture was stirred at room temperature overnight, after which time ^{1}H NMR indicated low conversion to the desired product.

2.5.3.5 *N*-benzylation of 4-(chloromethyl)pyridine with benzyl bromide

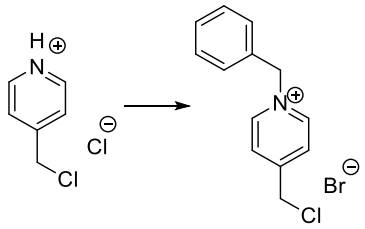

In a round-bottom flask equipped with a stir bar, benzyl bromide (10.00mmol, 1.189mL) was dissolved in methanol (10mL). Sodium carbonate (10.00mmol, 1.060g) was added. Separately, 4-(chloromethyl)pyridine hydrochloride (5.00mmol, 0.820g) was dissolved in methanol (10mL). The solution of 4-(chloromethyl)pyridine hydrochloride was added dropwise to the solution of benzyl bromide and the reaction mixture was stirred at room temperature for 24 hours, at which time ^{1}H NMR indicated low conversion to the desired product.

2.5.3.6 Ring-building from glyoxal and formaldehyde

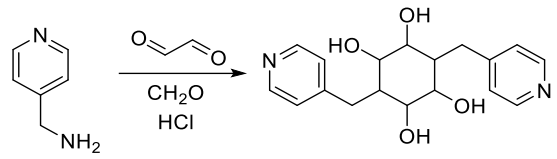

In water:

Aqueous 40% glyoxal (2.50mmol, 0.363mL) was diluted to 5mL with water. 4-(aminomethyl)pyridine (5.00mmol, 0.508mL) was added, and a yellow precipitate formed immediately. The precipitate was collected by vacuum filtration.

^{1}H NMR (DMSO-d6, 300MHz): δ 8.51 (d, J=5.72Hz, 4H), 7.44 (d, J=5.26Hz, 4H), 5.14 (d, J=7.14Hz, 4H), 4.18 (d, J=6.98Hz, 4H), 4.08 (s, 4H).

^{13}C NMR (DMSO-d6, 75MHz): δ 149.5, 143.8, 123.3, 83.5, 51.5.

In dichloromethane:

40% glyoxal (2.50mmol, 0.363mL) was taken up in 5mL of dichloromethane. Anhydrous magnesium sulfate was added to dry the mixture. 4-(aminomethyl)pyridine (5.00mmol, 0.508mL) was added with a few drops of formic acid. After 24 hours, ^{1}H NMR spectroscopy indicated the formation of a likely polymeric product.

In acetonitrile:

The procedure used for dichloromethane was repeated with 5mL of acetonitrile instead of 5mL of dichloromethane, with the same outcome.

2.5.4 Reactions of the linkers with transition metal salts

2.5.4.1 Table 3 entry 1

13 (0.10mmol, 28.7mg) was dissolved in ethanol (2mL). Separately, nickel hexafluorosilicate hexahydrate (0.05mmol, 15.4mg) was dissolved in water (2mL). The solution of nickel hexafluorosilicate hexahydrate was cooled on ice, and the solution of **13** was layered on top of it. A brown precipitate immediately began to form at the interface. A control experiment was performed in which potassium hexafluorosilicate was used in place of nickel hexafluorosilicate hexahydrate; no precipitate was observed.

2.5.4.2 Table 3 entry 2

13 (0.10mmol, 28.7mg) was dissolved in ethanol (2mL). Separately, copper sulfate pentahydrate (0.05mmol, 12.5mg) and ammonium hexafluorosilicate (0.05mmol, 8.9mg) were dissolved in water (2mL). The solution of copper sulfate pentahydrate and ammonium hexafluorosilicate was cooled on ice, and the solution of **13** was layered on top of it. A brown precipitate immediately began to form at the interface.

2.5.4.3 Table 3 entry 3

Separately, **13** (0.10mmol, 28.7mg) and copper(II) tetrafluoroborate hydrate (34.5mg) were each taken up in methanol (1mL). the solution of copper(II) tetrafluoroborate hydrate was cooled on ice, and methanol (0.25mL) was layered on top. This was cooled as well, and the solution of **13** was layered on top. After 24 hours, an amorphous brown precipitate had formed.

2.5.4.4 Table 3 entry 4

13 (0.1mmol, 28.7mg) and nickel hexafluorosilicate hexahydrate (0.05mmol, 15.4mg) were taken up in ethylene glycol (3mL), forming a brown precipitate. This suspension was microwaved at 120°C for 1 hour, after which time no change was observed.

2.5.4.5 Table 3 entry 5

Separately, **13** (0.10mmol, 28.7mg) and nickel(II) chloride hexahydrate (0.10mmol, 23.8mg) were dissolved in methanol (1mL). The solutions were mixed and stirred for 24 hours, during which time an amorphous brown precipitate had formed. This was collected by centrifugation. It was found to be sparingly soluble in DMSO, but could not be recrystallized.

2.5.4.6 Table 3 entry 6

13 (0.10mmol, 28.7mg) and nickel(II) chloride hexahydrate (0.05mmol, 11.9mg) were taken up in ethanol (3mL) and refluxed for 24 hours. The resulting brown precipitate was collected by centrifugation and found to be sparingly soluble in ethylene glycol, but could not be recrystallized.

2.5.4.7 Table 3 entry 7

13 (0.10mmol, 28.7mg), copper(II) tetrafluoroborate hydrate (17.3mg) and ammonium hexafluorosilicate (0.05mmol, 8.9mg) were taken up in water (10mL). After 3 days at room temperature, there was no visible change, so the reaction was microwaved at 120°C for 2 hours.

2.5.4.8 Table 3 entry 8

14 (0.10mmol, 28.7mg) was dissolved in methanol (1mL). Separately, nickel(II) hexafluorosilicate hexahydrate (0.05mmol, 15.4mg) was dissolved in a mixture of methanol (4mL) and water (2mL). The solutions were mixed, resulting in an immediate amorphous brown precipitate.

2.5.4.9 Table 3 entry 9

13 (0.10mmol, 28.7mg) and nickel(II) hexafluorosilicate hexahydrate (0.05mmol, 15.4mg) were taken up in methanol (3mL), resulting in an immediate brown precipitate. Aqueous 6M

hydrochloric acid was added dropwise until all solids had fully dissolved. A vapour diffusion was set up with triethylamine. After 24 hours, an amorphous brown precipitate had formed.

2.5.4.10 Table 3 entry 10

14 (0.10mmol, 28.7mg) was dissolved in methanol (2mL). Separately, copper(II) tetrafluoroborate hydrate (17.3mg) and ammonium hexafluorosilicate (0.05mmol, 8.9mg) were dissolved in water (2mL). The solution of **14** was layered onto the solution of copper(II) tetrafluoroborate hydrate (17.3mg) and ammonium hexafluorosilicate, and an amorphous brown precipitate began forming at the interface immediately.

2.5.4.11 Table 3 entry 11

13 (0.10mmol, 28.7mg) and nickel(II) hexafluorosilicate hexahydrate (0.05mmol, 15.4mg) were each dissolved in water (5mL). The solutions were mixed and refluxed for 3 days, during which time an amorphous brown precipitate formed.

3. References

(1) Zhou, Q.-L. Transition-Metal Catalysis and Organocatalysis: Where Can Progress Be Expected? *Angewandte Chemie International Edition* **2016**, *55* (18), 5352–5353. https://doi.org/10.1002/anie.201509164.

(2) The Nobel Prize in Chemistry 2010.

(3) Ludwig, J. R.; Schindler, C. S. Catalyst: Sustainable Catalysis. *Chem* **2017**, *2* (3), 313–316. https://doi.org/10.1016/J.CHEMPR.2017.02.014.

(4) Zweig, J. E.; Kim, D. E.; Newhouse, T. R. Methods Utilizing First-Row Transition Metals in Natural Product Total Synthesis. *Chemical Reviews*. American Chemical Society September 27, 2017, pp 11680–11752. https://doi.org/10.1021/acs.chemrev.6b00833.

(5) Hopkinson, M. N.; Richter, C.; Schedler, M.; Glorius, F. An Overview of N-Heterocyclic Carbenes. *Nature* **2014**, *510* (7506), 485–496. https://doi.org/10.1038/nature13384.

(6) Arduengo, A. J.; Harlow, R. L.; Kline, M. A Stable Crystalline Carbene. *J Am Chem Soc* **1991**, *113* (1), 361–363. https://doi.org/10.1021/ja00001a054.

(7) Herrmann, W. A.; Elison, M.; Fischer, J.; Köcher, C.; Artus, G. R. J. Metal Complexes of N-Heterocyclic Carbenes—A New Structural Principle for Catalysts in Homogeneous Catalysis. *Angewandte Chemie International Edition in English* **1995**, *34* (21), 2371–2374. https://doi.org/10.1002/anie.199523711.

(8) Nelson, D. J.; Nolan, S. P. Quantifying and Understanding the Electronic Properties of N-Heterocyclic Carbenes. *Chemical Society Reviews* **2013**, *42* (16), 6723–6753. https://doi.org/10.1039/c3cs60146c.

(9) Jahnke, M. C.; Pape, T.; Hahn, F. E. Synthesis and Catalytic Application of Palladium Complexes with Picoline-Functionalized Benzimidazolin-2-Ylidene Ligands. *European Journal of Inorganic Chemistry* **2009**, No. 13 SPEC. ISS., 1960–1969. https://doi.org/10.1002/ejic.200801214.

(10) Wanzlick, H.-W.; Schönherr, H.-J. Direct Synthesis of a Mercury Salt-Carbene Complex. *Angewandte Chemie International Edition in English* **1968**, *7* (2), 141–142. https://doi.org/10.1002/anie.196801412.

(11) Díez-González, S.; Marion, N.; Nolan, S. P. N-Heterocyclic Carbenes in Late Transition Metal Catalysis. *Chemical Reviews* **2009**, *109* (8), 3612–3676. https://doi.org/10.1021/cr900074m.

(12) Jamil, M. S. S.; Endot, N. A. Influence of Fluorine Substituents on the Electronic Properties of Selenium-N-Heterocyclic Carbene Compounds. *Molecules* **2020**, *25* (21). https://doi.org/10.3390/molecules25215161.

(13) Leyssens, T.; Peeters, D.; Orpen, A. G.; Harvey, J. N. How Important Is Metal - Ligand Back-Bonding toward YX3 Ligands (Y = N, P, C, Si)? An NBO Analysis. *Organometallics* **2007**, *26* (10), 2637–2645. https://doi.org/10.1021/om061151z.

(14) Lee, M. T.; Hu, C. H. Density Functional Study of N-Heterocyclic and Diamino Carbene Complexes: Comparison with Phosphines. *Organometallics* **2004**, *23* (5), 976–983. https://doi.org/10.1021/om0341451.

(15) Dorta, R.; Scott, N. M.; Costabile, C.; Cavallo, L.; Hoff, C. D.; Nolan, S. P. Steric and Electronic Properties of N-Heterocyclic Carbenes (NHC): A Detailed Study on Their Interaction with Ni(CO)4. *J Am Chem Soc* **2005**, *127* (8), 2485–2495. https://doi.org/10.1021/ja0438821.

(16) Ghavami, Z. S.; Anneser, M. R.; Kaiser, F.; Altmann, P. J.; Hofmann, B. J.; Schlagintweit, J. F.; Grivani, G.; Kühn, F. E. A Bench Stable Formal Cu(Iii): N - Heterocyclic Carbene Accessible from Simple Copper(Ii) Acetate. *Chemical Science* **2018**, *9* (43), 8307–8314. https://doi.org/10.1039/c8sc01834k.

(17) Zhou, Y.; Xi, Z.; Chen, W.; Wang, D. Dinickel(II) Complexes of Bis(N-Heterocyclic Carbene) Ligands Containing [Ni2(μ-OH)] Cores as Highly Efficient Catalysts for the Coupling of Aryl Chlorides. *Organometallics* **2008**, *27* (22), 5911–5920. https://doi.org/10.1021/om800711g.

(18) Bansal, S.; Shabade, A. B.; Punji, B. Advances in C(Sp2)−H/C(Sp2)−H Oxidative Coupling of (Hetero)Arenes Using 3d Transition Metal Catalysts. *Advanced Synthesis and Catalysis*. John Wiley and Sons Inc April 13, 2021, pp 1998–2022. https://doi.org/10.1002/adsc.202001498.

(19) Hupp, B.; Schiller, C.; Lenczyk, C.; Stanoppi, M.; Edkins, K.; Lorbach, A.; Steffen, A. Synthesis, Structures, and Photophysical Properties of a Series of Rare Near-IR Emitting Copper(I) Complexes. *Inorganic Chemistry* **2017**, *56* (15), 8996–9008. https://doi.org/10.1021/acs.inorgchem.7b00958.

(20) Whittaker, A. M.; Rucker, R. P.; Lalic, G. Catalytic SN2′-Selective Substitution of Allylic Chlorides with Arylboronic Esters. *Organic Letters* **2010**, *12* (14), 3216–3218. https://doi.org/10.1021/ol101171v.

(21) Santoro, O.; Collado, A.; Slawin, A. M. Z.; Nolan, S. P.; Cazin, C. S. J. A General Synthetic Route to [Cu(X)(NHC)] (NHC = N-Heterocyclic Carbene, X = Cl, Br, I) Complexes. *Chemical Communications* **2013**, *49* (89), 10483–10485. https://doi.org/10.1039/c3cc45488f.

(22) Suresh, L.; Finnstad, J.; Törnroos, K. W.; le Roux, E. Bis(Phenolate)-Functionalized N-Heterocyclic Carbene Complexes of Oxo- and Imido-Vanadium(V). *Inorganica Chimica Acta* **2021**, *521*, 120301. https://doi.org/10.1016/j.ica.2021.120301.

(23) Bellemin-Laponnaz, S.; Welter, R.; Brelot, L.; Dagorne, S. Synthesis and Structure of V(V) and Mn(III) NHC Complexes Supported by a Tridentate Bis-Aryloxide-N-Heterocyclic Carbene Ligand. *Journal of Organometallic Chemistry* **2009**, *694* (5), 604–606. https://doi.org/10.1016/j.jorganchem.2008.12.049.

(24) Liu, B.; Liu, X.; Chen, C.; Chen, C.; Chen, W. Carbene Transfer Reactivities of Nickel(II)-N-Heterocyclic Carbene Complexes and Their Applications in the Synthesis of Metal-NHC Complexes. *Organometallics* **2012**, *31* (1), 282–288. https://doi.org/10.1021/om200881s.

(25) Smith, J. M.; Long, J. R. First-Row Transition Metal Complexes of the Strongly Donating Pentadentate Ligand PY4Im. *Inorganic Chemistry* **2010**, *49* (23), 11223–11230. https://doi.org/10.1021/ic1018407.

(26) Romain, C.; Specklin, D.; Miqueu, K.; Sotiropoulos, J. M.; Fliedel, C.; Bellemin-Laponnaz, S.; Dagorne, S. Unusual Benzyl Migration Reactivity in NHC-Bearing Group 4 Metal Chelates: Synthesis, Characterization, and Mechanistic Investigations. *Organometallics* **2015**, *34* (20), 4854–4863. https://doi.org/10.1021/om501143t.

(27) Quadri, C. C.; Lalrempuia, R.; Hessevik, J.; Törnroos, K. W.; le Roux, E. Structural Characterization of Tridentate N-Heterocyclic Carbene Titanium(IV) Benzyloxide, Silyloxide, Acetate, and Azide Complexes and Assessment of Their Efficacies for Catalyzing the Copolymerization of Cyclohexene Oxide with CO2. *Organometallics* **2017**, *36* (22), 4477–4489. https://doi.org/10.1021/acs.organomet.7b00705.

(28) Pradeep, T.; Velusamy, M.; Mayilmurugan, R. Novel Iron(II)-N-Heterocyclic Carbene Catalysts for Efficient Transfer Hydrogenations under Mild Condition. *Molecular Catalysis* **2018**, *459*, 71–77. https://doi.org/10.1016/J.MCAT.2018.08.017.

(29) Fujisaki, H.; Ishizuka, T.; Shimoyama, Y.; Kotani, H.; Shiota, Y.; Yoshizawa, K.; Kojima, T. Selective Catalytic 2e--Oxidation of Organic Substrates by an FeIIcomplex Having an N-Heterocyclic Carbene Ligand in Water. *Chemical Communications* **2020**, *56* (68), 9783–9786. https://doi.org/10.1039/d0cc03289a.

(30) Luo, S.; Bruggeman, D. F.; Siegler, M. A.; Bouwman, E. Can Pendant Pyridyl Arm Assist the Proton Delivery in Electrocatalysis? *Inorganica Chimica Acta* **2018**, *477*, 24–30. https://doi.org/10.1016/J.ICA.2018.02.030.

(31) Chen, C.; Qiu, H.; Chen, W. Trinuclear Copper(I) Complex of 1,3-Bis(2-Pyridinylmethyl)Imidazolylidene as a Carbene-Transfer Reagent for the Preparation of Catalytically Active Nickel(II) and Palladium(II) Complexes. *Journal of Organometallic Chemistry* **2012**, *696* (26), 4166–4172. https://doi.org/10.1016/J.JORGANCHEM.2011.09.008.

(32) Cope, J. D.; Sheridan, P. E.; Galloway, C. J.; Awoyemi, R. F.; Stokes, S. L.; Emerson, J. P. Synthesis and Characterization of a Tetradentate, N-Heterocyclic Carbene Copper(II) Complex and Its Use as a Chan-Evans-Lam Coupling Catalyst. *Organometallics* **2020**, *39* (24), 4457–4464. https://doi.org/10.1021/acs.organomet.0c00552.

(33) Anneser, M. R.; Haslinger, S.; Pöthig, A.; Cokoja, M.; Basset, J. M.; Kühn, F. E. Synthesis and Characterization of an Iron Complex Bearing a Cyclic Tetra-N-Heterocyclic Carbene Ligand: An Artifical Heme Analogue? *Inorganic Chemistry* **2015**, *54* (8), 3797–3804. https://doi.org/10.1021/ic503043h.

(34) Cheng, J.; Wang, L.; Wang, P.; Deng, L. High-Oxidation-State 3d Metal (Ti-Cu) Complexes with N-Heterocyclic Carbene Ligation. *Chemical Reviews*. American Chemical Society October 10, 2018, pp 9930–9987. https://doi.org/10.1021/acs.chemrev.8b00096.

(35) O'Hearn, D. J.; Singer, R. D. Direct Synthesis of a Copper(II) N-Heterocyclic Carbene Complex in Air. *Organometallics* **2017**, *36* (17), 3175–3177. https://doi.org/10.1021/acs.organomet.7b00489.

(36) das Adhikary, S.; Samanta, T.; Roymahapatra, G.; Loiseau, F.; Jouvenot, D.; Giri, S.; Chattaraj, P. K.; Dinda, J. Synthesis{,} Structure and Electrochemical Behaviour of Ru(Ii)- and Pt(Ii)-Carbene Complexes of the NCN-Pincer 1{,}3-Bis(2-Pyridylmethyl)-1H-Benzimidazolium Chloride. *New J. Chem.* **2010**, *34* (9), 1974–1980. https://doi.org/10.1039/B9NJ00698B.

(37) Shimoyama, Y.; Ishizuka, T.; Kotani, H.; Shiota, Y.; Yoshizawa, K.; Mieda, K.; Ogura, T.; Okajima, T.; Nozawa, S.; Kojima, T. A Ruthenium(III)–Oxyl Complex Bearing Strong Radical Character. *Angewandte Chemie - International Edition* **2016**, *55* (45), 14041–14045. https://doi.org/10.1002/anie.201607861.

(38) Zhang, Z.; Yang, Y.; Sun, H.; Cao, R. Syntheses, Structures and Anion Exchange Properties of Accommodative Silver Chains Using a Positively Charged and Flexible Ligand. *Inorganica Chimica Acta* **2015**, *434*, 158–171. https://doi.org/10.1016/j.ica.2015.05.021.

(39) Magill, A. M.; Mcguinness, D. S.; Cavell, K. J.; Britovsek, G. J. P.; Gibson, V. C.; White, A. J. P.; Williams, D. J.; White, A. H.; Skelton, B. W. *Palladium(II) Complexes Containing Mono-, Bi-and Tridentate Carbene Ligands. Synthesis, Characterisation and Application as Catalysts in CC Coupling Reactions*; 2001.

(40) Chen, C.; Qiu, H.; Chen, W. Trinuclear Copper(I) Complex of 1,3-Bis(2-Pyridinylmethyl)Imidazolylidene as a Carbene-Transfer Reagent for the Preparation of Catalytically Active Nickel(II) and Palladium(II) Complexes. *Journal of Organometallic Chemistry* **2012**, *696* (26), 4166–4172. https://doi.org/10.1016/j.jorganchem.2011.09.008.

(41) Roy, S.; Mitra, P.; Patra, A. K. Cu(II) Complexes with Square Pyramidal (N2S)CuCl2 Chromophore: Jahn-Teller Distortion and Subsequent Effect on Spectral and Structural Properties. *Inorganica Chimica Acta* **2011**, *370* (1), 247–253. https://doi.org/10.1016/j.ica.2011.01.068.

(42) Lake, B. R. M.; Willans, C. E. Remarkable Stability of Copper(II)-N-Heterocyclic Carbene Complexes Void of an Anionic Tether. *Organometallics* **2014**, *33* (8), 2027–2038. https://doi.org/10.1021/om500178e.

(43) Nielsen, A.; Veltzé, S.; Bond, A. D.; McKenzie, C. J. Isomerism in Copper(II) Chloride Complexes of Bis(2-Pyridylmethyl)Amine and N-Substituted Derivatives: Synthesis and X-Ray Structural Characterisation. *Polyhedron* **2007**, *26* (8), 1649–1657. https://doi.org/10.1016/j.poly.2006.12.005.

(44) Catalano, V. J.; Munro, L. B.; Strasser, C. E.; Samin, A. F. Modulation of Metal-Metal Separations in a Series of Ag(I) and Intensely Blue Photoluminescent Cu(I) NHC-Bridged Triangular Clusters. *Inorganic Chemistry* **2011**, *50* (17), 8465–8476. https://doi.org/10.1021/ic201053t.

(45) Liu, B.; Ma, X.; Wu, F.; Chen, W. Simple Synthesis of Neutral and Cationic Cu-NHC Complexes. *Dalton Transactions* **2015**, *44* (4), 1836–1844. https://doi.org/10.1039/c4dt02986k.

(46) Díez-González, S.; Escudero-Adán, E. C.; Benet-Buchholz, J.; Stevens, E. D.; Slawin, A. M. Z.; Nolan, S. P. [(NHC)CuX] Complexes: Synthesis, Characterization and Catalytic Activities in Reduction Reactions and Click Chemistry. On the

Advantage of Using Well-Defined Catalytic Systems. *Dalton Transactions* **2010**, *39* (32), 7595–7606. https://doi.org/10.1039/C0DT00218F.

(47) Wang, X.; Liu, S.; Weng, L.; Jin, G. X. Preparation, Structure and Ethylene Polymerization Behavior of Mixed-Halide Nickel(II) Complexes and Cobalt(II) Complex Containing Imidazolium. *Journal of Organometallic Chemistry* **2005**, *690* (12), 2934–2940. https://doi.org/10.1016/j.jorganchem.2005.03.015.

(48) Hao, N.; McGlinchey, M. J.; Sayer, B. G.; Schrobilgen, G. J. A Nickel-61 NMR Study of Some D10 Nickel Complexes. *Journal of Magnetic Resonance (1969-1992)* **1982**, *46* (1), 158–162. https://doi.org/10.1016/0022-2364(82)90176-7.

(49) C. F. Macrae; I. Sovago; S. J. Cottrell; P. T. A. Galek; P. McCabe; E. Pidcock; M. Platings; G. P. Shields; J. S. Stevens; M. Towler; P. A. Wood. Mercury 4.0: From Visualization to Analysis, Design and Prediction. 2020, pp 226–235.

(50) Leung, D. Y. C.; Caramanna, G.; Maroto-Valer, M. M. An Overview of Current Status of Carbon Dioxide Capture and Storage Technologies. *Renewable and Sustainable Energy Reviews* **2014**, *39*, 426–443. https://doi.org/10.1016/J.RSER.2014.07.093.

(51) J, D. S.; Ken, C.; Damon, M. H. Future CO2 Emissions and Climate Change from Existing Energy Infrastructure. *Science (1979)* **2010**, *329* (5997), 1330–1333. https://doi.org/10.1126/science.1188566.

(52) Bui, M.; Adjiman, C. S.; Bardow, A.; Anthony, E. J.; Boston, A.; Brown, S.; Fennell, P. S.; Fuss, S.; Galindo, A.; Hackett, L. A.; Hallett, J. P.; Herzog, H. J.; Jackson, G.; Kemper, J.; Krevor, S.; Maitland, G. C.; Matuszewski, M.; Metcalfe, I. S.; Petit, C.;

Puxty, G.; Reimer, J.; Reiner, D. M.; Rubin, E. S.; Scott, S. A.; Shah, N.; Smit, B.; Trusler, J. P. M.; Webley, P.; Wilcox, J.; mac Dowell, N. Carbon Capture and Storage (CCS): The Way Forward. *Energy & Environmental Science* **2018**, *11* (5), 1062–1176. https://doi.org/10.1039/C7EE02342A.

(53) Reis Machado, A. S.; Nunes da Ponte, M. CO2 Capture and Electrochemical Conversion. *Current Opinion in Green and Sustainable Chemistry* **2018**, *11*, 86–90. https://doi.org/10.1016/J.COGSC.2018.05.009.

(54) Agboola, O. D.; Benson, N. U. Physisorption and Chemisorption Mechanisms Influencing Micro (Nano) Plastics-Organic Chemical Contaminants Interactions: A Review. *Frontiers in Environmental Science*. Frontiers Media S.A. May 28, 2021. https://doi.org/10.3389/fenvs.2021.678574.

(55) Sarmad, S.; Mikkola, J. P.; Ji, X. Carbon Dioxide Capture with Ionic Liquids and Deep Eutectic Solvents: A New Generation of Sorbents. *ChemSusChem*. Wiley-VCH Verlag January 20, 2017, pp 324–352. https://doi.org/10.1002/cssc.201600987.

(56) Yang, L.; Wang, H. Recent Advances in Carbon Dioxide Capture, Fixation, and Activation by Using N-Heterocyclic Carbenes. *ChemSusChem* **2014**, *7* (4), 962–998. https://doi.org/https://doi.org/10.1002/cssc.201301131.

(57) Das, R.; Nagaraja, C. M. Noble Metal-Free Cu(I)-Anchored NHC-Based MOF for Highly Recyclable Fixation of CO2 under RT and Atmospheric Pressure Conditions. *Green Chemistry* **2021**. https://doi.org/10.1039/d1gc01312b.

(58) North, M.; Pasquale, R.; Young, C. Synthesis of Cyclic Carbonates from Epoxides and CO2. *Green Chemistry* **2010**, *12* (9), 1514–1539. https://doi.org/10.1039/c0gc00065e.

(59) Mesías-Salazar, Á.; Rios Yepes, Y.; Martínez, J.; Rojas, R. S. Highly Active CO2 Fixation into Cyclic Carbonates Catalyzed by Tetranuclear Aluminum Benzodiimidazole-Diylidene Adducts. **2020**. https://doi.org/10.3390/catal1101.

(60) Butova, V. v; Soldatov, M. A.; Guda, A. A.; Lomachenko, K. A.; Lamberti, C. Metal-Organic Frameworks: Structure, Properties, Methods of Synthesis and Characterization. *Russian Chemical Reviews* **2016**, *85* (3), 280–307. https://doi.org/10.1070/rcr4554.

(61) Schoedel, A.; Yaghi, O. M. Porosity in Metal-Organic Compounds. *Macrocyclic and Supramolecular Chemistry* **2016**, No. November, 200–219. https://doi.org/10.1002/9781119053859.ch9.

(62) Li, W.; Tan, J. S. Two Co(II)-Organic Frameworks: Selective Gas Sorption and Treatment Activity on Thecal Cyst. *Journal of Molecular Structure* **2021**, *1237*, 130359. https://doi.org/10.1016/J.MOLSTRUC.2021.130359.

(63) Yan, P.; Yang, J.; Ma, D.; Zhang, S.; Zeng, S.; Feng, L.; Zhan, S.; Lin, Q. C2H2/CH4 and CO2/CH4 Separations on a Ethoxyl-Functionalized Cobalt(II)–Organic Framework with Open Metal Sites. *Microporous and Mesoporous Materials* **2020**, *293*, 109777. https://doi.org/10.1016/J.MICROMESO.2019.109777.

(64) Cui, X.; Chen, K.; Xing, H.; Yang, Q.; Krishna, R.; Bao, Z.; Wu, H.; Zhou, W.; Dong, X.; Han, Y.; Li, B.; Ren, Q.; Zaworotko, M. J.; Chen, B. Pore Chemistry and Size

Control in Hybrid Porous Materials for Acetylene Capture from Ethylene. *Science (1979)* **2016**, *353* (6295), 141 LP – 144. https://doi.org/10.1126/science.aaf2458.

(65) Paschke, T.; Dreisbach, F.; Ntroduction, I. Gas Storage Capacity of MOF Materials - Measuring High Pressure Methane Adsorption. **2013**, No. 2, 1–2.

(66) Čejka, J. Metal-Organic Frameworks. Applications from Catalysis to Gas Storage. Edited by David Farrusseng. *Angewandte Chemie International Edition* **2012**, *51* (20), 4782–4783. https://doi.org/10.1002/anie.201200812.

(67) Kumari, A.; Kaushal, S.; Singh, P. P. Bimetallic Metal Organic Frameworks Heterogeneous Catalysts: Design, Construction, and Applications. *Materials Today Energy* **2021**, *20*, 100667. https://doi.org/10.1016/J.MTENER.2021.100667.

(68) Hu, M. L.; Razavi, S. A. A.; Piroozzadeh, M.; Morsali, A. Sensing Organic Analytes by Metal-Organic Frameworks: A New Way of Considering the Topic. *Inorganic Chemistry Frontiers*. Royal Society of Chemistry April 7, 2020, pp 1598–1632. https://doi.org/10.1039/c9qi01617a.

(69) Wang, H.; Lustig, W. P.; Li, J. Sensing and Capture of Toxic and Hazardous Gases and Vapors by Metal-Organic Frameworks. *Chemical Society Reviews*. Royal Society of Chemistry July 7, 2018, pp 4729–4756. https://doi.org/10.1039/c7cs00885f.

(70) Chen, M.-L.; Qi, Z.-L.; Jin, W.-T.; Xu, Z.; Cheng, Y.-H.; Zhou, Z.-H. Cation Exchange in a Fluorescent Zinc-Based Metal–Organic Framework for Cadmium Ion Detection. *CrystEngComm* **2021**, *23* (42), 7442–7449. https://doi.org/10.1039/d1ce00931a.

(71) Karmakar, A.; Samanta, P.; Desai, A. v.; Ghosh, S. K. Guest-Responsive Metal-Organic Frameworks as Scaffolds for Separation and Sensing Applications. *Accounts of Chemical Research* **2017**, *50* (10), 2457–2469. https://doi.org/10.1021/acs.accounts.7b00151.

(72) Desai, A. v; Manna, B.; Karmakar, A.; Sahu, A.; Ghosh, S. K. A Water-Stable Cationic Metal–Organic Framework as a Dual Adsorbent of Oxoanion Pollutants. *Angewandte Chemie International Edition* **2016**, *55* (27), 7811–7815. https://doi.org/10.1002/anie.201600185.

(73) Kalaj, M.; Cohen, S. M. Postsynthetic Modification: An Enabling Technology for the Advancement of Metal-Organic Frameworks. *ACS Central Science* **2020**, *6* (7), 1046–1057. https://doi.org/10.1021/acscentsci.0c00690.

(74) Liu, J.; Wei, Y.; Bao, F.; Li, G.; Liu, H.; Wang, H. Pore-Size Tuning in Pillared-Layer Metal–Organic Framework with Self-Penetrated Rob Net for Selective Gas Adsorption and Efficient Dyes Adsorption in Aqueous Solution. *Polyhedron* **2019**, *169*, 58–65. https://doi.org/10.1016/j.poly.2019.05.003.

(75) Mukherjee, S.; Sikdar, N.; O'Nolan, D.; Franz, D. M.; Gascón, V.; Kumar, A.; Kumar, N.; Scott, H. S.; Madden, D. G.; Kruger, P. E.; Space, B.; Zaworotko, M. J. Trace CO2 Capture by an Ultramicroporous Physisorbent with Low Water Affinity. *Science Advances* **2019**, *5* (11), 1–8. https://doi.org/10.1126/sciadv.aax9171.

(76) Alhamami, M.; Doan, H.; Cheng, C. H. A Review on Breathing Behaviors of Metal-Organic-Frameworks (MOFs) for Gas Adsorption. *Materials*. 2014, pp 3198–3250. https://doi.org/10.3390/ma7043198.

(77) Rivera-Torrente, M.; Filez, M.; Hardian, R.; Reynolds, E.; Seoane, B.; Coulet, M. V.; Oropeza Palacio, F. E.; Hofmann, J. P.; Fischer, R. A.; Goodwin, A. L.; Llewellyn, P. L.; Weckhuysen, B. M. Metal-Organic Frameworks as Catalyst Supports: Influence of Lattice Disorder on Metal Nanoparticle Formation. *Chemistry - A European Journal* **2018**, *24* (29), 7498–7506. https://doi.org/10.1002/chem.201800694.

(78) Rossin, A.; Tuci, G.; Luconi, L.; Giambastiani, G. Metal-Organic Frameworks as Heterogeneous Catalysts in Hydrogen Production from Lightweight Inorganic Hydrides. *ACS Catalysis* **2017**, *7* (8), 5035–5045. https://doi.org/10.1021/acscatal.7b01495.

(79) Dhakshinamoorthy, A.; Asiri, A. M.; Garcia, H. Mixed-Metal or Mixed-Linker Metal Organic Frameworks as Heterogeneous Catalysts. *Catalysis Science and Technology*. Royal Society of Chemistry 2016, pp 5238–5261. https://doi.org/10.1039/c6cy00695g.

(80) Chughtai, A. H.; Ahmad, N.; Younus, H. A.; Laypkov, A.; Verpoort, F. Metal-Organic Frameworks: Versatile Heterogeneous Catalysts for Efficient Catalytic Organic Transformations. *Chemical Society Reviews*. Royal Society of Chemistry October 7, 2015, pp 6804–6849. https://doi.org/10.1039/c4cs00395k.

(81) Karmakar, A.; Desai, A. v.; Ghosh, S. K. Ionic Metal-Organic Frameworks (IMOFs): Design Principles and Applications. *Coordination Chemistry Reviews* **2016**, *307*, 313–341. https://doi.org/10.1016/j.ccr.2015.08.007.

(82) Jiang, M.; Li, B.; Cui, X.; Yang, Q.; Bao, Z.; Yang, Y.; Wu, H.; Zhou, W.; Chen, B.; Xing, H. Controlling Pore Shape and Size of Interpenetrated Anion-Pillared Ultramicroporous Materials Enables Molecular Sieving of CO2 Combined with Ultrahigh Uptake Capacity. *ACS Applied Materials and Interfaces* **2018**, *10* (19), 16628–16635. https://doi.org/10.1021/acsami.8b03358.

(83) Desveaux, B. E.; Wong, Y. T. A.; Lucier, B. E. G.; Terskikh, V. v.; Boyle, P. D.; Jiang, S.; Huang, Y. CO2 Behavior in a Highly Selective Ultramicroporous Framework: Insights from Single-Crystal X-Ray Diffraction and Solid-State Nuclear Magnetic Resonance Spectroscopy. *Journal of Physical Chemistry C* **2019**, *123* (29), 17798–17807. https://doi.org/10.1021/acs.jpcc.9b03221.

(84) Skarmoutsos, I.; Belmabkhout, Y.; Adil, K.; Eddaoudi, M.; Maurin, G. CO2 Capture Using the SIFSIX-2-Cu-i Metal-Organic Framework: A Computational Approach. *Journal of Physical Chemistry C* **2017**, *121* (49), 27462–27472. https://doi.org/10.1021/acs.jpcc.7b08964.

(85) Forrest, K. A.; Pham, T.; Space, B. Comparing the Mechanism and Energetics of CO2 Sorption in the SIFSIX Series. *CrystEngComm* **2017**, *19* (24), 3338–3347. https://doi.org/10.1039/c7ce00594f.

(86) Burd, S. D.; Ma, S.; Perman, J. A.; Sikora, B. J.; Snurr, R. Q.; Thallapally, P. K.; Tian, J.; Wojtas, L.; Zaworotko, M. J. Highly Selective Carbon Dioxide Uptake by [Cu(Bpy-n) 2(SiF 6)] (Bpy-1 = 4,4′-Bipyridine; Bpy-2 = 1,2-Bis(4-Pyridyl)Ethene). *J Am Chem Soc* **2012**, *134* (8), 3663–3666. https://doi.org/10.1021/ja211340t.

(87) Nugent, P.; Giannopoulou, E. G.; Burd, S. D.; Elemento, O.; Giannopoulou, E. G.; Forrest, K.; Pham, T.; Ma, S.; Space, B.; Wojtas, L.; Eddaoudi, M.; Zaworotko, M. J. Porous Materials with Optimal Adsorption Thermodynamics and Kinetics for Co2 Separation. *Nature* **2013**, *495* (7439), 80–84. https://doi.org/10.1038/nature11893.

(88) Siraj, I. T.; Spicer, M. D. Building Metal Organic Frameworks with Pyridine Fuctionalised Imidazolium Salts Spacers. *International Journal of Chemical Engineering and Applications* **2013**, *4* (4), 199–203. https://doi.org/10.7763/ijcea.2013.v4.294.

(89) O'hearn, D. J. The Design of an Imidazolium Functionalized SIFSIX Pillared Metal-Organic Framework, Halifax, NS, 2017.

(90) Tilley, J. W.; Levitan, P.; Kierstead, R. W. Synthesis of Heterocyclic Analogs of α-Methyldopa. *Journal of Heterocyclic Chemistry* **1979**, *16* (2), 333–337. https://doi.org/10.1002/jhet.5570160226.

(91) Deady, L. W.; Finlayson, W. L. Studies on a General Method for the Demethylation of Quaternized Nitrogen Heterocycles. *Synthetic Communications* **1980**, *10* (12), 947–950. https://doi.org/10.1080/00397918008061856.

(92) Aakeröy, C. B.; Wijethunga, T. K.; Desper, J.; Daković, M. Electrostatic Potential Differences and Halogen-Bond Selectivity. *Crystal Growth and Design* **2016**, *16* (5), 2662–2670. https://doi.org/10.1021/acs.cgd.5b01770.

(93) Sen, S.; Nair, N. N.; Yamada, T.; Kitagawa, H.; Bharadwaj, P. K. High Proton Conductivity by a Metal-Organic Framework Incorporating Zn 8O Clusters with

Aligned Imidazolium Groups Decorating the Channels. *J Am Chem Soc* **2012**, *134* (47), 19432–19437. https://doi.org/10.1021/ja3076378.

4. Appendix

4.1 Appendix A: NMR spectra

^{1}H NMR spectrum of **1** in DMSO-d6

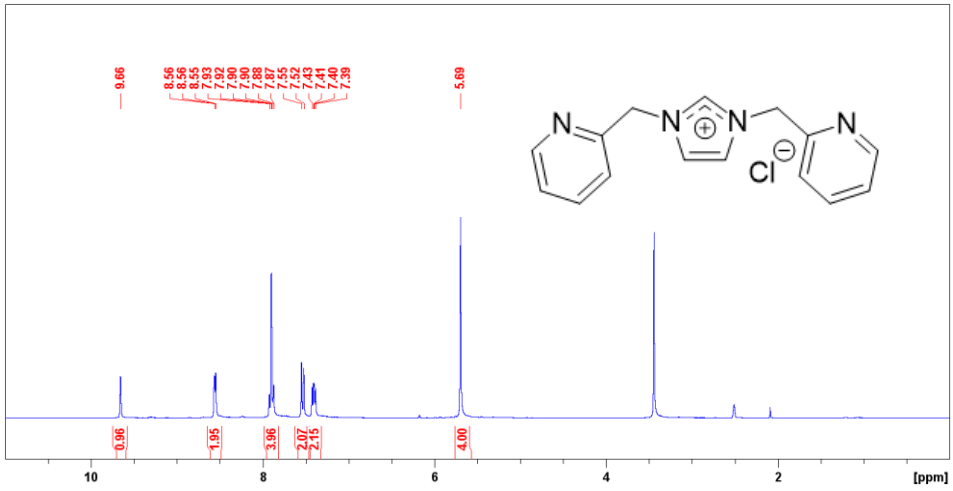

^{13}C NMR spectrum of **1** in DMSO-d6

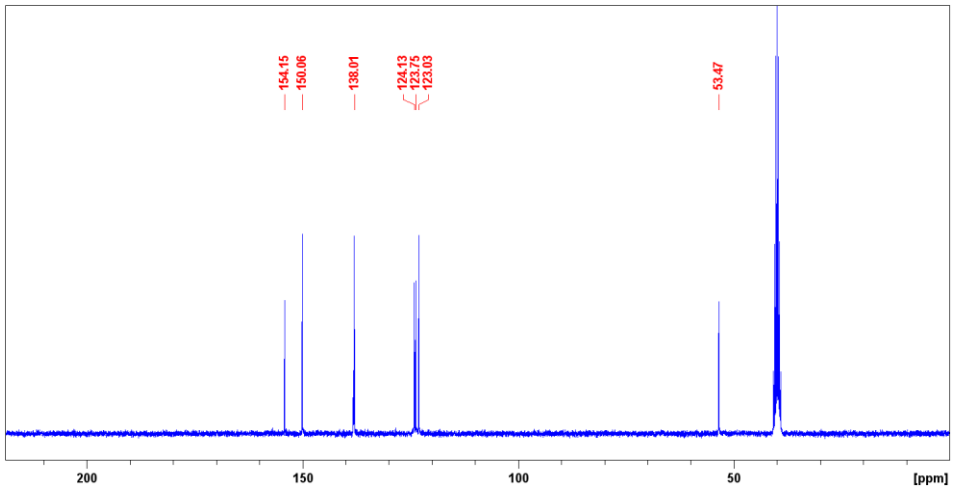

^{1}H NMR spectrum of **2** in DMSO-d6

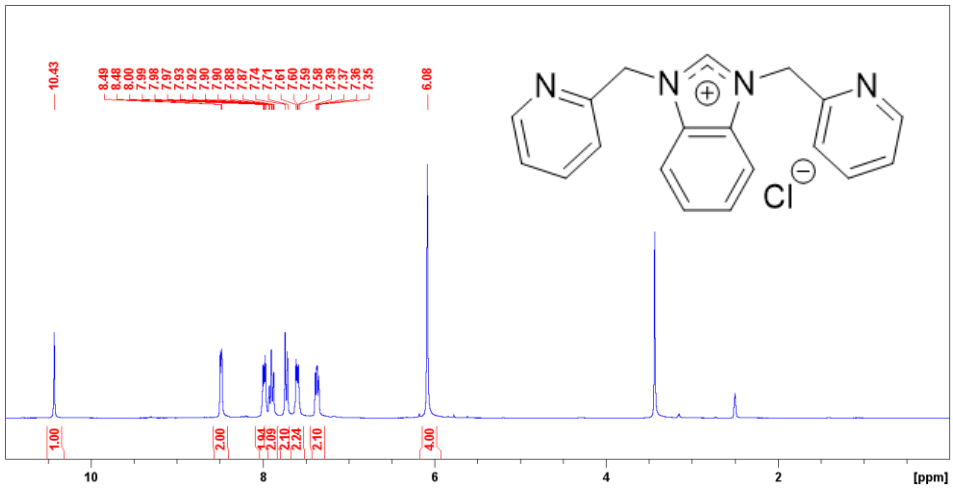

^{13}C NMR spectrum of **2** in DMSO-d6

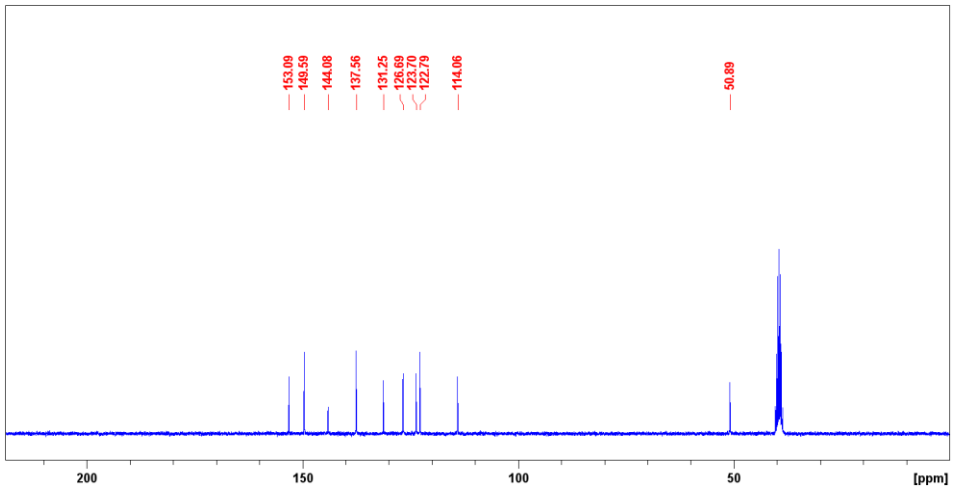

^{1}H NMR spectrum of **3/4/5** in CD_3OD

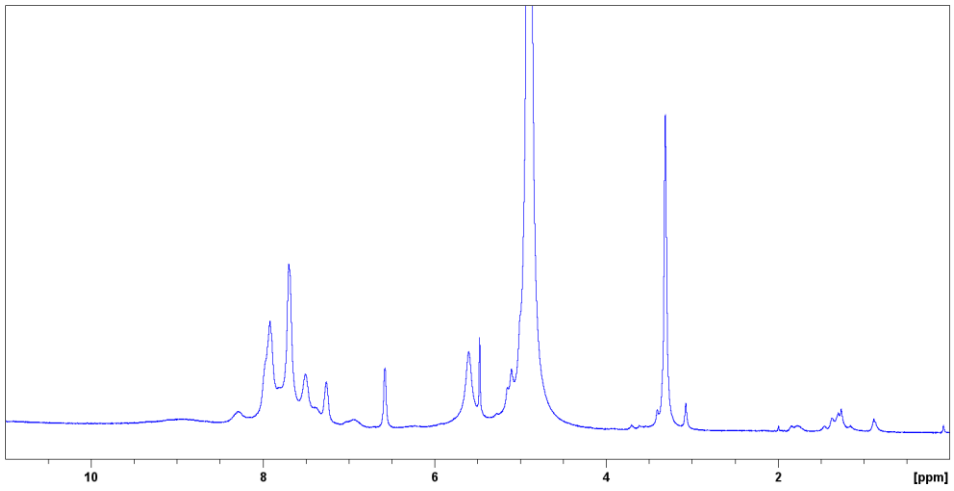

^{1}H-^{1}H COSY spectrum of **3/4/5** in CD_3OD

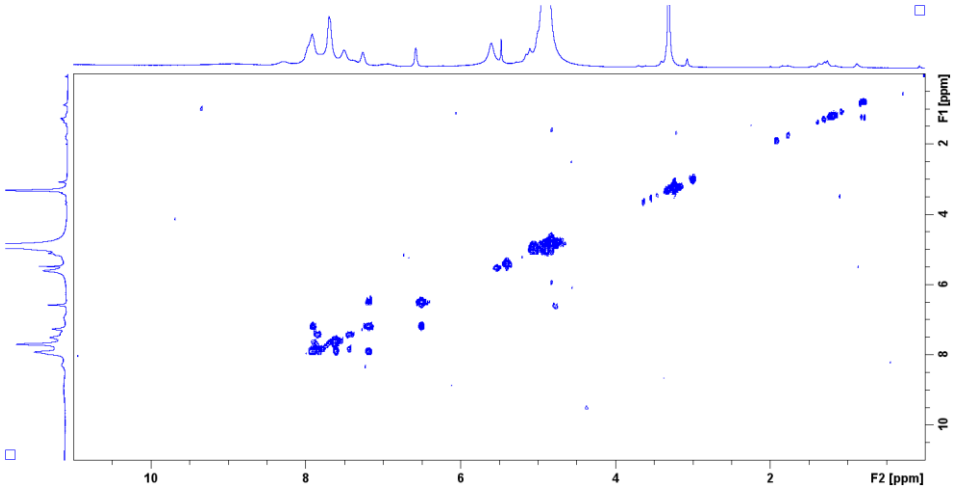

^{1}H-^{13}C HSQC spectrum of **3/4/5** in CD_3OD

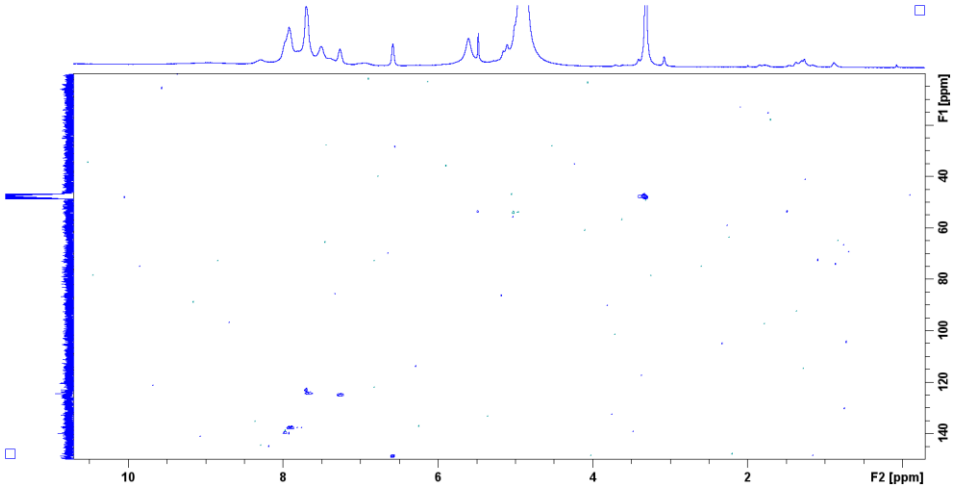

^{1}H NMR spectrum of **6** in CD_3OD

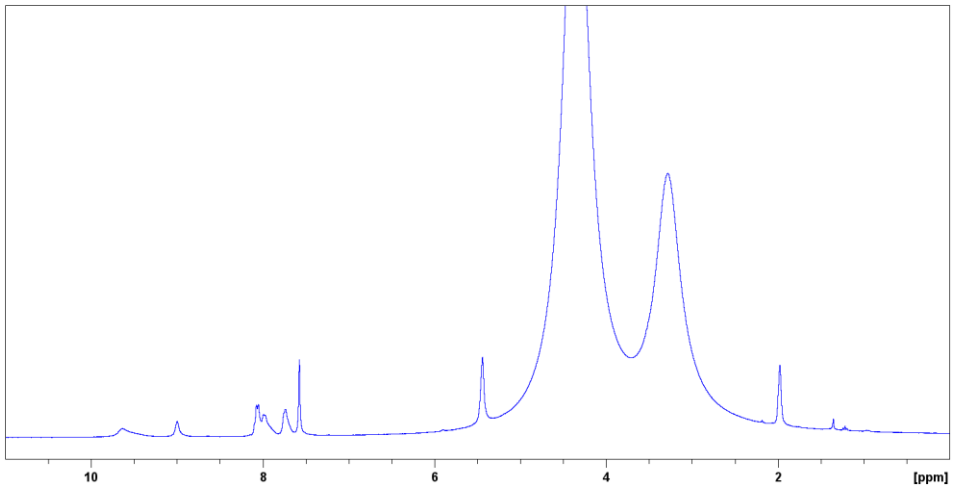

^{13}C NMR spectrum of **6** in CD_3OD

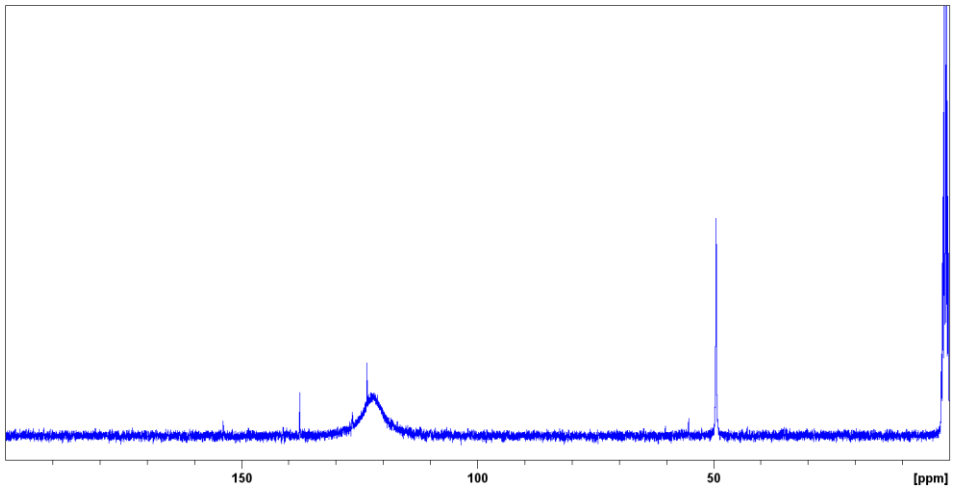

^{1}H-^{1}H COSY spectrum of **6** in CD_3OD

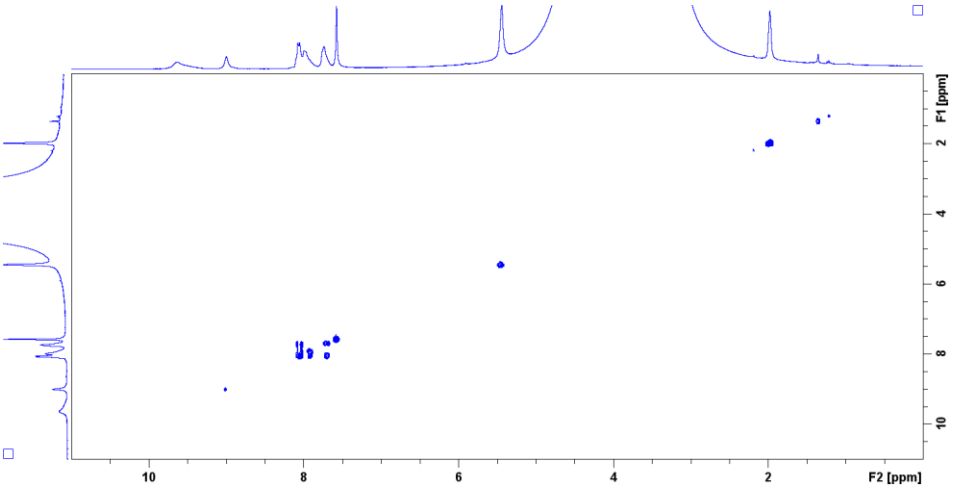

^{1}H-^{13}C HSQC spectrum of **6** in CD_3OD

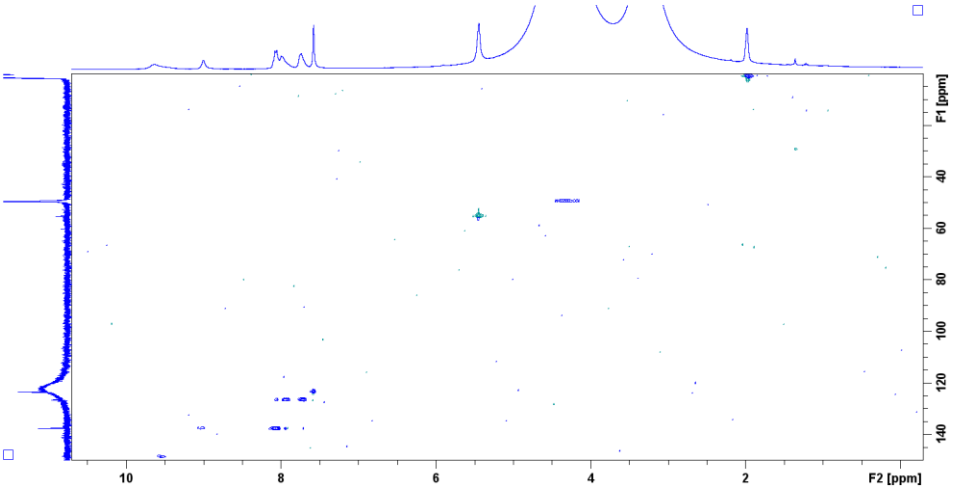

^{1}H NMR spectrum of **7** in CD_3OD

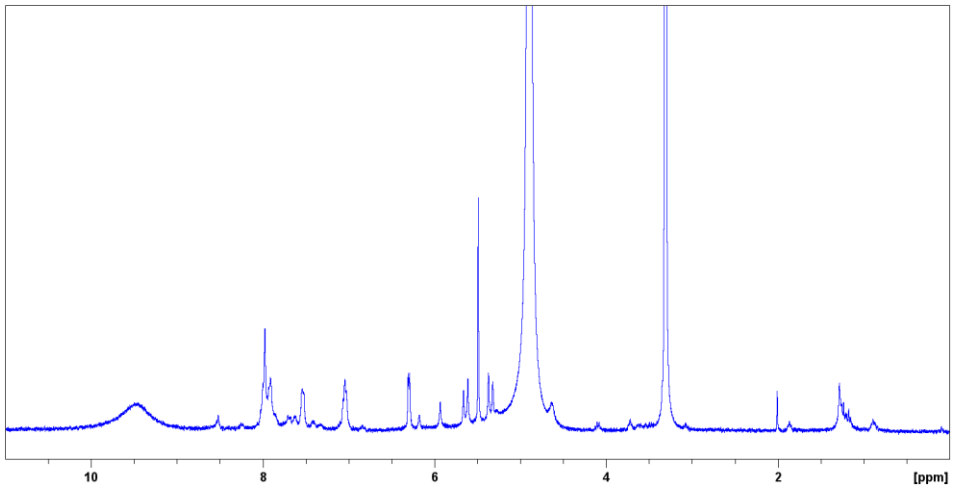

^{13}C NMR spectrum of **7** in CD_3OD

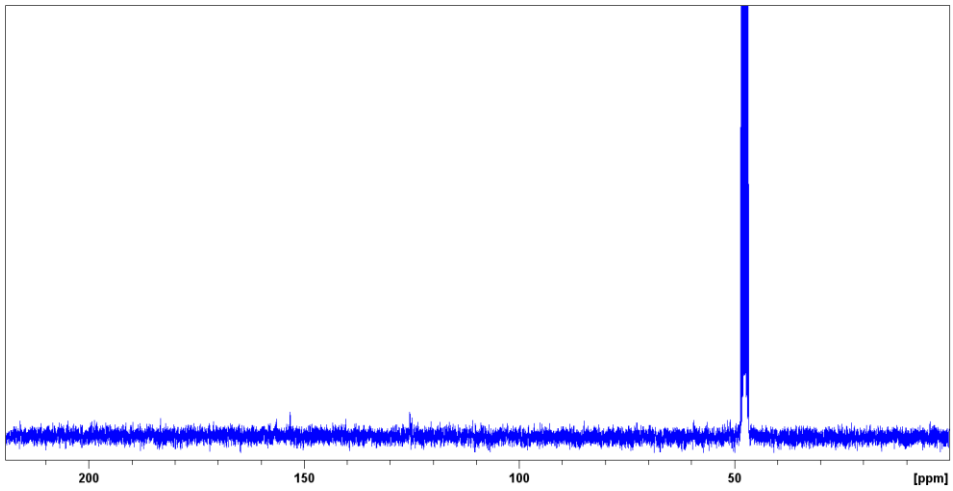

^{1}H-^{1}H COSY spectrum of **7** in CD_3OD

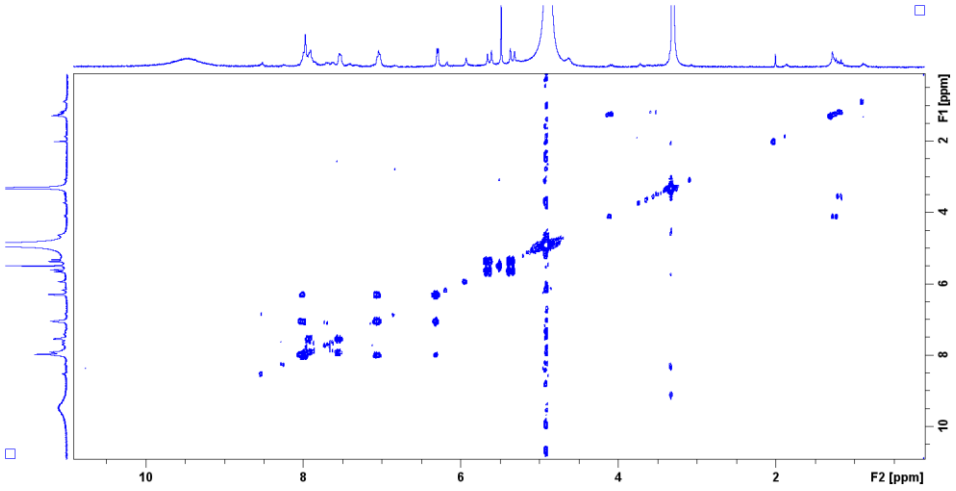

^{1}H-^{13}C HSQC spectrum of **7** in CD_3OD

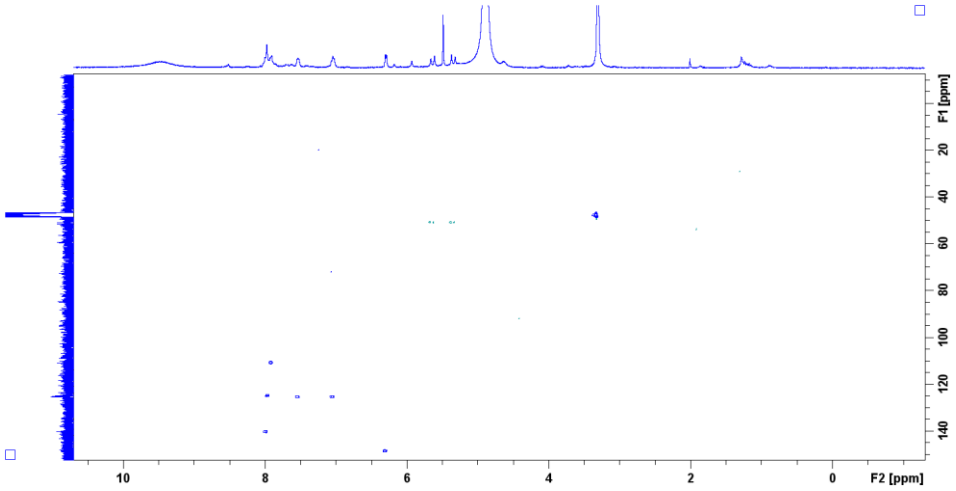

^{1}H NMR spectrum of **9** in CD_3OD

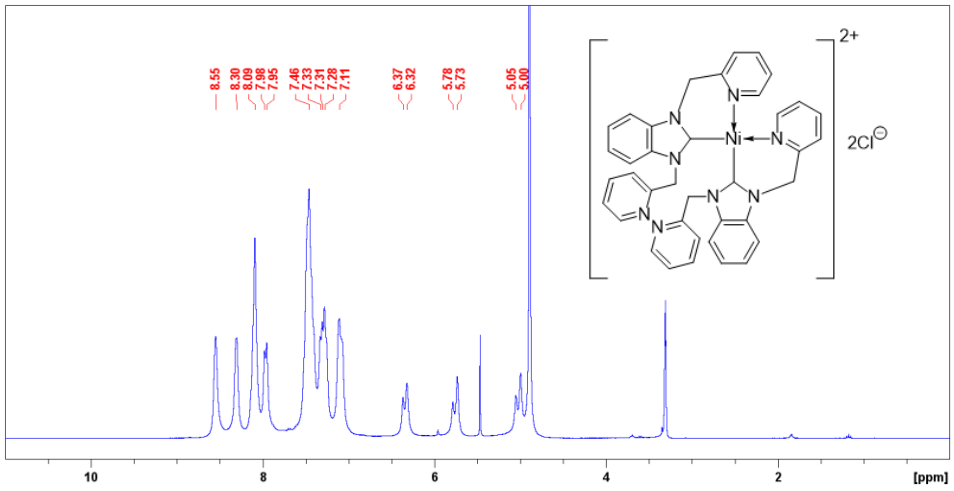

^{13}C NMR spectrum of **9** in CD_3OD

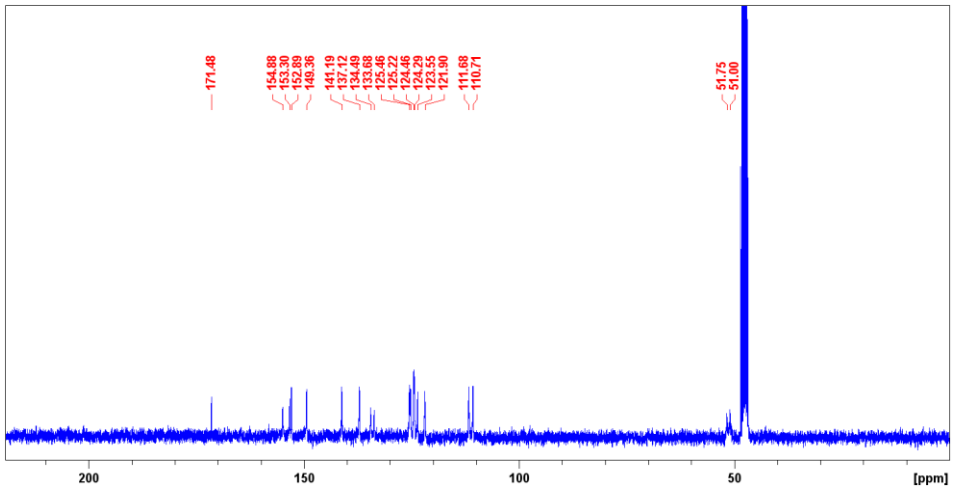

^{1}H-^{1}H COSY spectrum of **9** in CD_3OD

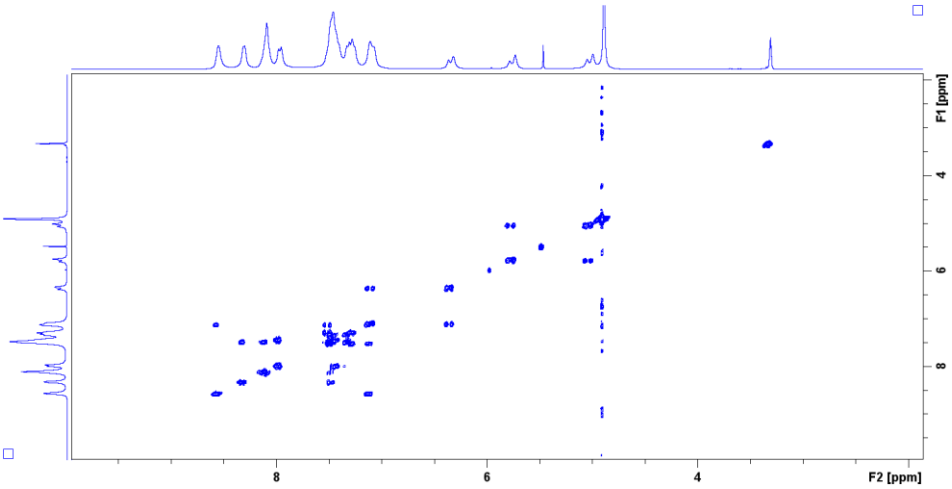

^{1}H-^{13}C HSQC spectrum of **9** in CD_3OD

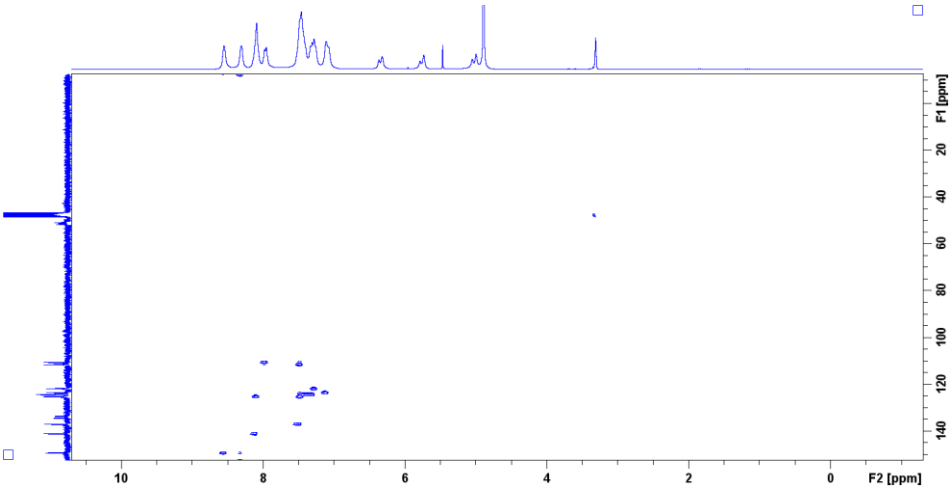

^{1}H NMR spectrum of **10** in DMSO-d_6

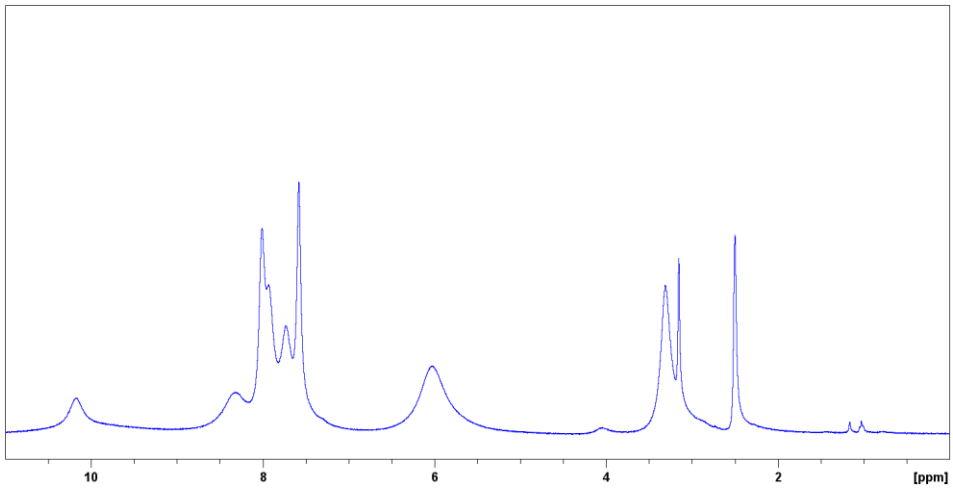

^{13}C NMR spectrum of **10** in DMSO-d_6

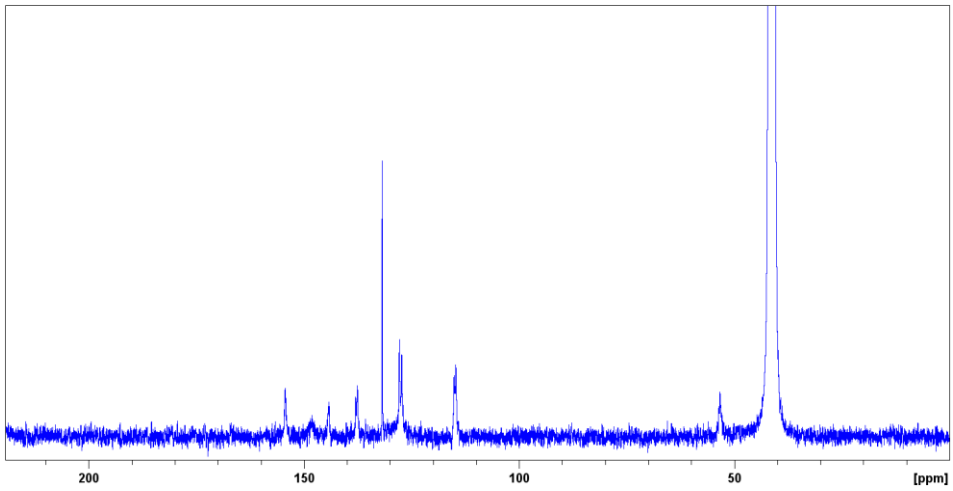

^{1}H NMR spectrum of **11/12** in CD_3OD

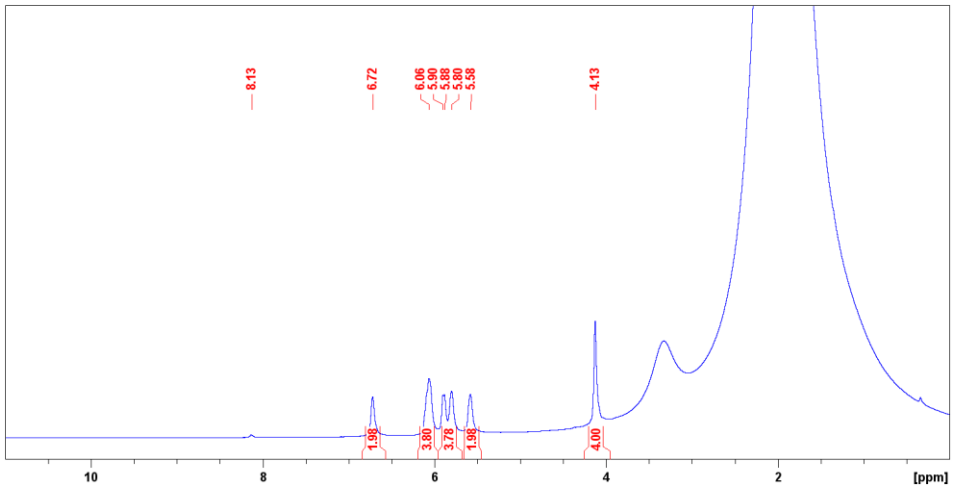

^{13}C NMR spectrum of **11/12** in CD_3OD

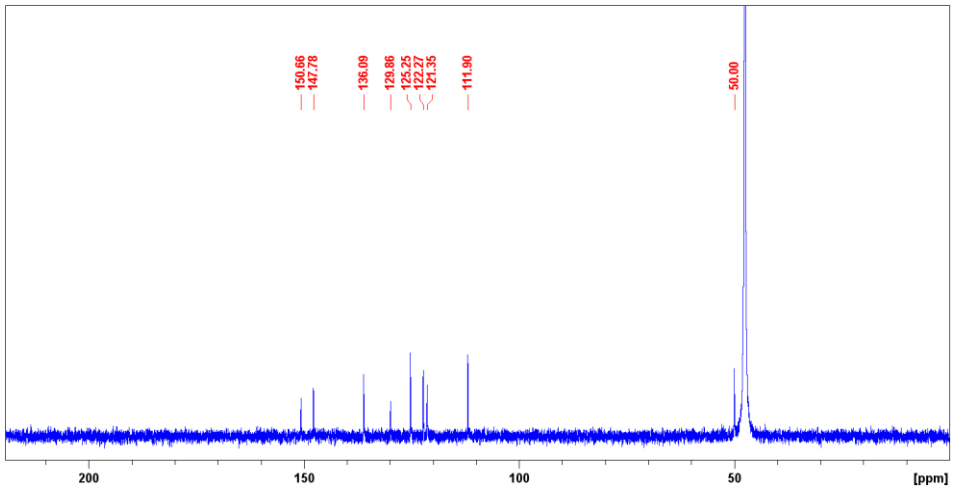

^{1}H NMR spectrum of **13** in DMSO-d6

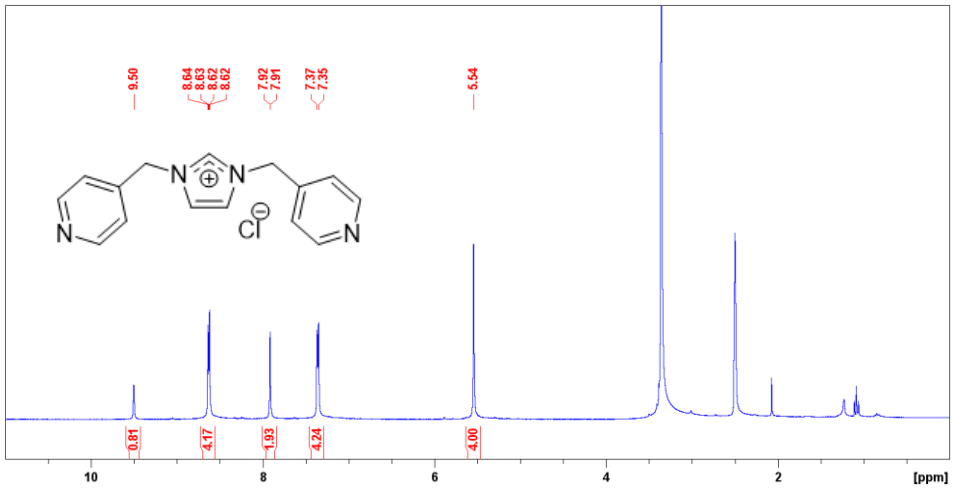

^{13}C NMR spectrum of **13** in DMSO-d6

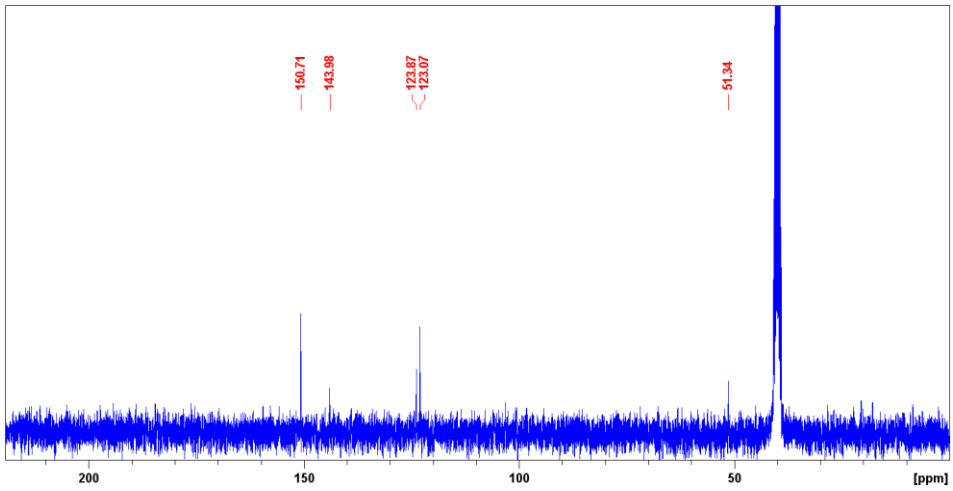

^{1}H-^{1}H COSY spectrum of **13** in DMSO-d6

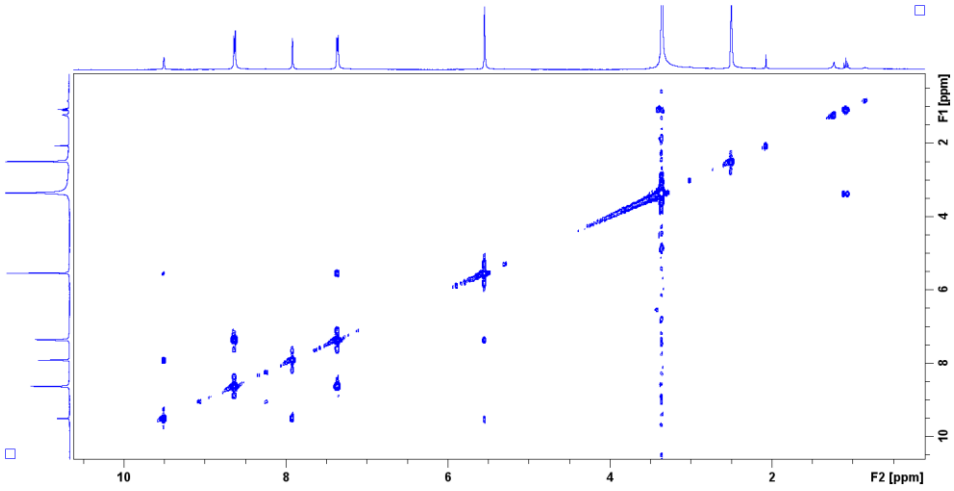

^{1}H-^{13}C HSQC spectrum of **13** in DMSO-d6

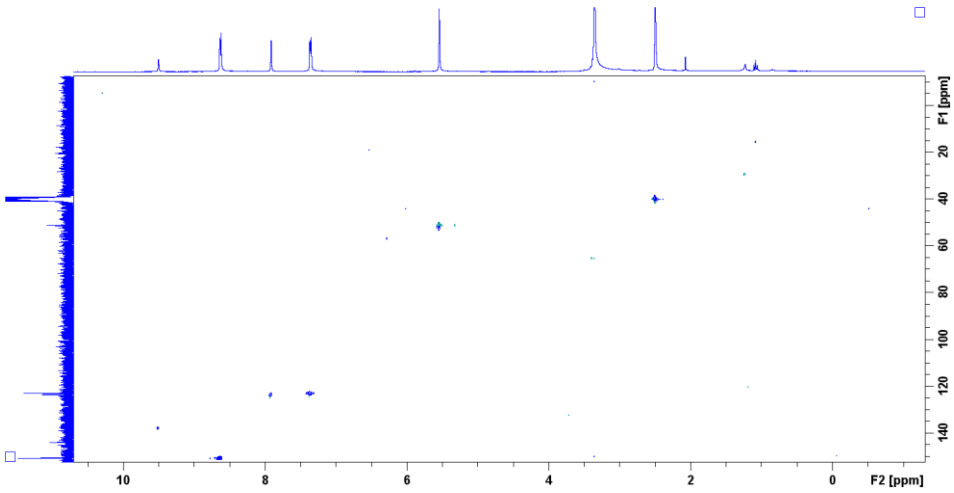

^{1}H NMR spectrum of **14** in DMSO-d6

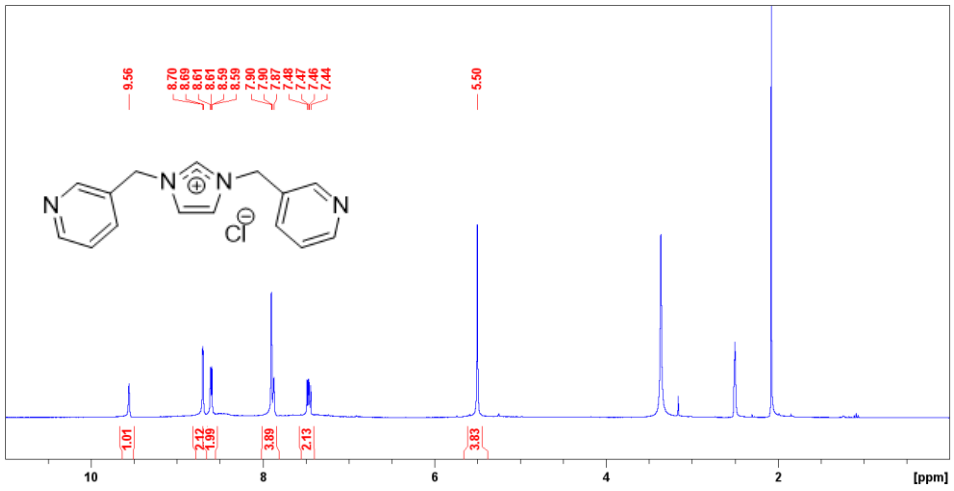

^{13}C NMR spectrum of **14** in DMSO-d6

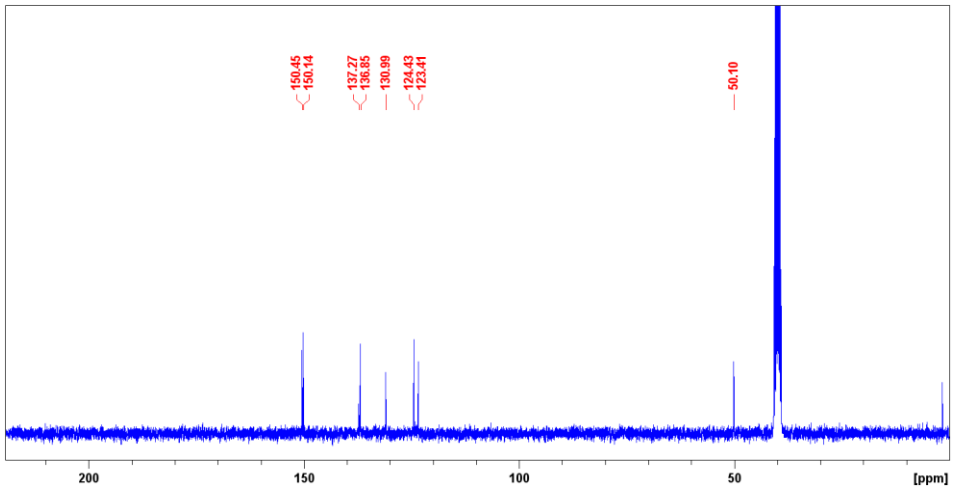

^{1}H-^{1}H COSY spectrum of **14** in DMSO-d6

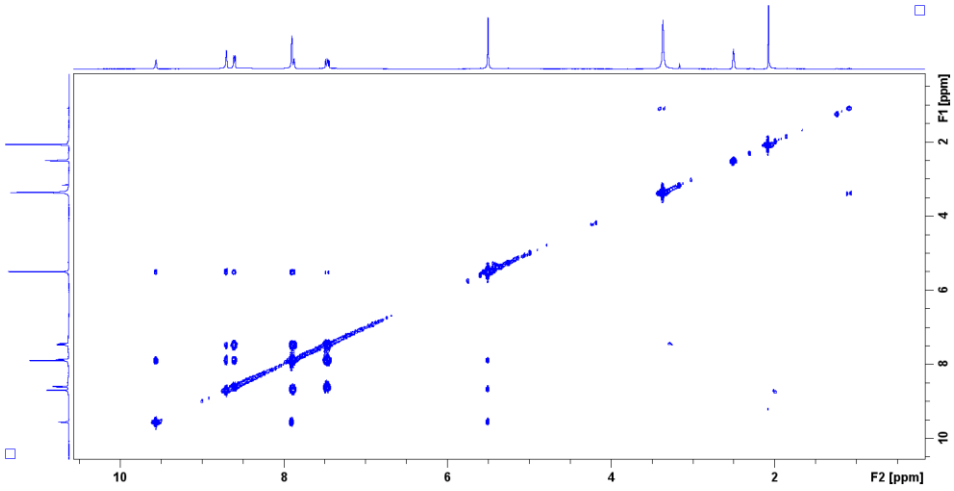

^{1}H-^{13}C HSQC spectrum of **14** in DMSO-d6

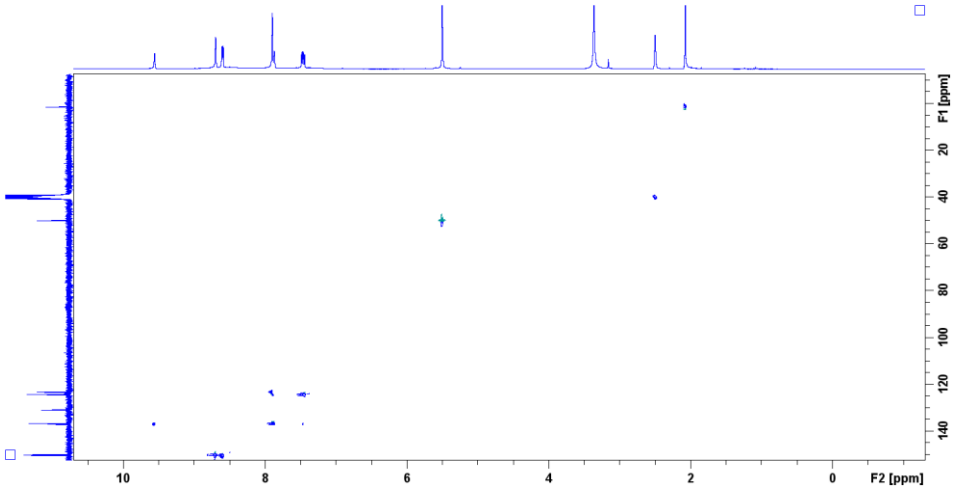

^{1}H NMR spectrum of **17** in $CDCl_3$

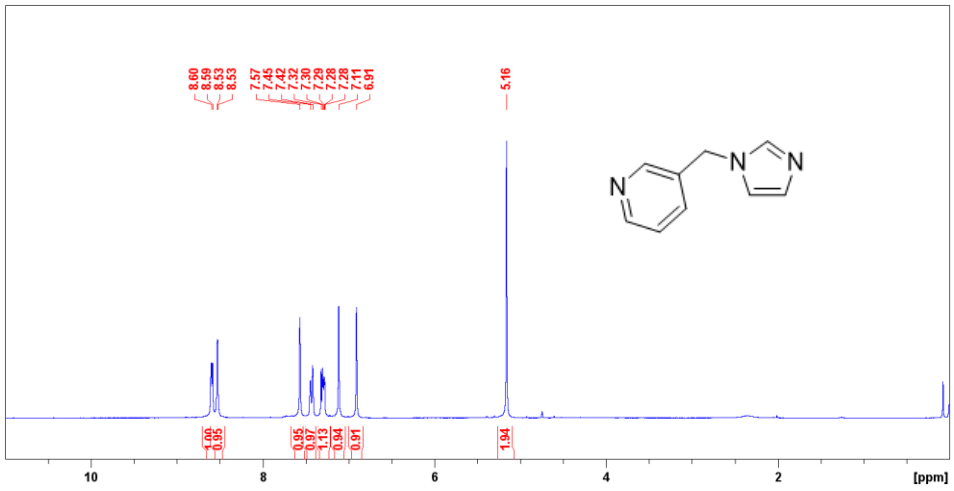

^{13}C NMR spectrum of **17** in $CDCl_3$

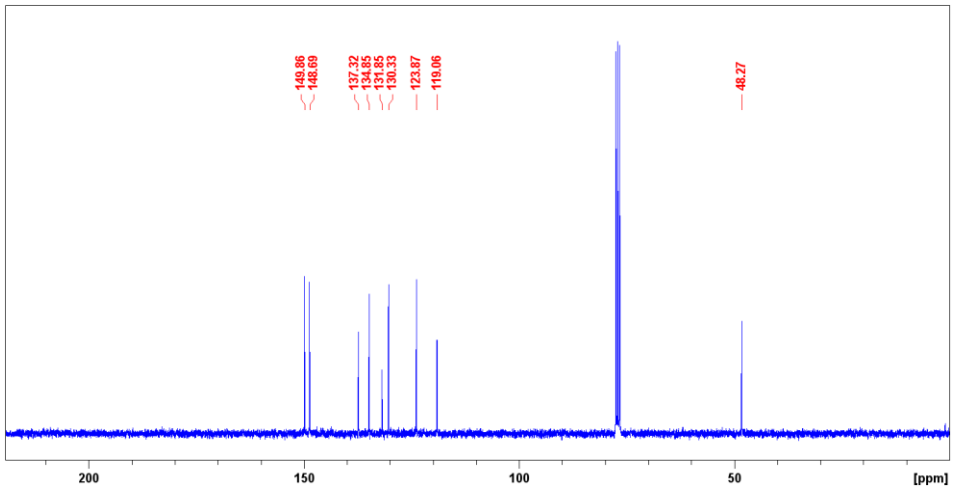

^{1}H NMR spectrum of **18** in $CDCl_3$

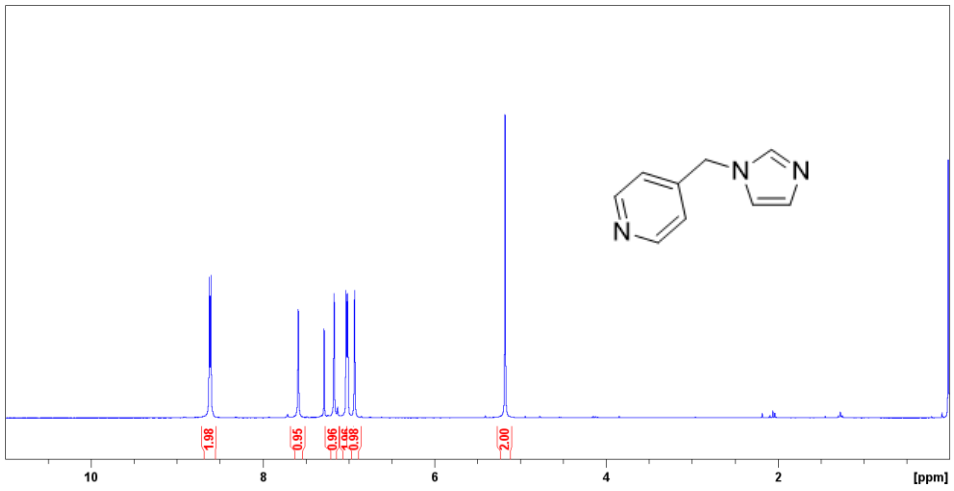

^{13}C NMR spectrum of **18** in $CDCl_3$

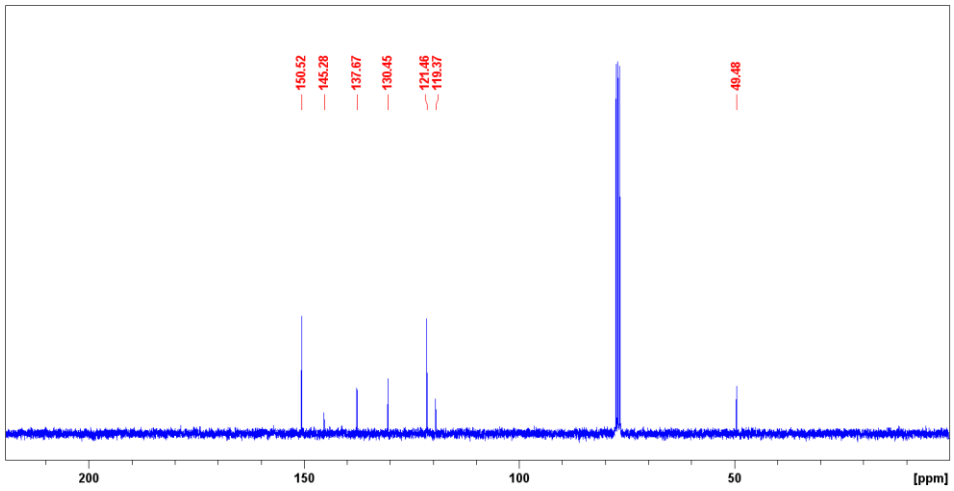

^{1}H NMR spectrum of **19** in $CDCl_3$

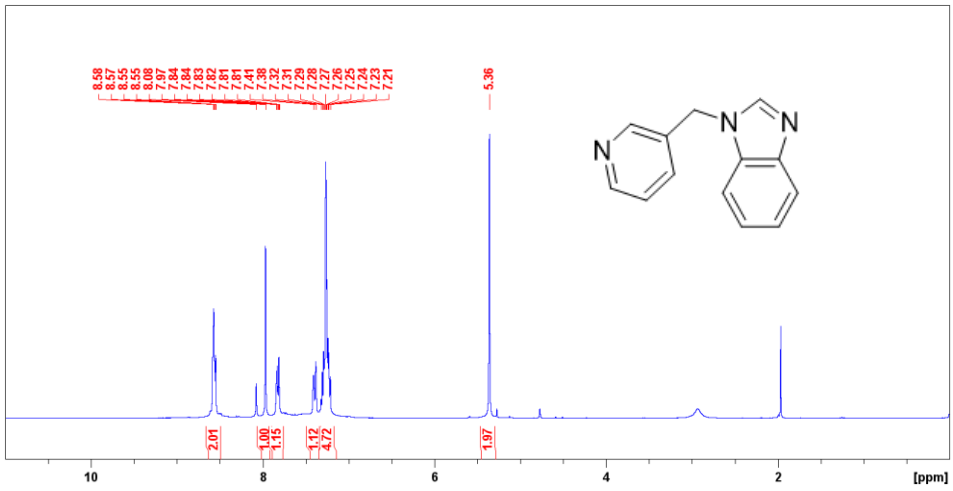

^{13}C NMR spectrum of **19** in $CDCl_3$

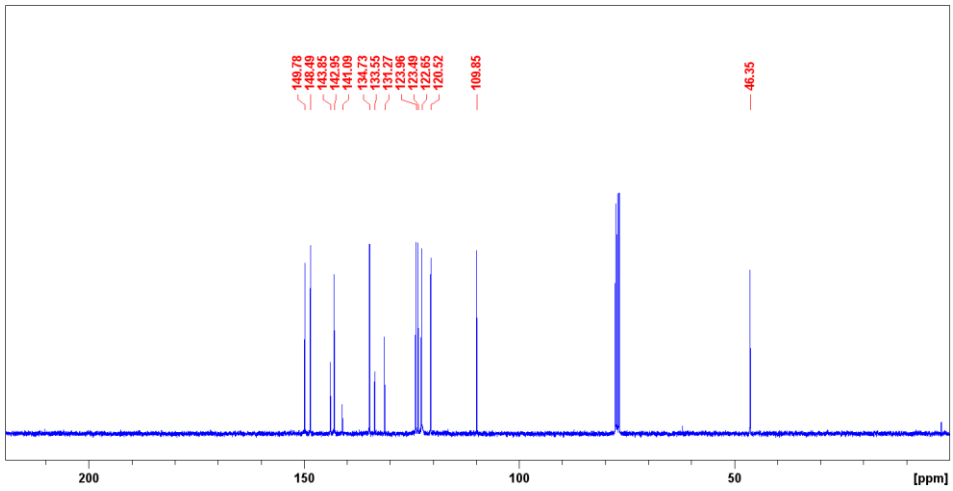

^{1}H NMR spectrum of **20** in $CDCl_3$

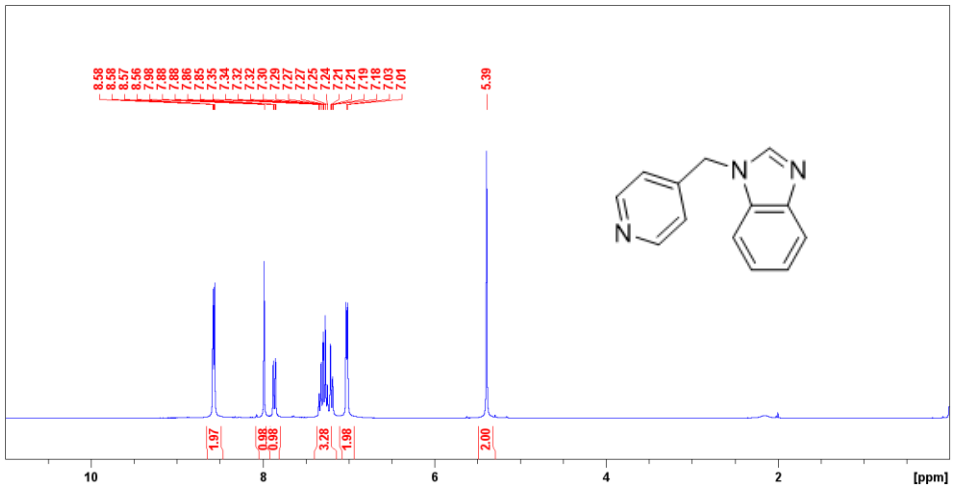

^{13}C NMR spectrum of **20** in $CDCl_3$

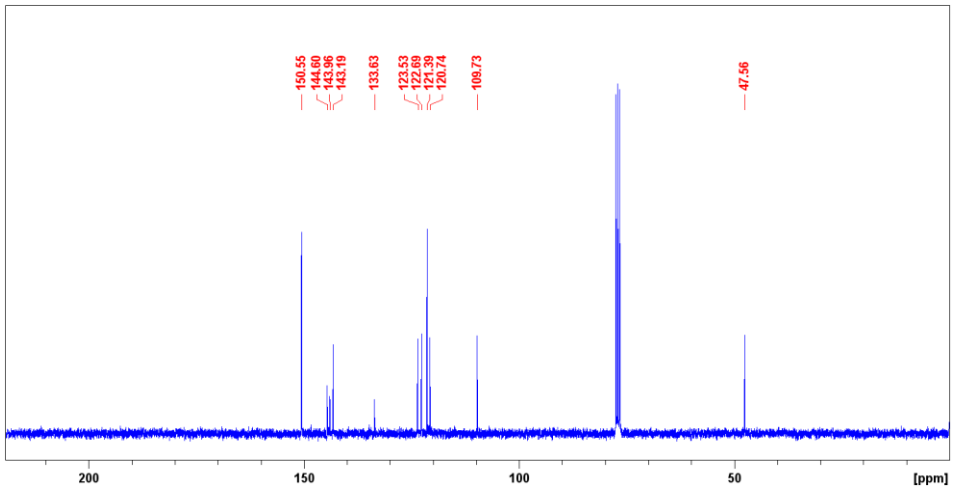

4.2 Appendix B: crystallographic data

Structural information for 2

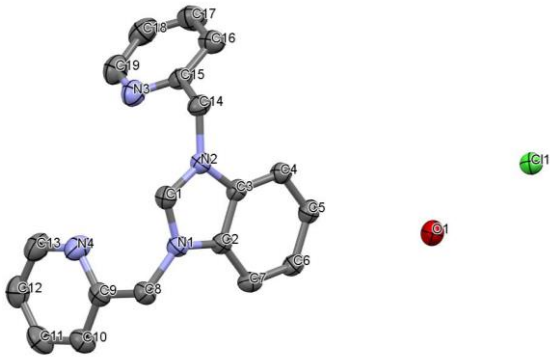

Space group	P b c a
Cell lengths	**a** 16.8078(6) **b** 10.2910(4) **c** 19.9404(7)
Cell angles	α 90 β 90 γ 90
Cell volume	3449.07
Z, Z’	**Z**: 8 **Z'**: 1
R-factor (%)	7.15

Bond lengths in **2**

Atom 1	**Atom 2**	**Length**	**Atom 1**	**Atom 2**	**Length**
N1	C1	1.331(4)	C4	C5	1.384(5)
N1	C2	1.390(4)	C5	C6	1.407(6)
N1	C8	1.469(5)	C6	C7	1.372(6)
N2	C1	1.332(4)	C8	C9	1.508(5)
N2	C3	1.390(4)	C9	C10	1.371(5)
N2	C14	1.471(5)	C10	C11	1.395(6)
N3	C15	1.344(5)	C11	C12	1.374(6)
N3	C19	1.334(5)	C12	C13	1.375(7)
N4	C9	1.338(5)	C14	C15	1.506(5)

N4	C13	1.335(5)	C15	C16	1.370(6)
C2	C3	1.398(4)	C16	C17	1.404(6)
C2	C7	1.394(5)	C17	C18	1.366(7)
C3	C4	1.389(4)	C18	C19	1.373(7)

Bond angles in **2**

Atom 1	**Atom 2**	**Atom 3**	**Angle**	**Atom 1**	**Atom 2**	**Atom 3**	**Angle**
C1	N1	C2	108.1(3)	C2	C7	C6	116.2(3)
C1	N1	C8	125.2(3)	N1	C8	C9	110.5(3)
C2	N1	C8	126.1(3)	N4	C9	C8	115.3(3)
C1	N2	C3	107.8(3)	N4	C9	C10	123.3(3)
C1	N2	C14	126.6(3)	C8	C9	C10	121.4(3)
C3	N2	C14	125.3(3)	C9	C10	C11	118.6(4)
C15	N3	C19	117.2(3)	C10	C11	C12	118.3(4)
C9	N4	C13	117.4(4)	C11	C12	C13	119.2(4)
N1	C1	N2	110.8(3)	N4	C13	C12	123.1(4)
N1	C2	C3	106.4(3)	N2	C14	C15	111.1(3)
N1	C2	C7	132.0(3)	N3	C15	C14	115.8(3)
C3	C2	C7	121.6(3)	N3	C15	C16	123.2(3)
N2	C3	C2	106.8(3)	C14	C15	C16	121.0(3)
N2	C3	C4	131.0(3)	C15	C16	C17	118.1(4)
C2	C3	C4	122.2(3)	C16	C17	C18	119.2(4)
C3	C4	C5	115.9(3)	C17	C18	C19	118.3(4)
C4	C5	C6	121.8(3)	N3	C19	C18	124.0(4)
C5	C6	C7	122.3(3)				

Structural information for 3

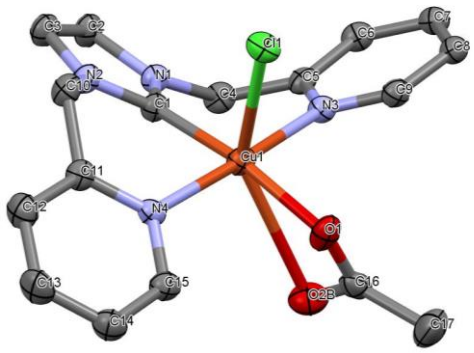

Space group	P $\bar{1}$
Cell lengths	**a** 7.6192(5) **b** 9.8671(6) **c** 14.3365(9)
Cell angles	**α** 108.553(2) **β** 91.958(2) **γ** 111.856(2)
Cell volume	933.977
Z, Z’	**Z**: 2 **Z'**: 1
R-factor (%)	4.51

Bond lengths in **3**

Atom 1	**Atom 2**	**Length**	**Atom 1**	**Atom 2**	**Length**
Cu1	Cl1	2.6051(8)	N2	C3	1.382(6)
Cu1	O1	1.950(3)	N2	C10	1.454(4)
Cu1	O2B	2.74(1)	N3	C5	1.357(4)
Cu1	N3	2.089(3)	N3	C9	1.338(5)
Cu1	N4	2.113(3)	N4	C11	1.348(5)
Cu1	C1	1.924(4)	N4	C15	1.346(5)
O1	C16	1.257(3)	C2	C3	1.351(5)
O2B	C16	1.27(2)	C4	C5	1.506(6)
N1	C1	1.344(4)	C5	C6	1.383(4)
N1	C2	1.384(5)	C6	C7	1.386(6)
N1	C4	1.462(4)	C7	C8	1.385(5)

N2	C1	1.338(4)	C8	C9	1.385(5)
C13	C14	1.375(6)	C10	C11	1.510(5)
C14	C15	1.387(5)	C11	C12	1.392(5)
C16	C17	1.512(7)	C12	C13	1.387(6)

Bonds angles in **3**

Atom 1	**Atom 2**	**Atom 3**	**Angle**	**Atom 1**	**Atom 2**	**Atom 3**	**Angle**
Cl1	Cu1	O1	95.54(8)	Cu1	C1	N2	125.9(2)
Cl1	Cu1	O2B	143.2(3)	N1	C1	N2	105.3(3)
Cl1	Cu1	N3	93.57(8)	N1	C2	C3	106.2(3)
Cl1	Cu1	N4	88.88(8)	N2	C3	C2	106.6(3)
Cl1	Cu1	C1	96.3(1)	N1	C4	C5	112.4(3)
O1	Cu1	O2B	49.0(3)	N3	C5	C4	119.0(3)
O1	Cu1	N3	91.2(1)	N3	C5	C6	121.5(3)
O1	Cu1	N4	92.7(1)	C4	C5	C6	119.5(3)
O1	Cu1	C1	168.2(1)	C5	C6	C7	119.9(3)
O2B	Cu1	N3	79.9(3)	C6	C7	C8	118.5(3)
O2B	Cu1	N4	100.5(3)	C7	C8	C9	118.7(3)
O2B	Cu1	C1	119.4(3)	N3	C9	C8	123.1(3)
N3	Cu1	N4	175.2(1)	N2	C10	C11	114.2(3)
N3	Cu1	C1	88.1(1)	N4	C11	C10	119.3(3)
N4	Cu1	C1	87.5(1)	N4	C11	C12	121.4(3)
Cu1	O1	C16	119.0(2)	C10	C11	C12	119.1(3)
Cu1	O2B	C16	78.8(6)	C11	C12	C13	119.8(4)
C1	N1	C2	110.9(3)	C12	C13	C14	118.9(4)
C1	N1	C4	122.7(3)	C13	C14	C15	118.7(4)
C2	N1	C4	126.4(3)	N4	C15	C14	123.1(3)
C1	N2	C3	111.0(3)	O1	C16	O2B	110.2(7)
C1	N2	C10	122.7(3)	O1	C16	C17	115.8(4)
C3	N2	C10	125.9(3)	O2B	C16	C17	133.0(7)
Cu1	N3	C5	125.8(2)	Cu1	N4	C15	118.9(2)
Cu1	N3	C9	115.3(2)	C11	N4	C15	118.2(3)
C5	N3	C9	118.2(3)	Cu1	C1	N1	127.9(2)
Cu1	N4	C11	122.8(2)				

Structural information for 4

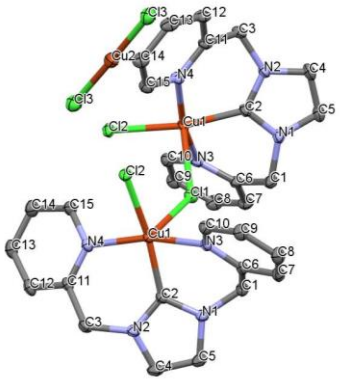

Space group	P 2/c
Cell lengths	**a** 11.5626(3) **b** 8.4390(2) **c** 16.3796(4)
Cell angles	α 90 β 90.4510(10) γ 90
Cell volume	1598.22
Z, Z’	**Z**: 2 **Z'**: 0.5
R-factor (%)	3.4

Bond lengths in **4**

Atom 1	**Atom 2**	**Length**	**Atom 1**	**Atom 2**	**Length**
Cu1	Cl1	2.3256(7)	C18	C19	1.386(5)
Cu1	Cl2	2.2690(7)	Cu1	Cl1	2.3256(7)
Cu1	Cl3	2.2991(7)	Cu1	Cl2	2.2690(7)
Cu1	N3	2.048(2)	Cu1	Cl3	2.2991(7)
Cu1	Cl1	2.6753(6)	Cu1	N3	2.048(2)
Cl1	Cu1	2.6753(6)	N1	C1	1.342(4)
N1	C1	1.342(4)	N1	C3	1.389(3)
N1	C3	1.389(3)	N1	C8	1.460(4)
N1	C8	1.460(4)	N2	C1	1.332(4)
N2	C1	1.332(4)	N2	C2	1.389(4)
N2	C2	1.389(4)	N2	C14	1.463(4)

N2	C14	1.463(4)	N3	C9	1.354(3)
N3	C9	1.354(3)	N3	C13	1.341(4)
N3	C13	1.341(4)	N4	C15	1.348(4)
N4	C15	1.348(4)	N4	C19	1.324(4)
N4	C19	1.324(4)	C2	C3	1.399(4)
C2	C3	1.399(4)	C2	C7	1.391(4)
C2	C7	1.391(4)	C3	C4	1.393(4)
C3	C4	1.393(4)	C4	C5	1.385(4)
C4	C5	1.385(4)	C5	C6	1.411(4)
C5	C6	1.411(4)	C6	C7	1.380(4)
C6	C7	1.380(4)	C8	C9	1.506(4)
C8	C9	1.506(4)	C9	C10	1.384(4)
C9	C10	1.384(4)	C10	C11	1.389(4)
C10	C11	1.389(4)	C11	C12	1.382(4)
C11	C12	1.382(4)	C12	C13	1.386(4)
C12	C13	1.386(4)	C14	C15	1.510(4)
C14	C15	1.510(4)	C15	C16	1.381(4)
C15	C16	1.381(4)	C16	C17	1.416(4)
C16	C17	1.416(4)	C17	C18	1.375(5)
C17	C18	1.375(5)	C18	C19	1.386(5)

Bonds angles in **4**

Atom 1	**Atom 2**	**Atom 3**	**Angle**	**Atom 1**	**Atom 2**	**Atom 3**	**Angle**
Cl1	Cu1	Cl2	92.21(2)	Cl1	Cu1	Cl1	90.94(2)
Cl1	Cu1	Cl3	166.70(3)	Cl1	Cu1	Cl2	95.83(2)
Cl1	Cu1	N3	88.46(6)	Cl1	Cu1	Cl3	101.74(2)
Cl1	Cu1	Cl1	90.94(2)	Cl1	Cu1	N3	96.43(6)
Cl2	Cu1	Cl3	90.50(3)	Cl1	Cu1	Cl2	92.21(2)
Cl2	Cu1	N3	167.71(7)	Cl1	Cu1	Cl3	166.70(3)
Cl2	Cu1	Cl1	95.83(2)	Cl1	Cu1	N3	88.46(6)
Cl3	Cu1	N3	86.16(6)	Cl2	Cu1	Cl3	90.50(3)
Cl3	Cu1	Cl1	101.74(2)	Cl2	Cu1	N3	167.71(7)
N3	Cu1	Cl1	96.43(6)	Cl3	Cu1	N3	86.16(6)
Cu1	Cl1	Cu1	89.06(2)	Cu1	Cl1	Cu1	89.06(2)
C1	N1	C3	108.7(2)	C1	N1	C3	108.7(2)
C1	N1	C8	126.6(2)	C1	N1	C8	126.6(2)
C3	N1	C8	124.7(2)	C3	N1	C8	124.7(2)
C1	N2	C2	108.9(2)	C1	N2	C2	108.9(2)
C1	N2	C14	126.3(2)	C1	N2	C14	126.3(2)
C2	N2	C14	124.7(2)	C2	N2	C14	124.7(2)
Cu1	N3	C9	121.2(2)	Cu1	N3	C9	121.2(2)
Cu1	N3	C13	120.1(2)	Cu1	N3	C13	120.1(2)

C9	N3	C13	118.4(2)	C9	N3	C13	118.4(2)
C15	N4	C19	118.2(3)	C15	N4	C19	118.2(3)
N1	C1	N2	109.5(2)	N1	C1	N2	109.5(2)
N2	C2	C3	106.6(2)	N2	C2	C3	106.6(2)
N2	C2	C7	131.5(3)	N2	C2	C7	131.5(3)
C3	C2	C7	122.0(3)	C3	C2	C7	122.0(3)
N1	C3	C2	106.3(2)	N1	C3	C2	106.3(2)
N1	C3	C4	131.8(3)	N1	C3	C4	131.8(3)
C2	C3	C4	121.9(3)	C2	C3	C4	121.9(3)
C3	C4	C5	116.2(3)	C3	C4	C5	116.2(3)
C4	C5	C6	121.8(3)	C4	C5	C6	121.8(3)
C5	C6	C7	121.9(3)	C5	C6	C7	121.9(3)
C2	C7	C6	116.3(3)	C2	C7	C6	116.3(3)
N1	C8	C9	113.0(2)	N1	C8	C9	113.0(2)
N3	C9	C8	115.3(2)	N3	C9	C8	115.3(2)
N3	C9	C10	121.7(3)	N3	C9	C10	121.7(3)
C8	C9	C10	122.9(2)	C8	C9	C10	122.9(2)
C9	C10	C11	119.4(3)	C9	C10	C11	119.4(3)
C10	C11	C12	118.9(3)	C10	C11	C12	118.9(3)
C11	C12	C13	118.6(3)	C11	C12	C13	118.6(3)
N3	C13	C12	122.9(3)	N3	C13	C12	122.9(3)
N2	C14	C15	111.1(2)	N2	C14	C15	111.1(2)
N4	C15	C14	114.6(3)	N4	C15	C14	114.6(3)
N4	C15	C16	122.3(3)	N4	C15	C16	122.3(3)
C14	C15	C16	123.1(3)	C14	C15	C16	123.1(3)
C15	C16	C17	118.9(3)	C15	C16	C17	118.9(3)
C16	C17	C18	117.8(3)	C16	C17	C18	117.8(3)
C17	C18	C19	119.2(3)	C17	C18	C19	119.2(3)
N4	C19	C18	123.5(3)	N4	C19	C18	123.5(3)

Structural information for 5

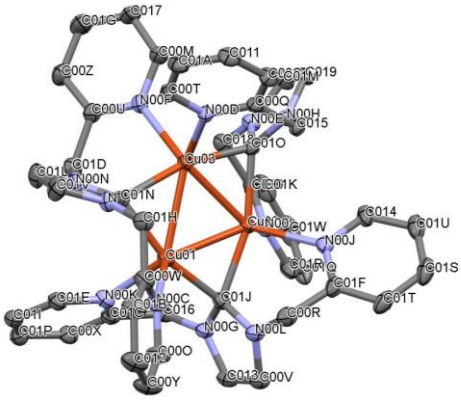

Space group	P 1
Cell lengths	**a** 11.3768(5) **b** 11.7673(5) **c** 12.2790(5)
Cell angles	α 114.5110(10) β 112.3100(10) γ 97.695(2)
Cell volume	1298.19
Z, Z’	**Z**: 4 **Z'**: 4
R-factor (%)	4.61

Bond lengths in **5**

Atom 1	**Atom 2**	**Length**	**Atom 1**	**Atom 2**	**Length**
Cu01	Cu02	2.5221(9)	C00M	C017	1.39(1)
Cu01	Cu03	2.5112(9)	N00N	C01D	1.460(6)
Cu01	N00C	2.172(5)	N00N	C01L	1.370(9)
Cu01	N00K	2.143(4)	N00N	C01N	1.372(8)
Cu01	C01J	2.021(6)	C00O	C00Y	1.386(9)
Cu01	C01N	2.032(5)	N	C01H	1.465(8)
Cu02	Cu03	2.5144(9)	N	C01N	1.369(5)
Cu02	N00I	2.155(4)	N	C01V	1.37(1)
Cu02	N00J	2.164(6)	C00Q	C00S	1.391(4)
Cu02	C01J	2.053(5)	C00Q	C015	1.512(7)
Cu02	C01O	2.027(5)	C00R	C01F	1.507(9)

Cu03	N00D	2.154(3)	C00S	C011	1.390(9)
Cu03	N00F	2.144(6)	C00T	C01A	1.384(5)
Cu03	C01N	2.020(5)	C00U	C00Z	1.38(1)
Cu03	C01O	2.032(5)	C00U	C01D	1.513(8)
N00C	C00O	1.342(8)	C00V	C013	1.351(8)
N00C	C00W	1.342(6)	C00W	C01B	1.387(8)
N00D	C00Q	1.341(7)	C00W	C01H	1.502(9)
N00D	C00T	1.352(7)	C00X	C01C	1.389(7)
N00E	C018	1.454(5)	C00X	C01P	1.39(1)
N00E	C01M	1.383(7)	C00Y	C012	1.395(7)
N00E	C01O	1.368(6)	C00Z	C01G	1.39(1)
N00F	C00M	1.344(8)	C010	C018	1.509(8)
N00F	C00U	1.335(7)	C010	C01K	1.398(6)
N00G	C013	1.385(8)	C011	C01A	1.377(9)
N00G	C016	1.460(7)	C012	C01B	1.38(1)
N00G	C01J	1.361(4)	C014	C01U	1.39(1)
N00H	C015	1.448(5)	C016	C01C	1.508(9)
N00H	C019	1.386(8)	C017	C01G	1.38(1)
N00H	C01O	1.371(5)	C019	C01M	1.357(6)
N00I	C010	1.342(9)	C01E	C01I	1.386(7)
N00I	C01R	1.340(8)	C01F	C01T	1.40(1)
N00J	C014	1.333(8)	C01I	C01P	1.382(6)
N00J	C01F	1.351(9)	C01K	C01W	1.39(1)
N00K	C01C	1.338(5)	C01L	C01V	1.370(9)
N00K	C01E	1.354(8)	C01Q	C01R	1.387(7)
N00L	C00R	1.465(6)	C01Q	C01W	1.37(1)
N00L	C00V	1.388(7)	C01S	C01T	1.38(1)
N00L	C01J	1.363(8)	C01S	C01U	1.39(1)

Bonds angles in **5**

Atom 1	**Atom 2**	**Atom 3**	**Angle**	**Atom 1**	**Atom 2**	**Atom 3**	**Angle**
Cu02	Cu01	Cu03	59.94(2)	C01L	N00N	C01N	112.3(5)
Cu02	Cu01	N00C	129.2(1)	N00C	C00O	C00Y	122.8(6)
Cu02	Cu01	N00K	124.8(1)	C01H	N	C01N	122.0(5)
Cu02	Cu01	C01J	52.3(1)	C01H	N	C01V	125.4(5)
Cu02	Cu01	C01N	111.3(1)	C01N	N	C01V	112.4(5)
Cu03	Cu01	N00C	123.2(1)	N00D	C00Q	C00S	122.3(5)
Cu03	Cu01	N00K	127.9(1)	N00D	C00Q	C015	117.6(4)
Cu03	Cu01	C01J	112.3(1)	C00S	C00Q	C015	120.0(4)
Cu03	Cu01	C01N	51.5(1)	N00L	C00R	C01F	110.9(5)
N00C	Cu01	N00K	93.8(2)	C00Q	C00S	C011	119.3(5)
N00C	Cu01	C01J	100.6(2)	N00D	C00T	C01A	123.2(5)

N00C	Cu01	C01N	93.3(2)	N00F	C00U	C00Z	123.2(5)
N00K	Cu01	C01J	92.3(2)	N00F	C00U	C01D	115.6(5)
N00K	Cu01	C01N	96.2(2)	C00Z	C00U	C01D	121.2(5)
C01J	Cu01	C01N	163.3(2)	N00L	C00V	C013	105.9(5)
Cu01	Cu02	Cu03	59.81(2)	N00C	C00W	C01B	122.1(5)
Cu01	Cu02	N00I	126.0(1)	N00C	C00W	C01H	116.4(5)
Cu01	Cu02	N00J	123.7(1)	C01B	C00W	C01H	121.4(5)
Cu01	Cu02	C01J	51.2(1)	C01C	C00X	C01P	119.5(5)
Cu01	Cu02	C01O	111.6(1)	C00O	C00Y	C012	119.0(6)
Cu03	Cu02	N00I	123.6(1)	C00U	C00Z	C01G	118.5(6)
Cu03	Cu02	N00J	126.9(1)	N00I	C010	C018	116.3(5)
Cu03	Cu02	C01J	111.0(1)	N00I	C010	C01K	122.7(5)
Cu03	Cu02	C01O	51.8(1)	C018	C010	C01K	120.9(5)
N00I	Cu02	N00J	97.1(2)	C00S	C011	C01A	118.7(5)
N00I	Cu02	C01J	97.4(2)	C00Y	C012	C01B	117.9(6)
N00I	Cu02	C01O	91.9(2)	N00G	C013	C00V	106.7(5)
N00J	Cu02	C01J	93.8(2)	N00J	C014	C01U	123.4(5)
N00J	Cu02	C01O	99.7(2)	N00H	C015	C00Q	112.0(4)
C01J	Cu02	C01O	162.6(2)	N00G	C016	C01C	112.7(4)
Cu01	Cu03	Cu02	60.25(2)	C00M	C017	C01G	118.8(7)
Cu01	Cu03	N00D	127.7(1)	N00E	C018	C010	110.8(4)
Cu01	Cu03	N00F	126.4(1)	N00H	C019	C01M	106.3(5)
Cu01	Cu03	C01N	51.9(1)	C00T	C01A	C011	118.8(5)
Cu01	Cu03	C01O	111.8(1)	C00W	C01B	C012	120.0(6)
Cu02	Cu03	N00D	122.7(1)	N00K	C01C	C00X	122.0(5)
Cu02	Cu03	N00F	128.1(1)	N00K	C01C	C016	117.4(5)
Cu02	Cu03	C01N	112.1(1)	C00X	C01C	C016	120.5(5)
Cu02	Cu03	C01O	51.6(1)	N00N	C01D	C00U	109.0(4)
N00D	Cu03	N00F	93.8(2)	N00K	C01E	C01I	123.0(5)
N00D	Cu03	C01N	101.7(2)	N00J	C01F	C00R	116.5(5)
N00D	Cu03	C01O	93.1(2)	N00J	C01F	C01T	123.1(6)
N00F	Cu03	C01N	92.1(2)	C00R	C01F	C01T	120.3(5)
N00F	Cu03	C01O	95.6(2)	C00Z	C01G	C017	118.8(7)
C01N	Cu03	C01O	162.9(2)	N	C01H	C00W	110.9(5)
Cu01	N00C	C00O	119.6(4)	C01E	C01I	C01P	118.4(5)
Cu01	N00C	C00W	121.9(4)	Cu01	C01J	Cu02	76.5(2)
C00O	N00C	C00W	118.2(5)	Cu01	C01J	N00G	114.9(4)
Cu03	N00D	C00Q	122.3(4)	Cu01	C01J	N00L	124.3(4)
Cu03	N00D	C00T	119.9(4)	Cu02	C01J	N00G	124.8(4)
C00Q	N00D	C00T	117.6(5)	Cu02	C01J	N00L	113.7(4)
C018	N00E	C01M	124.9(5)	N00G	C01J	N00L	102.9(4)
C018	N00E	C01O	122.6(4)	C010	C01K	C01W	118.7(6)
C01M	N00E	C01O	112.2(5)	N00N	C01L	C01V	106.4(6)
Cu03	N00F	C00M	119.3(4)	N00E	C01M	C019	106.6(5)
Cu03	N00F	C00U	122.6(4)	Cu01	C01N	Cu03	76.6(2)

C00M	N00F	C00U	118.1(5)	Cu01	C01N	N00N	124.4(4)
C013	N00G	C016	124.6(5)	Cu01	C01N	N	114.7(3)
C013	N00G	C01J	112.1(5)	Cu03	C01N	N00N	114.2(3)
C016	N00G	C01J	123.2(4)	Cu03	C01N	N	124.6(4)
C015	N00H	C019	124.9(4)	N00N	C01N	N	102.7(4)
C015	N00H	C01O	122.7(4)	Cu02	C01O	Cu03	76.6(2)
C019	N00H	C01O	112.1(4)	Cu02	C01O	N00E	115.7(3)
Cu02	N00I	C010	122.3(4)	Cu02	C01O	N00H	126.6(3)
Cu02	N00I	C01R	120.5(4)	Cu03	C01O	N00E	121.2(4)
C010	N00I	C01R	117.2(5)	Cu03	C01O	N00H	113.9(3)
Cu02	N00J	C014	120.9(4)	N00E	C01O	N00H	102.8(4)
Cu02	N00J	C01F	121.6(4)	C00X	C01P	C01I	118.9(6)
C014	N00J	C01F	117.5(5)	C01R	C01Q	C01W	119.0(6)
Cu01	N00K	C01C	122.0(4)	N00I	C01R	C01Q	123.5(6)
Cu01	N00K	C01E	119.3(4)	C01T	C01S	C01U	119.2(6)
C01C	N00K	C01E	118.1(5)	C01F	C01T	C01S	118.4(6)
C00R	N00L	C00V	124.0(5)	C014	C01U	C01S	118.4(6)
C00R	N00L	C01J	123.2(5)	N	C01V	C01L	106.2(6)
C00V	N00L	C01J	112.3(5)	C01K	C01W	C01Q	118.8(6)
N00F	C00M	C017	122.5(6)	O00B	C020	C01X	88.0(9)
C01D	N00N	C01L	124.3(5)	N01Z	C01Y	C1	179(1)
C01D	N00N	C01N	122.6(4)				

Structural information for 6

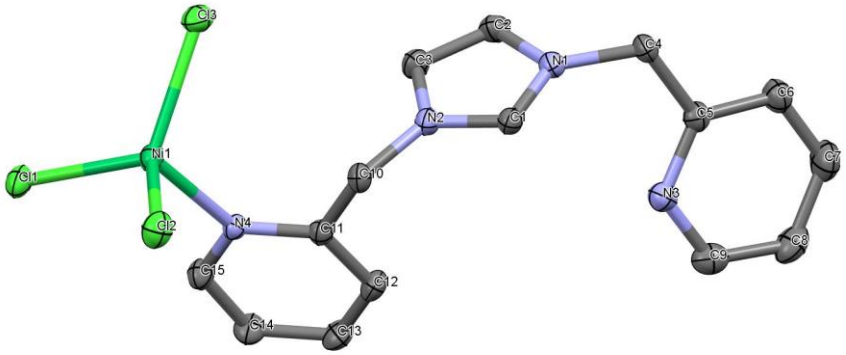

Space group	P 2_1 2_1 2_1
Cell lengths	**a** 8.2819(3) **b** 13.1635(5) **c** 15.8805(6)
Cell angles	**α** 90 **β** 90 γ 90
Cell volume	1731.27
Z, Z’	**Z**: 4 **Z'**: 1
R-factor (%)	2.14

Bond lengths in **6**

Atom 1	**Atom 2**	**Length**	**Atom 1**	**Atom 2**	**Length**
Ni1	Cl1	2.2608(7)	N4	C11	1.348(3)
Ni1	Cl2	2.2458(7)	N4	C15	1.342(3)
Ni1	Cl3	2.2476(6)	C2	C3	1.357(3)
Ni1	N4	2.030(2)	C4	C5	1.507(3)
N1	C1	1.329(3)	C5	C6	1.393(3)
N1	C2	1.379(3)	C6	C7	1.378(4)
N1	C4	1.464(3)	C7	C8	1.385(4)
N2	C1	1.326(3)	C8	C9	1.384(4)
N2	C3	1.382(3)	C10	C11	1.509(3)
N2	C10	1.470(3)	C11	C12	1.393(3)
N3	C5	1.339(3)	C12	C13	1.382(3)

N3	C9	1.338(3)	C13	C14	1.384(4)
C14	C15	1.384(3)			

Bonds angles in **6**

Atom 1	**Atom 2**	**Atom 3**	**Angle**	**Atom 1**	**Atom 2**	**Atom 3**	**Angle**
Cl1	Ni1	Cl2	107.24(3)	N1	C2	C3	106.8(2)
Cl1	Ni1	Cl3	115.50(2)	N2	C3	C2	106.6(2)
Cl1	Ni1	N4	105.04(5)	N1	C4	C5	112.0(2)
Cl2	Ni1	Cl3	118.84(3)	N3	C5	C4	117.3(2)
Cl2	Ni1	N4	102.07(5)	N3	C5	C6	122.8(2)
Cl3	Ni1	N4	106.41(5)	C4	C5	C6	119.8(2)
C1	N1	C2	109.1(2)	C5	C6	C7	118.7(2)
C1	N1	C4	124.6(2)	C6	C7	C8	119.0(2)
C2	N1	C4	126.3(2)	C7	C8	C9	118.4(2)
C1	N2	C3	109.2(2)	N3	C9	C8	123.5(2)
C1	N2	C10	125.6(2)	N2	C10	C11	109.2(2)
C3	N2	C10	125.1(2)	N4	C11	C10	118.6(2)
C5	N3	C9	117.5(2)	N4	C11	C12	121.5(2)
Ni1	N4	C11	124.0(1)	C10	C11	C12	119.9(2)
Ni1	N4	C15	117.5(1)	C11	C12	C13	119.6(2)
C11	N4	C15	118.4(2)	C12	C13	C14	118.7(2)
N1	C1	N2	108.3(2)	C13	C14	C15	118.9(2)
N4	C15	C14	122.9(2)				

Structural information for 7

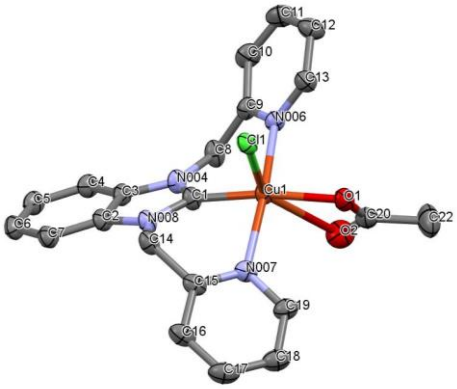

Space group	P 2_1/n
Cell lengths	**a** 12.5284(6) **b** 12.9661(5) **c** 15.6660(7)
Cell angles	α 90 β 112.876(2) γ 90
Cell volume	2344.7
Z, Z’	**Z**: 4 **Z'**: 1
R-factor (%)	4.51

Bond lengths in **7**

Atom 1	**Atom 2**	**Length**	**Atom 1**	**Atom 2**	**Length**
Cu1	Cl1	2.5503(7)	C9	C10	1.392(3)
Cu1	O1	1.975(2)	C9	C8	1.509(3)
Cu1	O2	2.728(3)	C13	C12	1.386(4)
Cu1	N006	2.108(2)	C2	C3	1.396(3)
Cu1	N007	2.127(2)	C2	C7	1.390(3)
Cu1	C1	1.929(2)	C15	C14	1.506(4)
O1	C20	1.263(3)	C15	C16	1.392(3)
N004	C1	1.352(2)	C10	C11	1.374(4)
N004	C3	1.393(3)	C3	C4	1.394(3)
N004	C8	1.456(3)	C12	C11	1.398(3)
O2	C20	1.246(3)	C20	C22	1.509(5)

N006	C9	1.353(2)	C19	C18	1.385(4)
N006	C13	1.337(3)	C7	C6	1.392(3)
N007	C15	1.347(3)	C4	C5	1.387(4)
N007	C19	1.345(3)	C5	C6	1.400(3)
N008	C1	1.341(3)	C16	C17	1.379(4)
N008	C2	1.397(3)	C18	C17	1.378(4)
N008	C14	1.456(2)			

Bonds angles in **7**

Atom 1	**Atom 2**	**Atom 3**	**Angle**	**Atom 1**	**Atom 2**	**Atom 3**	**Angle**
Cl1	Cu1	O1	93.69(5)	C10	C9	C8	119.9(2)
Cl1	Cu1	O2	146.49(5)	N006	C13	C12	123.6(2)
Cl1	Cu1	N006	94.68(6)	Cu1	C1	N004	127.3(2)
Cl1	Cu1	N007	91.29(6)	Cu1	C1	N008	125.7(2)
Cl1	Cu1	C1	103.98(7)	N004	C1	N008	107.0(2)
O1	Cu1	O2	53.12(7)	N008	C2	C3	105.6(2)
O1	Cu1	N006	90.71(7)	N008	C2	C7	132.1(2)
O1	Cu1	N007	94.48(7)	C3	C2	C7	122.3(2)
O1	Cu1	C1	162.30(9)	N007	C15	C14	118.8(2)
O2	Cu1	N006	82.63(7)	N007	C15	C16	122.4(2)
O2	Cu1	N007	95.44(7)	C14	C15	C16	118.9(2)
O2	Cu1	C1	109.19(8)	N008	C14	C15	111.5(2)
N006	Cu1	N007	171.83(8)	C9	C10	C11	119.8(2)
N006	Cu1	C1	86.83(9)	N004	C3	C2	106.4(2)
N007	Cu1	C1	86.31(9)	N004	C3	C4	131.8(2)
Cu1	O1	C20	109.2(2)	C2	C3	C4	121.8(2)
C1	N004	C3	110.2(2)	C13	C12	C11	117.6(2)
C1	N004	C8	122.5(2)	O1	C20	O2	123.3(2)
C3	N004	C8	127.3(2)	O1	C20	C22	115.9(3)
Cu1	O2	C20	74.1(2)	O2	C20	C22	120.8(3)
Cu1	N006	C9	124.4(2)	N007	C19	C18	122.9(2)
Cu1	N006	C13	116.4(2)	C2	C7	C6	115.9(2)
C9	N006	C13	118.3(2)	C3	C4	C5	115.9(2)
Cu1	N007	C15	121.8(2)	C4	C5	C6	122.3(2)
Cu1	N007	C19	120.6(2)	C15	C16	C17	119.2(2)
C15	N007	C19	117.6(2)	C10	C11	C12	119.2(2)
C1	N008	C2	110.9(2)	N004	C8	C9	112.1(2)
C1	N008	C14	120.8(2)	C7	C6	C5	121.8(2)
C2	N008	C14	128.3(2)	C19	C18	C17	119.0(2)
N006	C9	C10	121.3(2)	C16	C17	C18	118.8(2)
N006	C9	C8	118.7(2)				

Structural information for 8

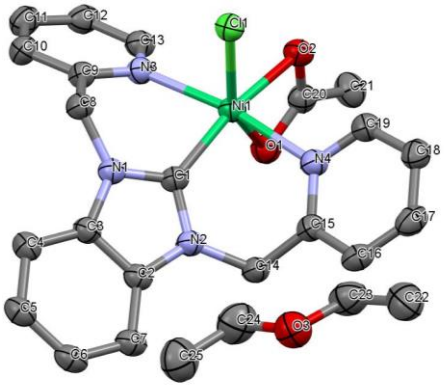

Space group	P 2_1/n
Cell lengths	**a** 12.0206(4) **b** 13.4929(4) **c** 15.8346(5)
Cell angles	**α** 90 **β** 111.5230(10) **γ** 90
Cell volume	2389.17
Z, Z’	**Z**: 4 **Z'**: 1
R-factor (%)	4.6

Bond lengths in **8**

Atom 1	**Atom 2**	**Length**	**Atom 1**	**Atom 2**	**Length**
Ni1	Cl1	2.4081(6)	C3	C4	1.392(3)
Ni1	O1	2.196(2)	C4	C5	1.393(3)
Ni1	O2	2.099(2)	C5	C6	1.403(3)
Ni1	N3	2.179(2)	C6	C7	1.388(3)
Ni1	N4	2.168(2)	C8	C9	1.512(3)
Ni1	C1	1.970(2)	C9	C10	1.393(3)
O1	C20	1.261(2)	C10	C11	1.385(4)
O2	C20	1.265(3)	C11	C12	1.380(4)
N1	C1	1.348(3)	C12	C13	1.388(3)
N1	C3	1.394(2)	C14	C15	1.512(3)
N1	C8	1.459(2)	C15	C16	1.384(3)

N2	C1	1.348(2)	C16	C17	1.383(3)
N2	C2	1.385(3)	C17	C18	1.385(3)
N2	C14	1.468(3)	C18	C19	1.391(3)
N3	C9	1.350(3)	C20	C21	1.508(4)
N3	C13	1.344(3)	O3	C23	1.405(4)
N4	C15	1.358(2)	O3	C24	1.412(5)
N4	C19	1.341(3)	C22	C23	1.522(6)
C2	C3	1.399(3)	C24	C25	1.509(6)
C2	C7	1.399(2)			

Bonds angles in **8**

Atom 1	**Atom 2**	**Atom 3**	**Angle**	**Atom 1**	**Atom 2**	**Atom 3**	**Angle**
Cl1	Ni1	O1	153.41(5)	N2	C2	C3	105.9(2)
Cl1	Ni1	O2	92.14(5)	N2	C2	C7	132.2(2)
Cl1	Ni1	N3	91.14(5)	C3	C2	C7	121.9(2)
Cl1	Ni1	N4	93.04(5)	N1	C3	C2	105.5(2)
Cl1	Ni1	C1	101.21(6)	N1	C3	C4	132.4(2)
O1	Ni1	O2	61.27(6)	C2	C3	C4	122.1(2)
O1	Ni1	N3	92.83(6)	C3	C4	C5	116.1(2)
O1	Ni1	N4	87.11(7)	C4	C5	C6	121.9(2)
O1	Ni1	C1	105.34(7)	C5	C6	C7	122.1(2)
O2	Ni1	N3	97.72(7)	C2	C7	C6	116.0(2)
O2	Ni1	N4	90.37(7)	N1	C8	C9	112.3(2)
O2	Ni1	C1	166.42(8)	N3	C9	C8	119.0(2)
N3	Ni1	N4	170.75(7)	N3	C9	C10	122.2(2)
N3	Ni1	C1	84.62(8)	C8	C9	C10	118.8(2)
N4	Ni1	C1	86.47(8)	C9	C10	C11	119.2(2)
Ni1	O1	C20	86.9(1)	C10	C11	C12	119.0(2)
Ni1	O2	C20	91.2(1)	C11	C12	C13	118.6(2)
C1	N1	C3	111.2(2)	N3	C13	C12	123.3(2)
C1	N1	C8	120.8(2)	N2	C14	C15	111.7(2)
C3	N1	C8	127.7(2)	N4	C15	C14	118.5(2)
C1	N2	C2	111.5(2)	N4	C15	C16	122.0(2)
C1	N2	C14	121.2(2)	C14	C15	C16	119.4(2)
C2	N2	C14	127.3(2)	C15	C16	C17	119.4(2)
Ni1	N3	C9	122.2(1)	C16	C17	C18	119.2(2)
Ni1	N3	C13	120.1(1)	C17	C18	C19	118.2(2)
C9	N3	C13	117.7(2)	N4	C19	C18	123.3(2)
Ni1	N4	C15	122.9(1)	O1	C20	O2	120.3(2)
Ni1	N4	C19	118.2(1)	O1	C20	C21	121.0(2)
C15	N4	C19	117.8(2)	O2	C20	C21	118.7(2)
Ni1	C1	N1	126.5(2)	C23	O3	C24	111.6(3)

Ni1	C1	N2	127.6(2)	O3	C23	C22	108.2(3)
N1	C1	N2	105.8(2)	O3	C24	C25	108.7(3)

Structural information for 9

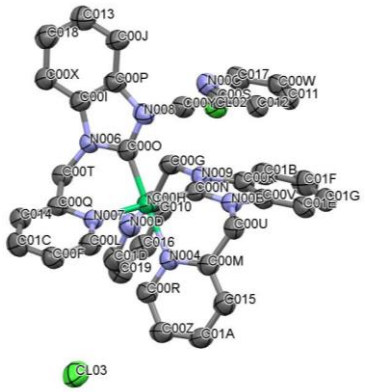

Space group	P 2_1/n
Cell lengths	**a** 13.917(1) **b** 18.8769(13) **c** 15.225(1)
Cell angles	α 90 β 91.848(3) γ 90
Cell volume	3997.57
Z, Z’	**Z**: 1 **Z'**: 0.25
R-factor (%)	27.32

Bond lengths in **9**

Atom 1	**Atom 2**	**Length**	**Atom 1**	**Atom 2**	**Length**
NI01	N004	1.9657	C00I	C00P	1.3897
NI01	N007	1.9481	C00I	C00X	1.3823
NI01	C00N	1.8528	C00J	C00P	1.3957
NI01	C00O	1.8702	C00J	C013	1.3856
N004	C00M	1.3544	C00K	C00V	1.3868
N004	C00R	1.3331	C00K	C01B	1.4070
N006	C00I	1.3983	C00M	C00U	1.4867
N006	C00O	1.3522	C00M	C015	1.3833
N006	C00T	1.4506	C00Q	C00T	1.4975
N007	C00L	1.3412	C00Q	C014	1.3704
N007	C00Q	1.3661	C00R	C00Z	1.3982

N008	C00O	1.3450	C00S	C00Y	1.5152
N008	C00P	1.4186	C00S	C012	1.3668
N008	C00Y	1.4650	C00V	C01E	1.3630
N009	C00G	1.4331	C00W	C011	1.3481
N009	C00K	1.4040	C00W	C017	1.3887
N009	C00N	1.3848	C00X	C018	1.3841
N00B	C00N	1.3113	C00Z	C01A	1.3607
N00B	C00U	1.4789	C010	C016	1.3826
N00B	C00V	1.3896	C011	C012	1.3796
N00C	C00S	1.3429	C013	C018	1.4251
N00C	C017	1.3524	C014	C01C	1.4029
N00D	C00H	1.3304	C015	C01A	1.3878
N00D	C01D	1.3435	C016	C019	1.3768
C00F	C00L	1.3882	C019	C01D	1.3536
C00F	C01C	1.3574	C01B	C01F	1.3599
C00G	C00H	1.4985	C01E	C01G	1.3497
C00H	C010	1.3842	C01F	C01G	1.4319

Bonds angles in **9**

Atom 1	**Atom 2**	**Atom 3**	**Angle**	**Atom 1**	**Atom 2**	**Atom 3**	**Angle**
N004	NI01	N007	93.49	NI01	C00N	N00B	123.74
N004	NI01	C00N	85.90	N009	C00N	N00B	106.75
N004	NI01	C00O	176.17	NI01	C00O	N006	119.74
N007	NI01	C00N	174.27	NI01	C00O	N008	132.97
N007	NI01	C00O	88.18	N006	C00O	N008	107.24
C00N	NI01	C00O	92.78	N008	C00P	C00I	106.60
NI01	N004	C00M	120.41	N008	C00P	C00J	130.33
NI01	N004	C00R	121.14	C00I	C00P	C00J	123.03
C00M	N004	C00R	118.45	N007	C00Q	C00T	117.28
C00I	N006	C00O	110.98	N007	C00Q	C014	121.25
C00I	N006	C00T	126.91	C00T	C00Q	C014	121.41
C00O	N006	C00T	121.94	N004	C00R	C00Z	121.94
NI01	N007	C00L	120.95	N00C	C00S	C00Y	117.07
NI01	N007	C00Q	120.77	N00C	C00S	C012	122.87
C00L	N007	C00Q	118.26	C00Y	C00S	C012	120.02
C00O	N008	C00P	109.55	N006	C00T	C00Q	109.95
C00O	N008	C00Y	126.78	N00B	C00U	C00M	107.87
C00P	N008	C00Y	123.48	N00B	C00V	C00K	103.64
C00G	N009	C00K	125.11	N00B	C00V	C01E	135.76
C00G	N009	C00N	126.81	C00K	C00V	C01E	120.59
C00K	N009	C00N	107.28	C011	C00W	C017	118.81
C00N	N00B	C00U	119.42	C00I	C00X	C018	117.54

C00N	N00B	C00V	113.53	N008	C00Y	C00S	113.42
C00U	N00B	C00V	124.70	C00R	C00Z	C01A	120.03
C00S	N00C	C017	117.58	C00H	C010	C016	117.74
C00L	C00F	C01C	118.89	C00W	C011	C012	120.13
N009	C00G	C00H	110.39	C00S	C012	C011	118.47
N00D	C00H	C00G	115.39	C00J	C013	C018	123.36
N00D	C00H	C010	123.58	C00Q	C014	C01C	119.54
C00G	C00H	C010	120.92	C00M	C015	C01A	120.01
N006	C00I	C00P	105.62	C010	C016	C019	119.52
N006	C00I	C00X	132.74	N00C	C017	C00W	121.98
C00P	C00I	C00X	121.64	C00X	C018	C013	119.81
C00P	C00J	C013	114.59	C016	C019	C01D	118.04
N009	C00K	C00V	108.68	C00Z	C01A	C015	118.00
N009	C00K	C01B	129.48	C00K	C01B	C01F	115.23
C00V	C00K	C01B	121.82	C00F	C01C	C014	119.20
N007	C00L	C00F	122.82	N00D	C01D	C019	124.61
N004	C00M	C00U	118.15	C00V	C01E	C01G	120.55
N004	C00M	C015	121.50	C01B	C01F	C01G	123.70
C00U	C00M	C015	120.26	C01E	C01G	C01F	118.09
NI01	C00N	N009	128.34				

Structural information for 10

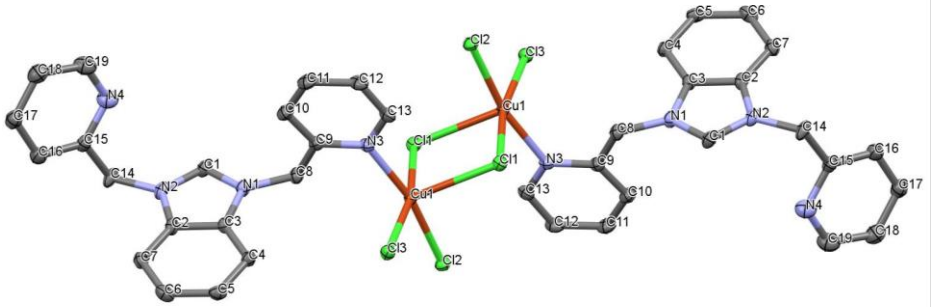

Space group	P 2_1/c
Cell lengths	**a** 10.1136(3) **b** 13.6081(4) **c** 13.8942(5)
Cell angles	α 90 β 92.5610(10) γ 90
Cell volume	1910.31
Z, Z’	**Z**: 4 **Z'**: 1
R-factor (%)	5.39

Bond lengths in **10**

Atom 1	**Atom 2**	**Length**	**Atom 1**	**Atom 2**	**Length**
Cu1	Cl1	2.3256(7)	C18	C19	1.386(5)
Cu1	Cl2	2.2690(7)	Cu1	Cl1	2.3256(7)
Cu1	Cl3	2.2991(7)	Cu1	Cl2	2.2690(7)
Cu1	N3	2.048(2)	Cu1	Cl3	2.2991(7)
Cu1	Cl1	2.6753(6)	Cu1	N3	2.048(2)
Cl1	Cu1	2.6753(6)	N1	C1	1.342(4)
N1	C1	1.342(4)	N1	C3	1.389(3)
N1	C3	1.389(3)	N1	C8	1.460(4)
N1	C8	1.460(4)	N2	C1	1.332(4)
N2	C1	1.332(4)	N2	C2	1.389(4)
N2	C2	1.389(4)	N2	C14	1.463(4)

N2	C14	1.463(4)	N3	C9	1.354(3)
N3	C9	1.354(3)	N3	C13	1.341(4)
N3	C13	1.341(4)	N4	C15	1.348(4)
N4	C15	1.348(4)	N4	C19	1.324(4)
N4	C19	1.324(4)	C2	C3	1.399(4)
C2	C3	1.399(4)	C2	C7	1.391(4)
C2	C7	1.391(4)	C3	C4	1.393(4)
C3	C4	1.393(4)	C4	C5	1.385(4)
C4	C5	1.385(4)	C5	C6	1.411(4)
C5	C6	1.411(4)	C6	C7	1.380(4)
C6	C7	1.380(4)	C8	C9	1.506(4)
C8	C9	1.506(4)	C9	C10	1.384(4)
C9	C10	1.384(4)	C10	C11	1.389(4)
C10	C11	1.389(4)	C11	C12	1.382(4)
C11	C12	1.382(4)	C12	C13	1.386(4)
C12	C13	1.386(4)	C14	C15	1.510(4)
C14	C15	1.510(4)	C15	C16	1.381(4)
C15	C16	1.381(4)	C16	C17	1.416(4)
C16	C17	1.416(4)	C17	C18	1.375(5)
C17	C18	1.375(5)	C18	C19	1.386(5)

Bonds angles in **10**

Atom 1	**Atom 2**	**Atom 3**	**Angle**	**Atom 1**	**Atom 2**	**Atom 3**	**Angle**
Cl1	Cu1	Cl2	92.21(2)	Cl1	Cu1	Cl1	90.94(2)
Cl1	Cu1	Cl3	166.70(3)	Cl1	Cu1	Cl2	95.83(2)
Cl1	Cu1	N3	88.46(6)	Cl1	Cu1	Cl3	101.74(2)
Cl1	Cu1	Cl1	90.94(2)	Cl1	Cu1	N3	96.43(6)
Cl2	Cu1	Cl3	90.50(3)	Cl1	Cu1	Cl2	92.21(2)
Cl2	Cu1	N3	167.71(7)	Cl1	Cu1	Cl3	166.70(3)
Cl2	Cu1	Cl1	95.83(2)	Cl1	Cu1	N3	88.46(6)
Cl3	Cu1	N3	86.16(6)	Cl2	Cu1	Cl3	90.50(3)
Cl3	Cu1	Cl1	101.74(2)	Cl2	Cu1	N3	167.71(7)
N3	Cu1	Cl1	96.43(6)	Cl3	Cu1	N3	86.16(6)
Cu1	Cl1	Cu1	89.06(2)	Cu1	Cl1	Cu1	89.06(2)
C1	N1	C3	108.7(2)	C1	N1	C3	108.7(2)
C1	N1	C8	126.6(2)	C1	N1	C8	126.6(2)
C3	N1	C8	124.7(2)	C3	N1	C8	124.7(2)
C1	N2	C2	108.9(2)	C1	N2	C2	108.9(2)
C1	N2	C14	126.3(2)	C1	N2	C14	126.3(2)
C2	N2	C14	124.7(2)	C2	N2	C14	124.7(2)
Cu1	N3	C9	121.2(2)	Cu1	N3	C9	121.2(2)
Cu1	N3	C13	120.1(2)	Cu1	N3	C13	120.1(2)

C9	N3	C13	118.4(2)	C9	N3	C13	118.4(2)
C15	N4	C19	118.2(3)	C15	N4	C19	118.2(3)
N1	C1	N2	109.5(2)	N1	C1	N2	109.5(2)
N2	C2	C3	106.6(2)	N2	C2	C3	106.6(2)
N2	C2	C7	131.5(3)	N2	C2	C7	131.5(3)
C3	C2	C7	122.0(3)	C3	C2	C7	122.0(3)
N1	C3	C2	106.3(2)	N1	C3	C2	106.3(2)
N1	C3	C4	131.8(3)	N1	C3	C4	131.8(3)
C2	C3	C4	121.9(3)	C2	C3	C4	121.9(3)
C3	C4	C5	116.2(3)	C3	C4	C5	116.2(3)
C4	C5	C6	121.8(3)	C4	C5	C6	121.8(3)
C5	C6	C7	121.9(3)	C5	C6	C7	121.9(3)
C2	C7	C6	116.3(3)	C2	C7	C6	116.3(3)
N1	C8	C9	113.0(2)	N1	C8	C9	113.0(2)
N3	C9	C8	115.3(2)	N3	C9	C8	115.3(2)
N3	C9	C10	121.7(3)	N3	C9	C10	121.7(3)
C8	C9	C10	122.9(2)	C8	C9	C10	122.9(2)
C9	C10	C11	119.4(3)	C9	C10	C11	119.4(3)
C10	C11	C12	118.9(3)	C10	C11	C12	118.9(3)
C11	C12	C13	118.6(3)	C11	C12	C13	118.6(3)
N3	C13	C12	122.9(3)	N3	C13	C12	122.9(3)
N2	C14	C15	111.1(2)	N2	C14	C15	111.1(2)
N4	C15	C14	114.6(3)	N4	C15	C14	114.6(3)
N4	C15	C16	122.3(3)	N4	C15	C16	122.3(3)
C14	C15	C16	123.1(3)	C14	C15	C16	123.1(3)
C15	C16	C17	118.9(3)	C15	C16	C17	118.9(3)
C16	C17	C18	117.8(3)	C16	C17	C18	117.8(3)
C17	C18	C19	119.2(3)	C17	C18	C19	119.2(3)
N4	C19	C18	123.5(3)	N4	C19	C18	123.5(3)

Structural information for 11

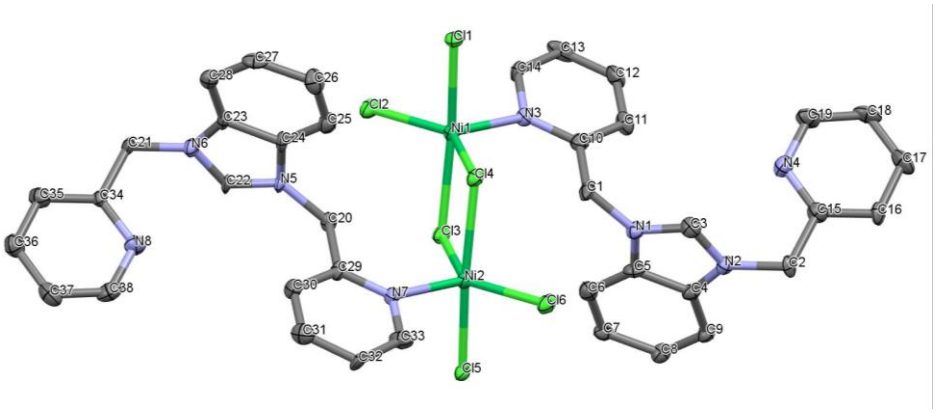

Space group	P 2_1
Cell lengths	**a** 8.4285(6) **b** 22.1022(15) **c** 10.3208(7)
Cell angles	**α** 90 **β** 97.424(3) **γ** 90
Cell volume	1906.53
Z, Z’	**Z**: 4 **Z'**: 2
R-factor (%)	5.87

Bond lengths in **11**

Atom 1	**Atom 2**	**Length**	**Atom 1**	**Atom 2**	**Length**
Ni1	Cl1	2.330(3)	C7	C8	1.40(2)
Ni1	Cl2	2.313(4)	C8	C9	1.39(2)
Ni1	Cl3	2.463(3)	C10	C11	1.39(2)
Ni1	Cl4	2.378(4)	C11	C12	1.40(2)
Ni1	N3	2.06(1)	C12	C13	1.36(2)
Ni2	Cl3	2.383(4)	C13	C14	1.37(2)
Ni2	Cl4	2.451(3)	C15	C16	1.40(2)
Ni2	Cl5	2.317(3)	C16	C17	1.42(2)
Ni2	Cl6	2.312(4)	C17	C18	1.37(2)
Ni2	N7	2.05(1)	C18	C19	1.37(2)
N1	C1	1.46(1)	C20	C29	1.53(2)

N1	C3	1.35(2)	C21	C34	1.51(2)
N1	C5	1.39(1)	C23	C24	1.41(2)
N2	C2	1.47(2)	C23	C28	1.38(2)
N2	C3	1.34(1)	C24	C25	1.37(2)
N2	C4	1.40(2)	C25	C26	1.39(2)
N3	C10	1.36(2)	C26	C27	1.43(2)
N3	C14	1.36(2)	C27	C28	1.39(2)
N4	C15	1.33(2)	C29	C30	1.39(2)
N4	C19	1.35(2)	C30	C31	1.38(2)
N5	C20	1.46(1)	C31	C32	1.40(2)
N5	C22	1.32(2)	C32	C33	1.39(2)
N5	C24	1.40(1)	C34	C35	1.40(2)
N6	C21	1.45(2)	C35	C36	1.37(2)
N6	C22	1.33(1)	C36	C37	1.40(2)
N6	C23	1.39(2)	C37	C38	1.39(2)
N7	C29	1.35(2)	C2	C15	1.53(2)
N7	C33	1.34(2)	C4	C5	1.39(2)
N8	C34	1.35(2)	C4	C9	1.40(1)
N8	C38	1.34(2)	C5	C6	1.41(2)
C1	C10	1.50(2)	C6	C7	1.38(2)

Bonds angles in **11**

Atom 1	**Atom 2**	**Atom 3**	**Angle**	**Atom 1**	**Atom 2**	**Atom 3**	**Angle**
Cl1	Ni1	Cl2	92.6(1)	Cl1	Ni1	Cl2	92.6(1)
Cl1	Ni1	Cl3	171.7(1)	Cl1	Ni1	Cl3	171.7(1)
Cl1	Ni1	Cl4	90.4(1)	Cl1	Ni1	Cl4	90.4(1)
Cl1	Ni1	N3	94.2(3)	Cl1	Ni1	N3	94.2(3)
Cl2	Ni1	Cl3	88.5(1)	Cl2	Ni1	Cl3	88.5(1)
Cl2	Ni1	Cl4	139.4(1)	Cl2	Ni1	Cl4	139.4(1)
Cl2	Ni1	N3	107.6(3)	Cl2	Ni1	N3	107.6(3)
Cl3	Ni1	Cl4	83.4(1)	Cl3	Ni1	Cl4	83.4(1)
Cl3	Ni1	N3	93.3(3)	Cl3	Ni1	N3	93.3(3)
Cl4	Ni1	N3	112.5(3)	Cl4	Ni1	N3	112.5(3)
Cl3	Ni2	Cl4	83.6(1)	Cl3	Ni2	Cl4	83.6(1)
Cl3	Ni2	Cl5	90.2(1)	Cl3	Ni2	Cl5	90.2(1)
Cl3	Ni2	Cl6	139.1(1)	Cl3	Ni2	Cl6	139.1(1)
Cl3	Ni2	N7	112.8(3)	Cl3	Ni2	N7	112.8(3)
Cl4	Ni2	Cl5	171.6(1)	Cl4	Ni2	Cl5	171.6(1)
Cl4	Ni2	Cl6	88.6(1)	Cl4	Ni2	Cl6	88.6(1)
Cl4	Ni2	N7	93.8(3)	Cl4	Ni2	N7	93.8(3)
Cl5	Ni2	Cl6	92.5(1)	Cl5	Ni2	Cl6	92.5(1)
Cl5	Ni2	N7	93.8(3)	Cl5	Ni2	N7	93.8(3)

Cl6	Ni2	N7	107.7(3)	Cl6	Ni2	N7	107.7(3)
Ni1	Cl3	Ni2	96.3(1)	Ni1	Cl3	Ni2	96.3(1)
Ni1	Cl4	Ni2	96.7(1)	Ni1	Cl4	Ni2	96.7(1)
C1	N1	C3	126(1)	C1	N1	C3	126(1)
C1	N1	C5	125(1)	C1	N1	C5	125(1)
C3	N1	C5	109(1)	C3	N1	C5	109(1)
C2	N2	C3	122(1)	C2	N2	C3	122(1)
C2	N2	C4	128(1)	C2	N2	C4	128(1)
C3	N2	C4	109(1)	C3	N2	C4	109(1)
Ni1	N3	C10	130.2(9)	Ni1	N3	C10	130.2(9)
Ni1	N3	C14	112.5(8)	Ni1	N3	C14	112.5(8)
C10	N3	C14	117(1)	C10	N3	C14	117(1)
C15	N4	C19	118(1)	C15	N4	C19	118(1)
C20	N5	C22	125(1)	C20	N5	C22	125(1)
C20	N5	C24	126(1)	C20	N5	C24	126(1)
C22	N5	C24	108(1)	C22	N5	C24	108(1)
C21	N6	C22	123(1)	C21	N6	C22	123(1)
C21	N6	C23	126(1)	C21	N6	C23	126(1)
C22	N6	C23	109(1)	C22	N6	C23	109(1)
Ni2	N7	C29	129.9(9)	Ni2	N7	C29	129.9(9)
Ni2	N7	C33	111.5(9)	Ni2	N7	C33	111.5(9)
C29	N7	C33	118(1)	C29	N7	C33	118(1)
C34	N8	C38	116(1)	C34	N8	C38	116(1)
N1	C1	C10	113(1)	N1	C1	C10	113(1)
N2	C2	C15	111(1)	N2	C2	C15	111(1)
N1	C3	N2	109(1)	N1	C3	N2	109(1)
N2	C4	C5	106(1)	N2	C4	C5	106(1)
N2	C4	C9	132(1)	N2	C4	C9	132(1)
C5	C4	C9	122(1)	C5	C4	C9	122(1)
N1	C5	C4	107(1)	N1	C5	C4	107(1)
N1	C5	C6	132(1)	N1	C5	C6	132(1)
C4	C5	C6	121(1)	C4	C5	C6	121(1)
C5	C6	C7	117(1)	C5	C6	C7	117(1)
C6	C7	C8	123(1)	C6	C7	C8	123(1)
C7	C8	C9	121(1)	C7	C8	C9	121(1)
C4	C9	C8	117(1)	C4	C9	C8	117(1)
N3	C10	C1	116(1)	N3	C10	C1	116(1)
N3	C10	C11	122(1)	N3	C10	C11	122(1)
C1	C10	C11	122(1)	C1	C10	C11	122(1)
C10	C11	C12	119(1)	C10	C11	C12	119(1)
C11	C12	C13	118(1)	C11	C12	C13	118(1)
C12	C13	C14	121(1)	C12	C13	C14	121(1)
N3	C14	C13	122(1)	N3	C14	C13	122(1)
N4	C15	C2	118(1)	N4	C15	C2	118(1)
N4	C15	C16	123(1)	N4	C15	C16	123(1)

C2	C15	C16	119(1)	C2	C15	C16	119(1)
C15	C16	C17	117(1)	C15	C16	C17	117(1)
C16	C17	C18	119(1)	C16	C17	C18	119(1)
C17	C18	C19	119(1)	C17	C18	C19	119(1)
N4	C19	C18	123(1)	N4	C19	C18	123(1)
N5	C20	C29	111(1)	N5	C20	C29	111(1)
N6	C21	C34	111(1)	N6	C21	C34	111(1)
N5	C22	N6	111(1)	N5	C22	N6	111(1)
N6	C23	C24	105(1)	N6	C23	C24	105(1)
N6	C23	C28	133(1)	N6	C23	C28	133(1)
C24	C23	C28	122(1)	C24	C23	C28	122(1)
N5	C24	C23	107(1)	N5	C24	C23	107(1)
N5	C24	C25	130(1)	N5	C24	C25	130(1)
C23	C24	C25	123(1)	C23	C24	C25	123(1)
C24	C25	C26	117(1)	C24	C25	C26	117(1)
C25	C26	C27	120(1)	C25	C26	C27	120(1)
C26	C27	C28	123(1)	C26	C27	C28	123(1)
C23	C28	C27	116(1)	C23	C28	C27	116(1)
N7	C29	C20	117(1)	N7	C29	C20	117(1)
N7	C29	C30	122(1)	N7	C29	C30	122(1)
C20	C29	C30	121(1)	C20	C29	C30	121(1)
C29	C30	C31	120(1)	C29	C30	C31	120(1)
C30	C31	C32	119(1)	C30	C31	C32	119(1)
C31	C32	C33	117(1)	C31	C32	C33	117(1)
N7	C33	C32	124(1)	N7	C33	C32	124(1)
N8	C34	C21	117(1)	N8	C34	C21	117(1)
N8	C34	C35	124(1)	N8	C34	C35	124(1)
C21	C34	C35	119(1)	C21	C34	C35	119(1)
C34	C35	C36	119(1)	C34	C35	C36	119(1)
C35	C36	C37	119(1)	C35	C36	C37	119(1)
C36	C37	C38	118(1)	C36	C37	C38	118(1)
N8	C38	C37	124(1)	N8	C38	C37	124(1)

Structural information for 12

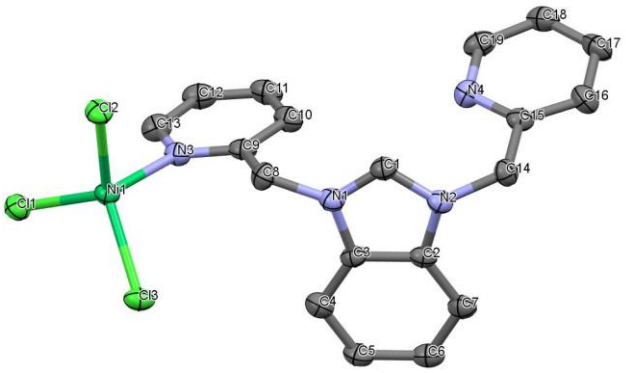

Space group	P 2_1/n
Cell lengths	**a** 9.5129(2) **b** 21.7068(7) **c** 9.8014(3)
Cell angles	α 90 β 104.9170(10) γ 90
Cell volume	1955.73
Z, Z’	**Z**: 4 **Z'**: 1
R-factor (%)	6.31

Bond lengths in **12**

Atom 1	**Atom 2**	**Length**	**Atom 1**	**Atom 2**	**Length**
Ni1	Cl2	2.250(1)	C2	C7	1.392(7)
Ni1	Cl3	2.242(1)	C3	C4	1.383(8)
Ni1	Cl1	2.240(1)	C4	C5	1.381(7)
Ni1	N3	2.024(3)	C5	C6	1.407(7)
N1	C1	1.324(6)	C6	C7	1.384(9)
N1	C3	1.398(6)	C8	C9	1.519(6)
N1	C8	1.452(5)	C9	C10	1.383(6)
N2	C1	1.334(5)	C10	C11	1.389(7)
N2	C2	1.393(7)	C11	C12	1.375(7)
N2	C14	1.461(6)	C12	C13	1.376(6)
N3	C9	1.347(6)	C14	C15	1.516(6)

N3	C13	1.349(6)	C15	C16	1.373(7)
N4	C15	1.338(6)	C16	C17	1.391(8)
N4	C19	1.349(6)	C17	C18	1.391(8)
C2	C3	1.394(6)	C18	C19	1.379(8)

Bonds angles in **12**

Atom 1	**Atom 2**	**Atom 3**	**Angle**	**Atom 1**	**Atom 2**	**Atom 3**	**Angle**
Cl2	Ni1	Cl3	125.56(5)	C2	C3	C4	122.8(4)
Cl2	Ni1	Cl1	115.66(5)	C3	C4	C5	115.8(4)
Cl2	Ni1	N3	100.2(1)	C4	C5	C6	122.1(5)
Cl3	Ni1	Cl1	102.71(5)	C5	C6	C7	121.7(5)
Cl3	Ni1	N3	106.0(1)	C2	C7	C6	116.2(4)
Cl1	Ni1	N3	104.6(1)	N1	C8	C9	111.1(4)
C1	N1	C3	109.0(4)	N3	C9	C8	116.5(4)
C1	N1	C8	126.1(4)	N3	C9	C10	121.9(4)
C3	N1	C8	124.6(4)	C8	C9	C10	121.6(4)
C1	N2	C2	108.3(4)	C9	C10	C11	119.0(4)
C1	N2	C14	122.8(4)	C10	C11	C12	119.2(5)
C2	N2	C14	126.5(4)	C11	C12	C13	118.9(5)
Ni1	N3	C9	124.2(3)	N3	C13	C12	122.6(5)
Ni1	N3	C13	117.4(3)	N2	C14	C15	111.8(4)
C9	N3	C13	118.3(4)	N4	C15	C14	117.0(4)
C15	N4	C19	116.6(4)	N4	C15	C16	124.1(5)
N1	C1	N2	110.1(4)	C14	C15	C16	118.8(4)
N2	C2	C3	106.8(4)	C15	C16	C17	118.6(5)
N2	C2	C7	131.8(4)	C16	C17	C18	118.5(5)
C3	C2	C7	121.4(4)	C17	C18	C19	118.5(5)
N1	C3	C2	105.8(4)	N4	C19	C18	123.7(5)
N1	C3	C4	131.4(4)				

4.3 Mass spectral data

ESI-MS (+) of **1**

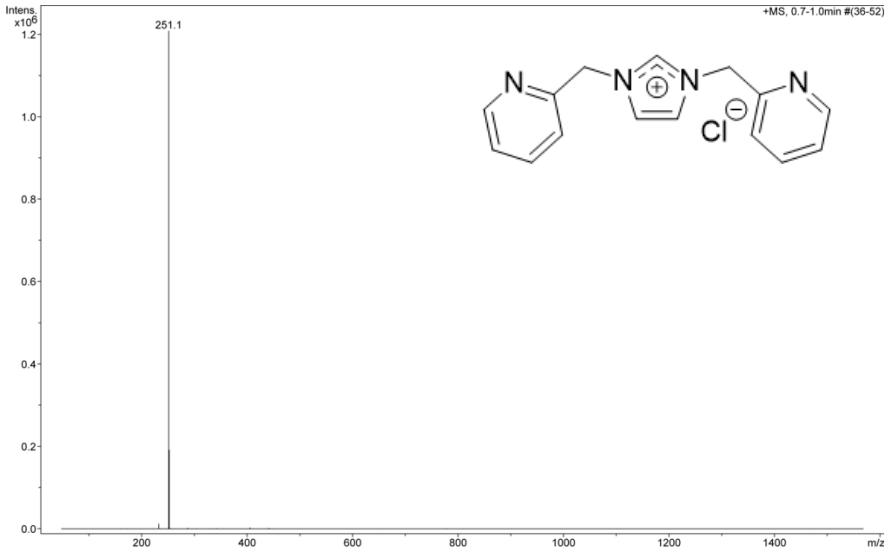

HRMS (+) of **1**

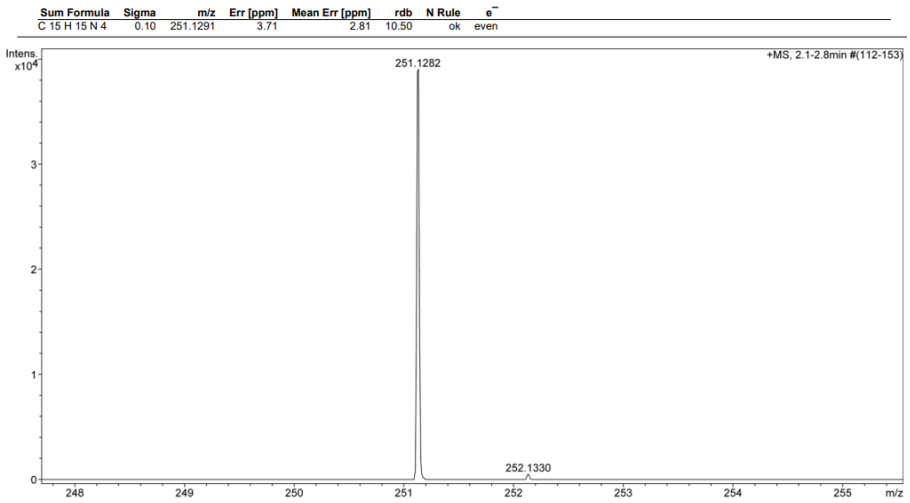

ESI-MS (+) of **2**

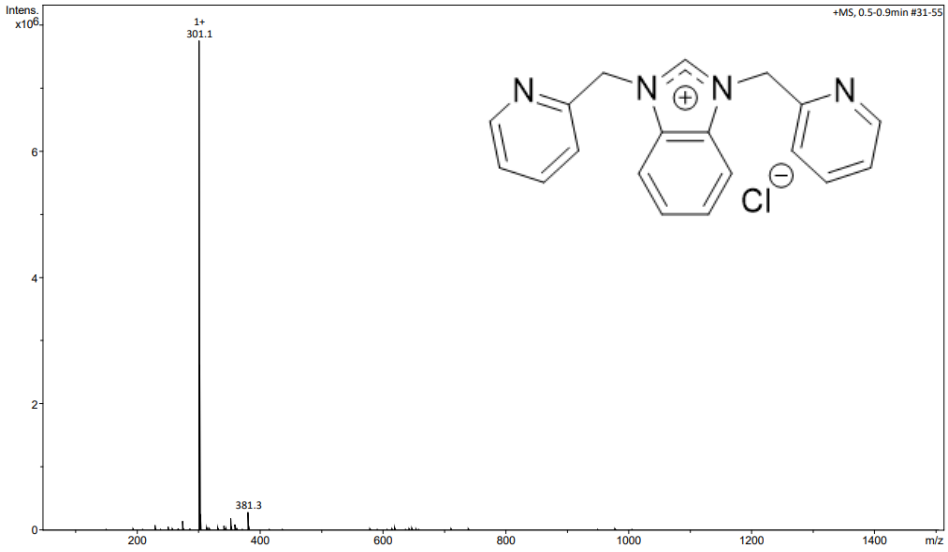

HRMS (+) of **2**

Meas. m/z	Ion Formula	m/z	err [ppm]
301.144764	C19H17N4	301.144773	0.0

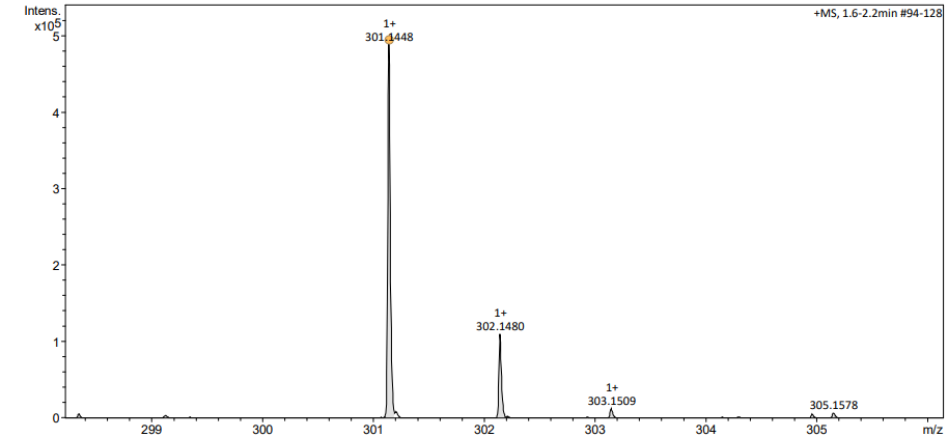

ESI-MS (+) of **3/4/5**

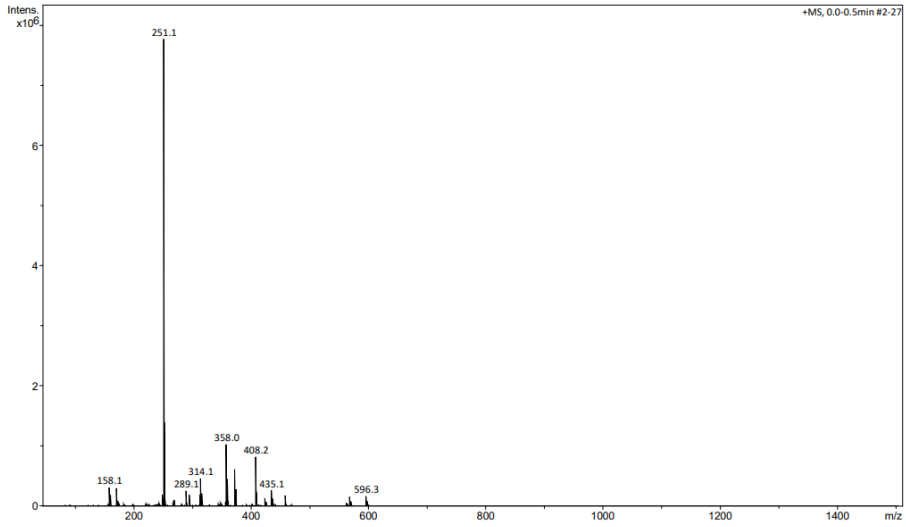

ESI-MS (-) of **3/4/5**

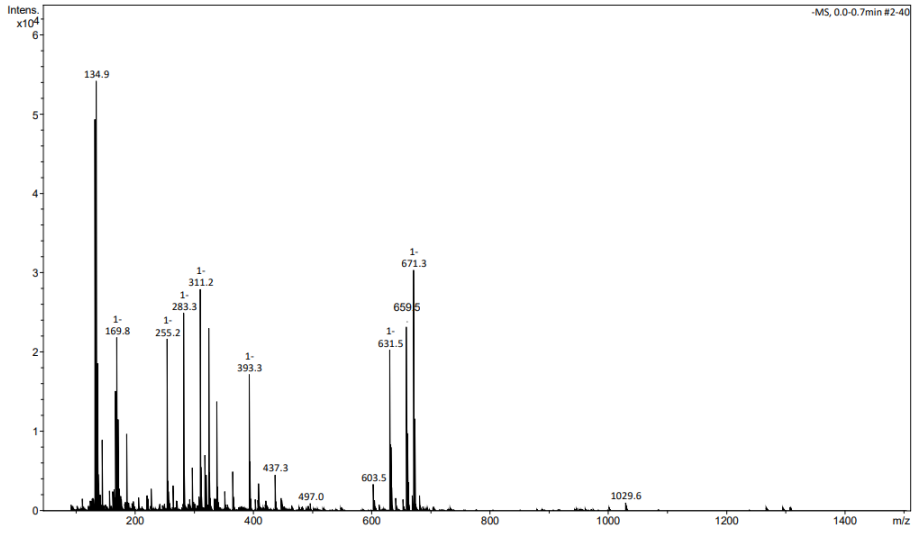

ESI-MS (+) of **6**

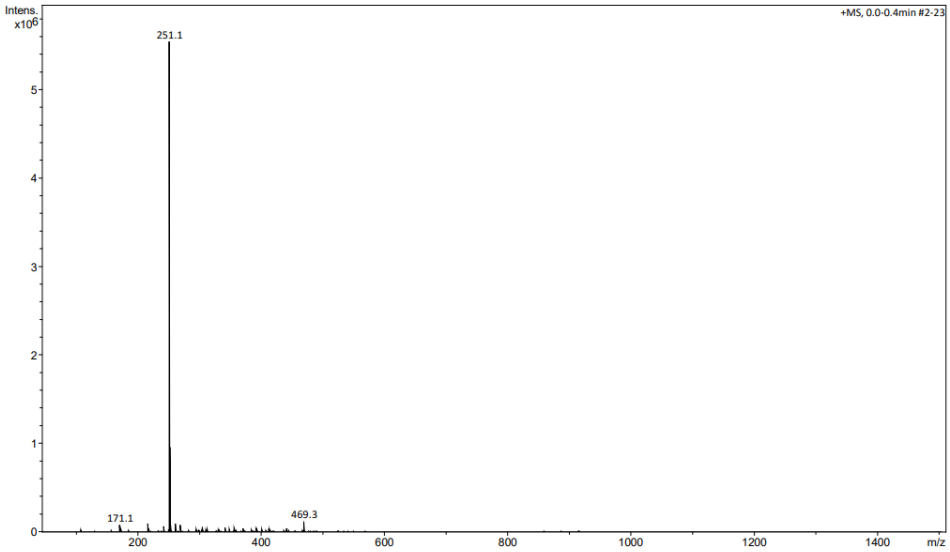
Intens.
x10^6
+MS, 0.0-0.4min #2-23
251.1
171.1
469.3
0
1
2
3
4
5
200
400
600
800
1000
1200
1400
m/z

ESI-MS (+) of **7**

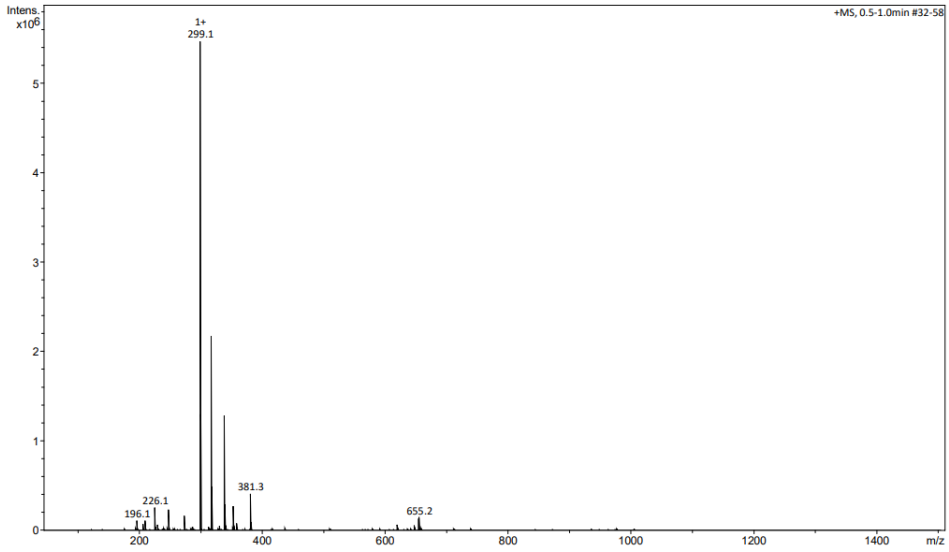
Intens.
x10^6
+MS, 0.5-1.0min #32-58
1+
299.1
226.1
196.1
381.3
655.2
m/z

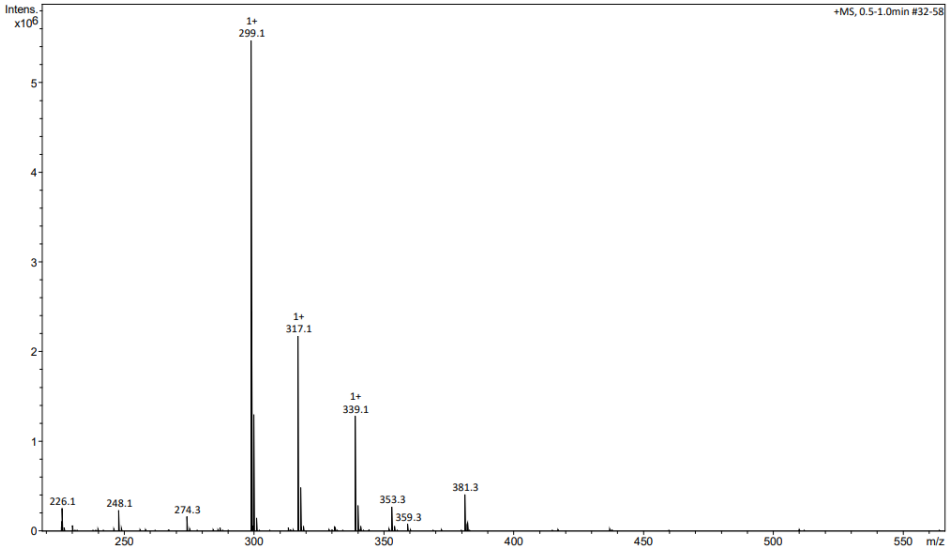
Intens.
x10^6
+MS, 0.5-1.0min #32-58
1+
299.1
1+
317.1
1+
339.1
226.1
248.1
274.3
353.3
359.3
381.3
m/z

ESI-MS (+) of **9**

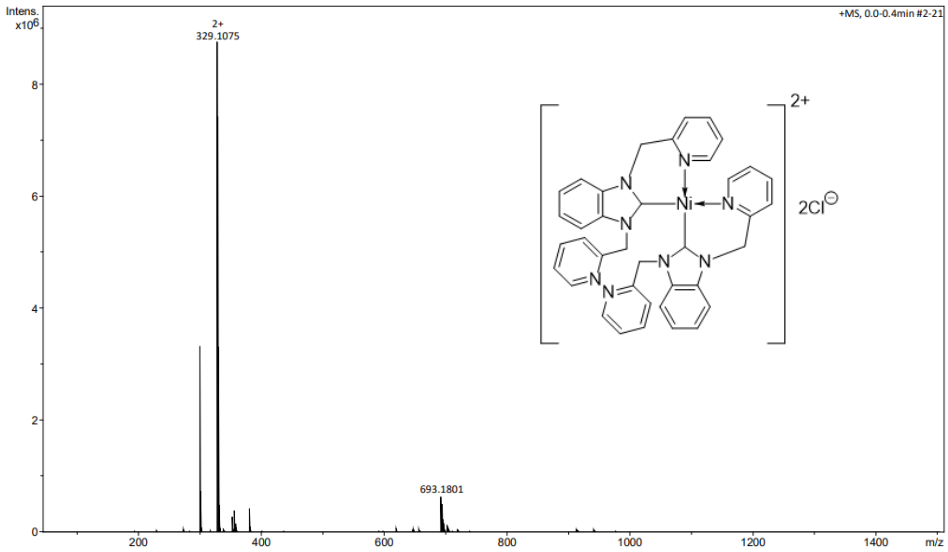

HRMS (+) of **9**

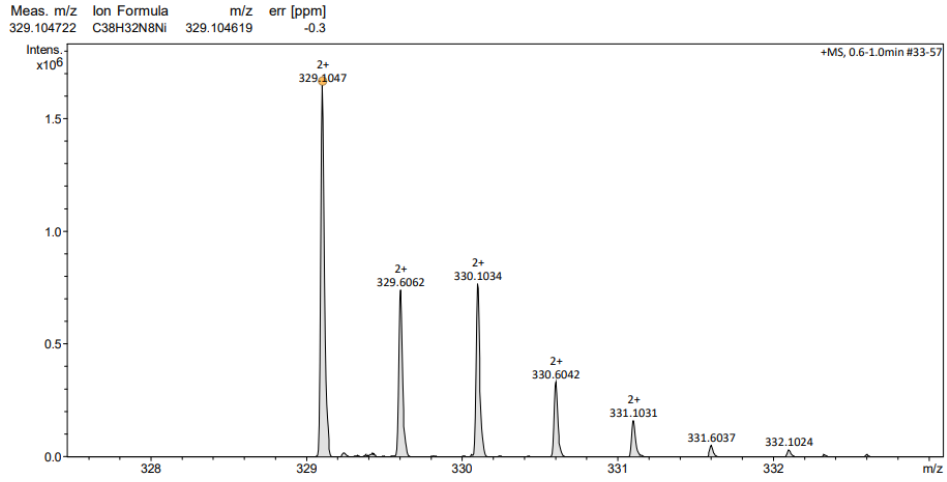

ESI-MS (+) of **10**

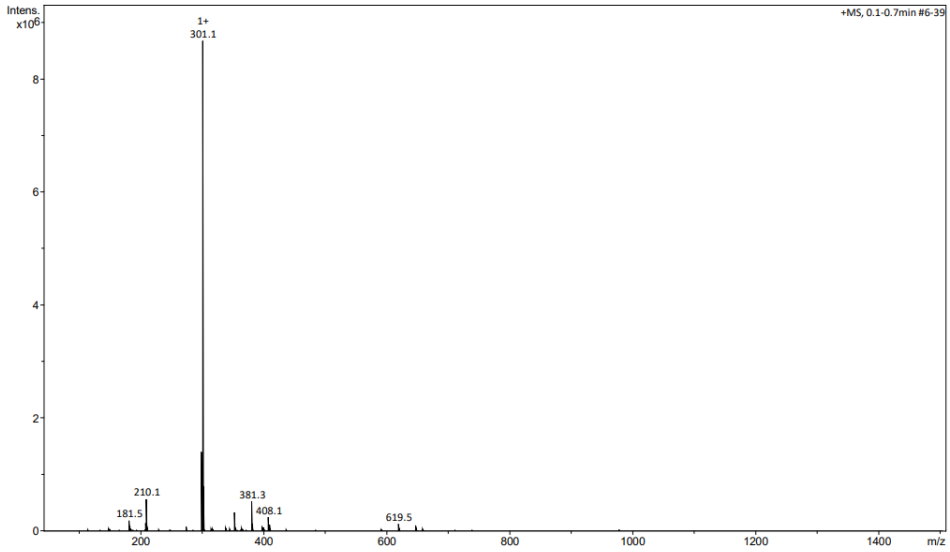
Intens.
x10^6
+MS, 0.1-0.7min #6-39
1+
301.1
210.1
181.5
381.3
408.1
619.5
m/z

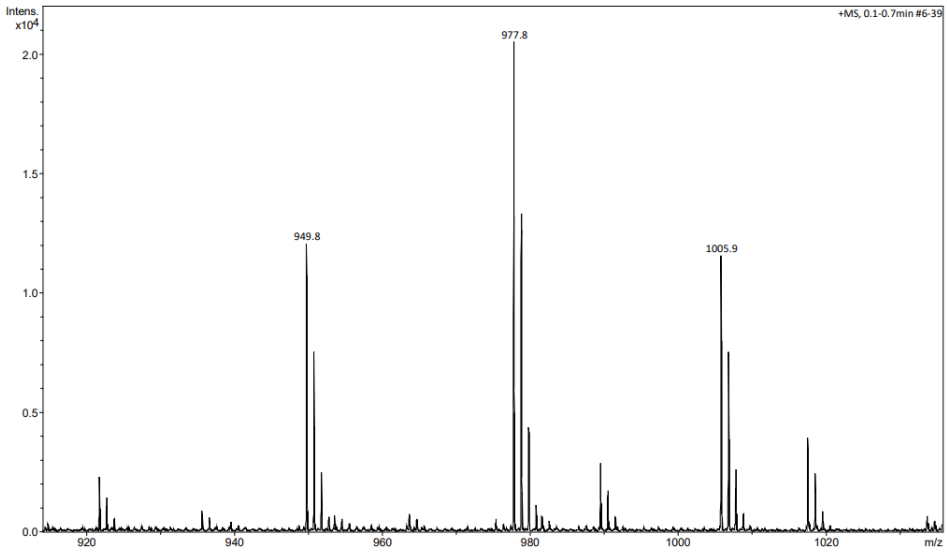
Intens.
x10^4
+MS, 0.1-0.7min #6-39
977.8
949.8
1005.9
m/z

ESI-MS (+) of **11/12**

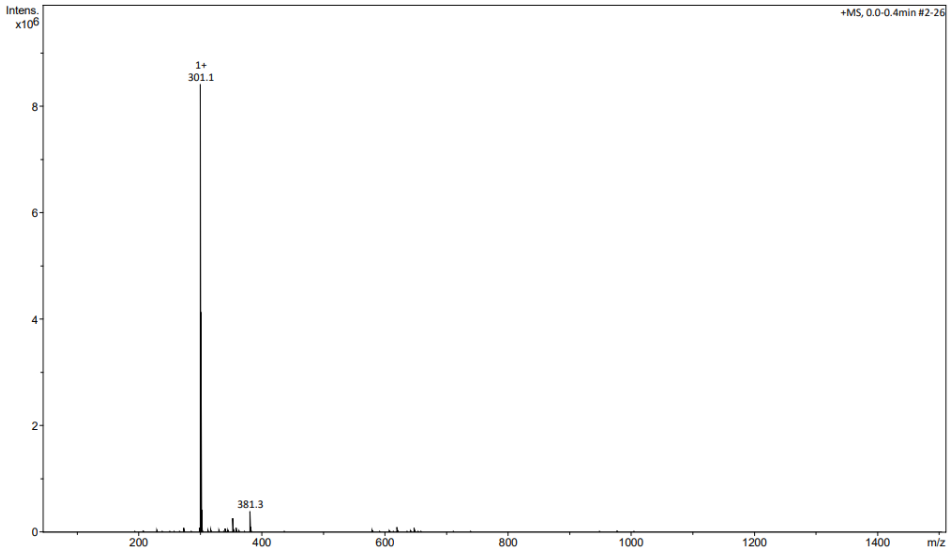

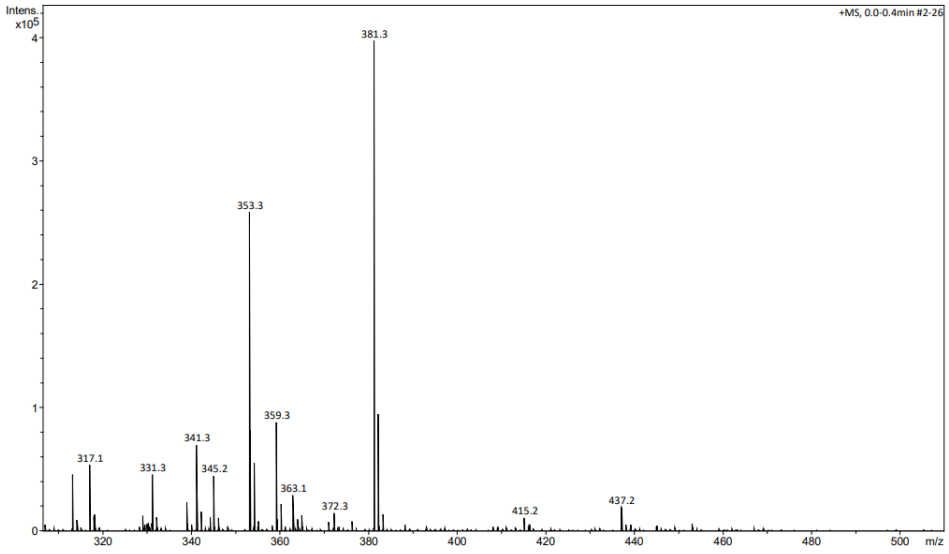

ESI-MS (+) of **13**

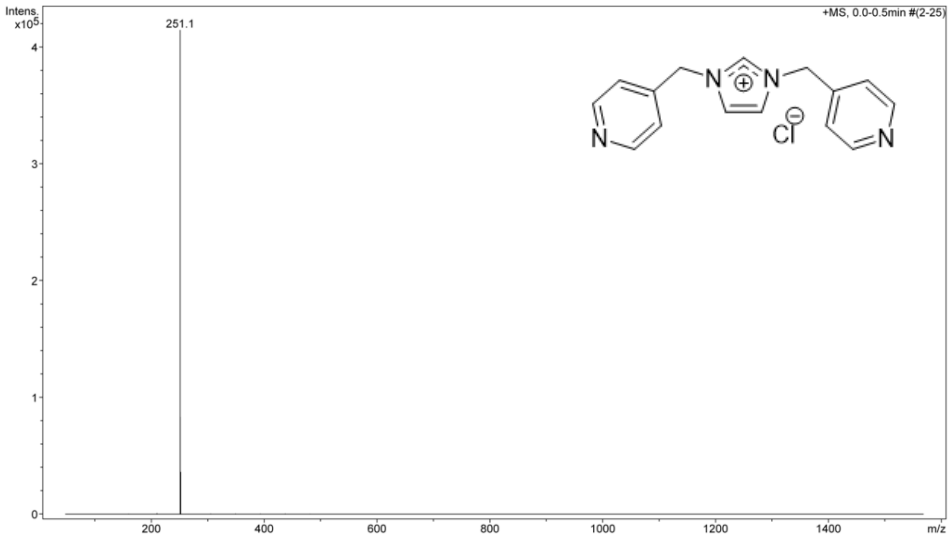

HRMS (+) of **13**

Sum Formula	Sigma	m/z	Err [ppm]	Mean Err [ppm]	rdb	N Rule	e⁻
C 15 H 15 N 4	0.07	251.1291	2.64	2.52	10.50	ok	even

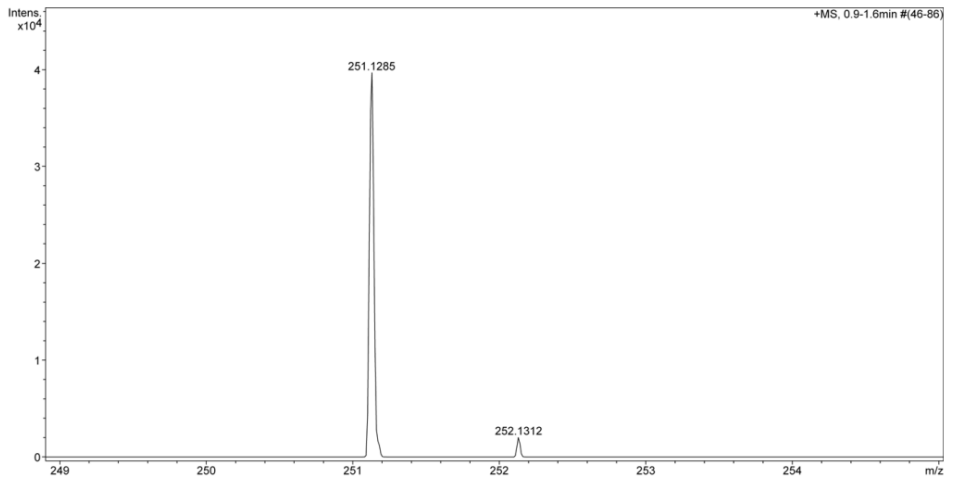

ESI-MS (+) of **14**

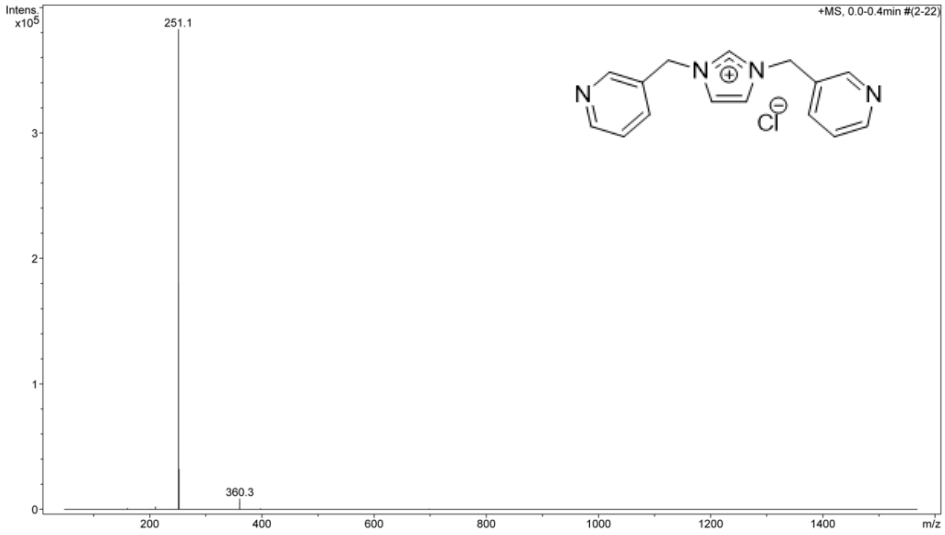

HRMS (+) of **14**

Sum Formula	Sigma	m/z	Err [ppm]	Mean Err [ppm]	rdb	N Rule	e⁻
C 15 H 15 N 4	0.07	251.1291	2.34	2.38	10.50	ok	even

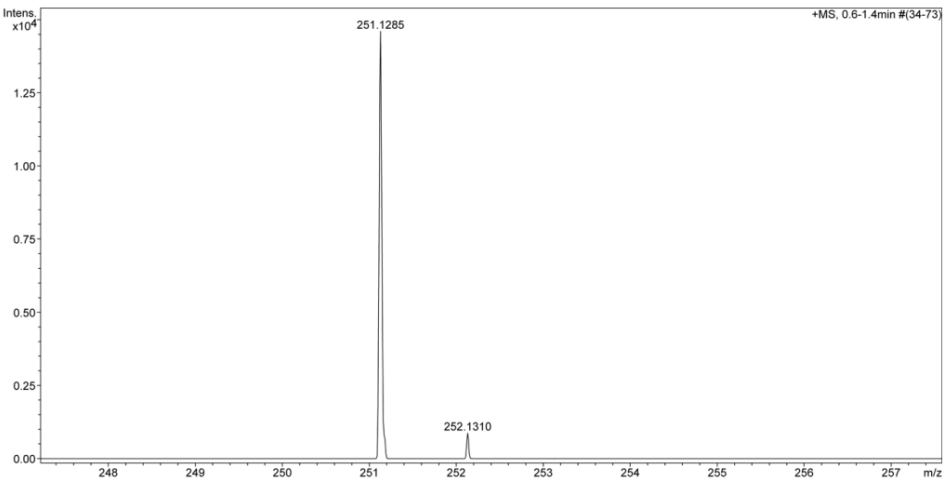

ESI-MS (+) of **17**

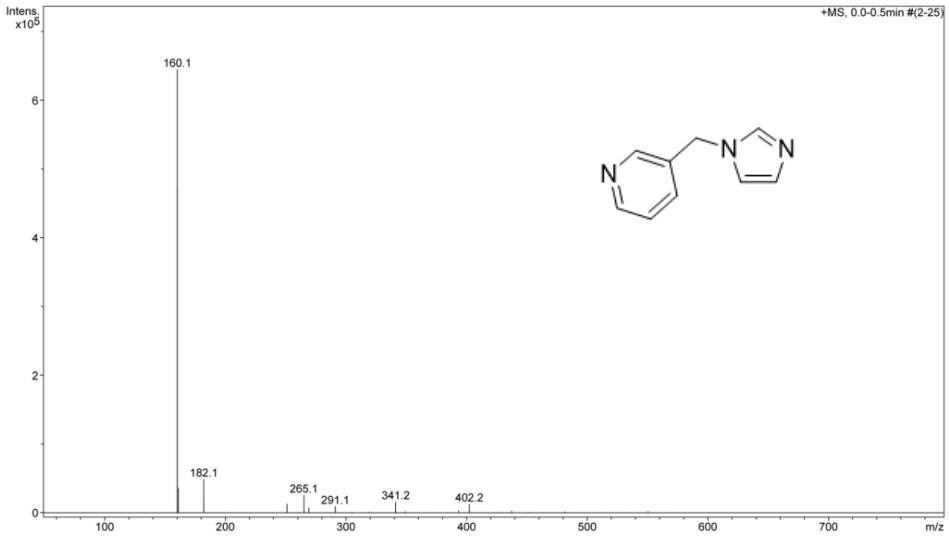

HRMS (+) of **17**

Sum Formula	Sigma	m/z	Err [ppm]	Mean Err [ppm]	rdb	N Rule	e⁻
C 9 H 10 N 3	0.04	160.0869	4.19	3.92	6.50	ok	even

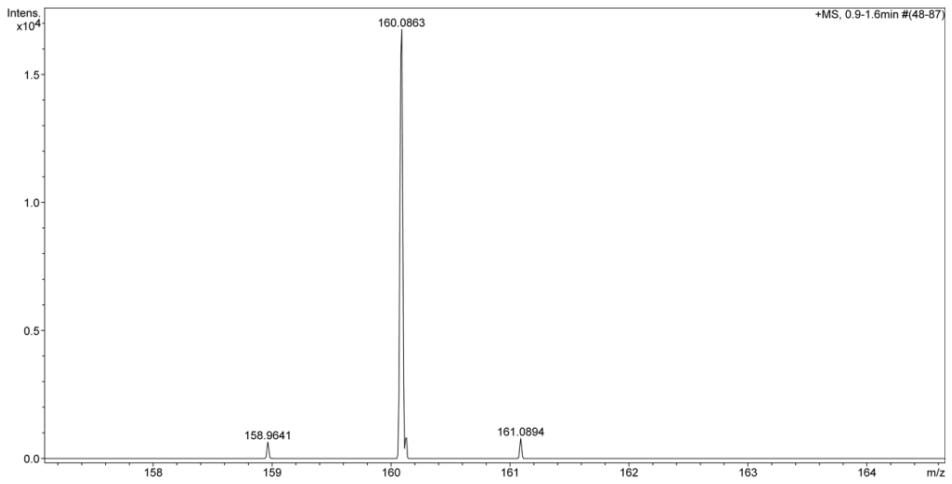

HRMS (+) of **18**

Sum Formula	Sigma	m/z	Err [ppm]	Mean Err [ppm]	rdb	N Rule	e⁻
C 9 H 10 N 3	0.04	160.0869	4.12	3.97	6.50	ok	even

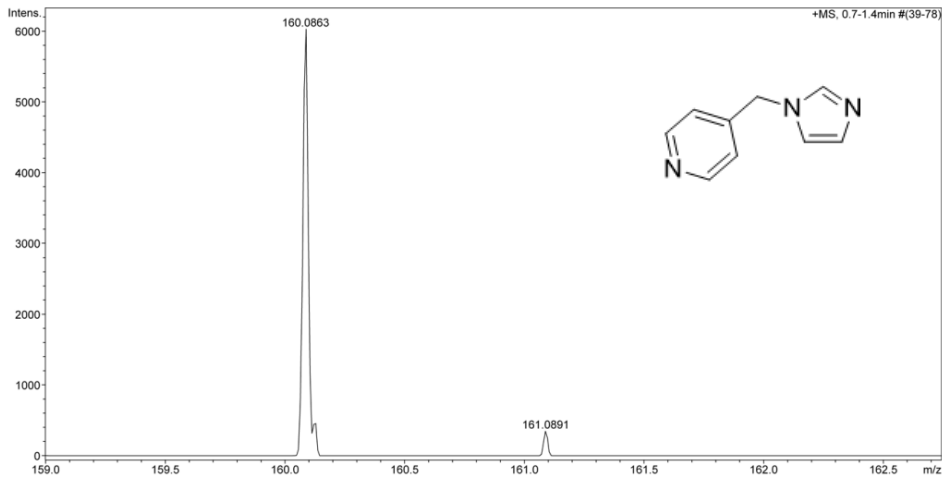

ESI-MS (+) of **19**

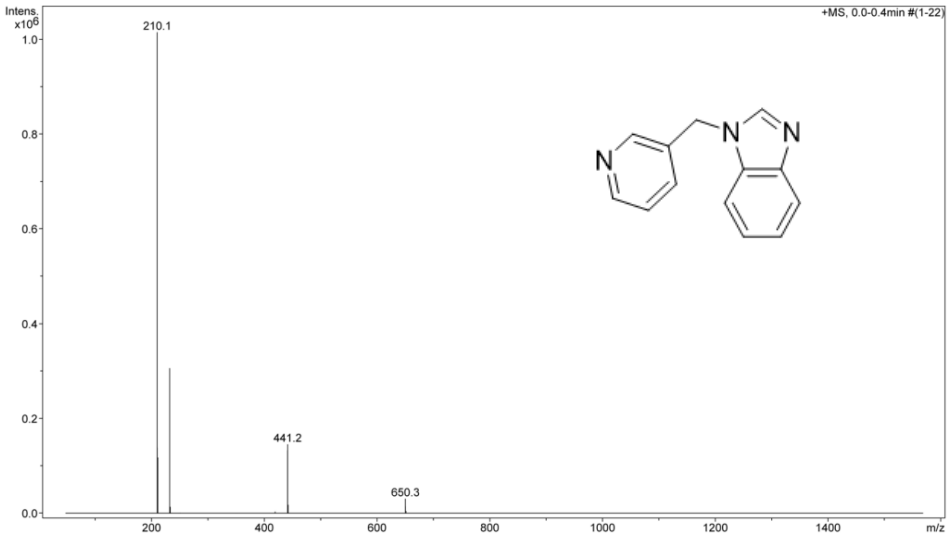

HRMS (+) of **19**

Sum Formula	Sigma	m/z	Err [ppm]	Mean Err [ppm]	rdb	N Rule	e⁻
C 13 H 12 N 3	0.04	210.1026	-3.12	-2.48	9.50	ok	even

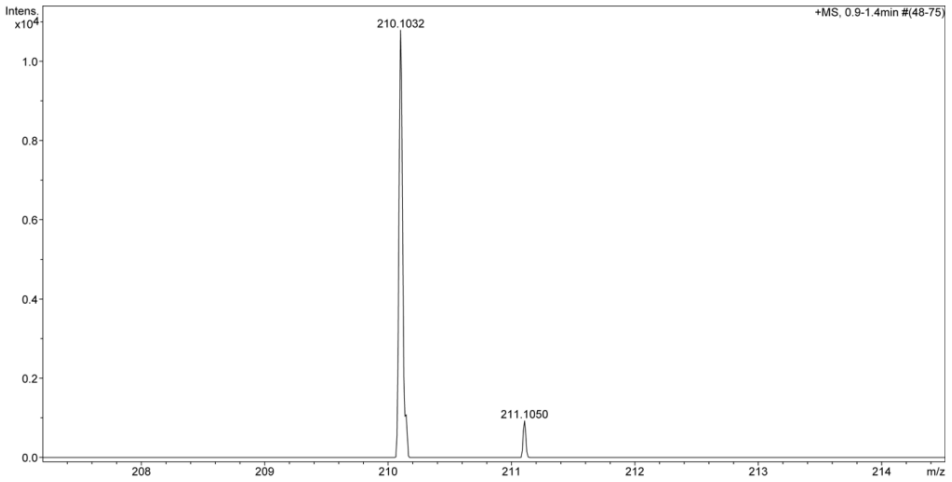

ESI-MS (+) of **20**

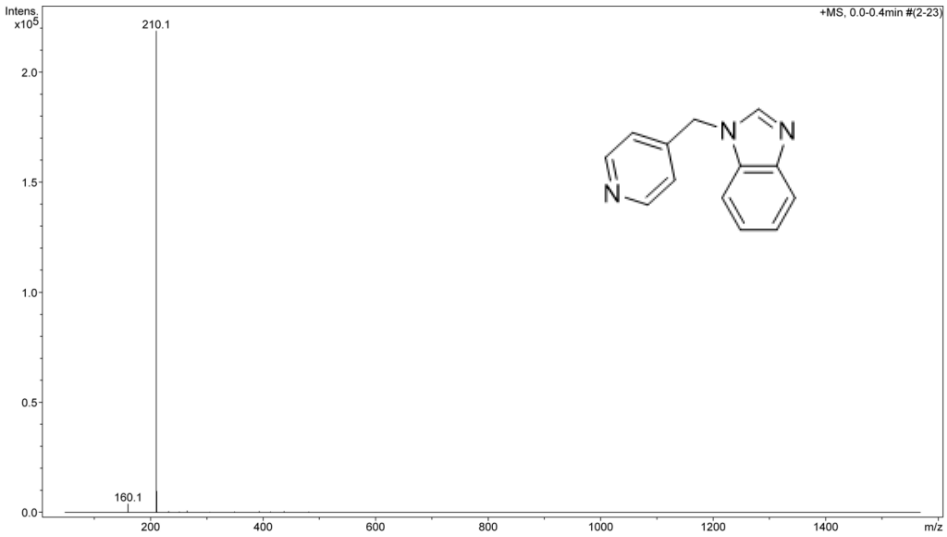

HRMS (+) of **20**

Sum Formula	Sigma	m/z	Err [ppm]	Mean Err [ppm]	rdb	N Rule	e⁻
C 13 H 12 N 3	0.07	210.1026	-2.29	-1.69	9.50	ok	even